Chem Soc Rev

REVIEW ARTICLE

View Article Online
View Journal | View Issue

Cite this: *Chem. Soc. Rev.*, 2024, **53**, 8713

Exploring pathological link between antimicrobial and amyloid peptides

Yijing Tang,†[a] Yanxian Zhang,†[b] Dong Zhang,[c] Yonglan Liu,[d] Ruth Nussinov*[ef] and Jie Zheng*[a]

Amyloid peptides (AMYs) and antimicrobial peptides (AMPs) are considered as the two distinct families of peptides, characterized by their unique sequences, structures, biological functions, and specific pathological targets. However, accumulating evidence has revealed intriguing pathological connections between these peptide families in the context of microbial infection and neurodegenerative diseases. Some AMYs and AMPs share certain structural and functional characteristics, including the ability to self-assemble, the presence of β-sheet-rich structures, and membrane-disrupting mechanisms. These shared features enable AMYs to possess antimicrobial activity and AMPs to acquire amyloidogenic properties. Despite limited studies on AMYs–AMPs systems, the cross-seeding phenomenon between AMYs and AMPs has emerged as a crucial factor in the bidirectional communication between the pathogenesis of neurodegenerative diseases and host defense against microbial infections. In this review, we examine recent developments in the potential interplay between AMYs and AMPs, as well as their pathological implications for both infectious and neurodegenerative diseases. By discussing the current progress and challenges in this emerging field, this account aims to inspire further research and investments to enhance our understanding of the intricate molecular crosstalk between AMYs and AMPs. This knowledge holds great promise for the development of innovative therapies to combat both microbial infections and neurodegenerative disorders.

Received 21st January 2024

DOI: 10.1039/d3cs00878a

rsc.li/chem-soc-rev

[a] *Department of Chemical, Biomolecular, and Corrosion Engineering, The University of Akron, Ohio 44325, USA. E-mail: zhengj@uakron.edu*
[b] *Division of Endocrinology and Diabetes, Department of Pediatrics, School of Medicine, Stanford University, Palo Alto, CA 94304, USA*
[c] *The Wallace H. Coulter Department of Biomedical Engineering, Georgia Institute of Technology and Emory University, Atlanta, Georgia 30332, USA*
[d] *Cancer Innovation Laboratory, National Cancer Institute, Frederick, MD 21702, USA*
[e] *Computational Structural Biology Section, Frederick National Laboratory for Cancer Research, Frederick, MD 21702, USA. E-mail: nussinor@mail.nih.gov*
[f] *Department of Human Molecular Genetics and Biochemistry Sackler School of Medicine, Tel Aviv University, Tel Aviv 69978, Israel*
† Authors contribute equally to this paper.

Yijing Tang

Yijing Tang received her BE in Polymer Science and materials from Beijing University of Chemical Technology and her MS in Polymer Science from the University of Akron. After completing her PhD study in 2024 under the supervision of Prof. Jie Zheng at the University of Akron, she joined the group of Prof. Brian Bacskai and Prof. Steven Hou at the Massachusetts General Hospital and Harvard Medical School as a Postdoc research fellow. Since then, her research has primarily focused on developing in vivo fluorescent labeling techniques to monitor real-time progression and dynamics of neurodegeneration.

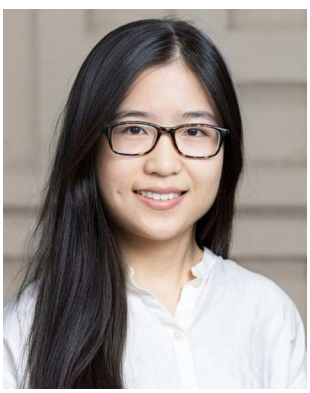

Yanxian Zhang

Dr Yanxian Zhang earned her PhD in Chemical, Biomolecular, and Corrosion Engineering from the University of Akron, focusing on amyloid peptide cross-seeding and inhibitor development. Her work revealed critical interactions between antimicrobial human α-defensins and amyloid peptides, notably inhibiting amyloid aggregation. Since 2021, she has been a postdoctoral researcher at Stanford University, developing biopharmaceuticals by merging molecular biology, chemical engineering, and protein engineering to enhance stability and optimize pharmacological profiles.

1. Introduction

Amyloids and antimicrobial peptides are generally considered as two distinct families characterized by their diverse sequences, structures, biological functions, and targets. Amyloid peptides (AMYs) are widely recognized as causative agents in the development of many neurodegenerative diseases, including Alzheimer's disease (AD), type II diabetes (T2D), and Parkinson's disease (PD).[1–4] The prevailing "amyloid cascade hypothesis" for the past 30 years postulates that the accumulation of misfolded amyloid aggregates, characterized by their highly ordered, β-sheet structures (namely amyloids),[5] in human tissues is a key pathological feature of neurodegenerative diseases. Unlike the pathological characteristics of amyloid peptides, antimicrobial peptides (AMPs), particularly those broad-spectrum antibacterial ones, are aimed at combating diseases caused by the infection and inflammation of various pathogens (*e.g.*, viruses, parasites, bacteria, fungi).[6]

Despite the disparate functions of AMYs and AMPs, numerous studies revealed that certain amyloid and antimicrobial peptides unexpectedly exhibit additional functions typically associated with the other class.[7] AMPs, such as protegrin-1,[8] plantaricin A,[9] uperin 3.5,[10] magainin,[11,12] dermaseptin S9,[13] have demonstrated their ability to form amyloid-like fibrils enriched in β-sheet structures, resembling the characteristic

Dong Zhang

Dr Dong Zhang earned his PhD in Chemical, Biomolecular, and Corrosion Engineering from The University of Akron in 2022, under the supervision of Professor Jie Zheng. He is currently a postdoctoral fellow in Professor Younan Xia's group at the Georgia Institute of Technology. His research focuses on the rational design and synthesis of polymers and nanomaterials for applications in environmental, biological, and biomedical fields.

Yonglan Liu

Dr Yonglan Liu earned her PhD in Chemical Engineering from the University of Akron. She currently is a research scientist at the Cancer Innovation Laboratory, National Cancer Institute, National Institutes of Health. Her research centers on computational biology, biophysics, and chemistry, with specialized expertise in cancer biology, neurodegenerative diseases, neurodevelopmental disorders, structural biology, drug discovery, and materials science. Dr. Liu employs machine learning and molecular dynamics simulations to innovate in these fields of study, aiming to revolutionize our understanding and treatment of complex diseases. Her work is driven by a passion for bridging interdisciplinary approaches to tackle critical biomedical challenges.

Ruth Nussinov

Ruth Nussinov is at the Frederick National Laboratory of Cancer Research, NCI, an adjunct Professor at the Chemistry Department at the University of Maryland, and emeritus at the Medical school at Tel Aviv University. She authored over 750 scientific papers, is Editor-in-Chief of Current Opinion in Structural Biology, was Editor-in-Chief of PLoS Computational Biology, is Associate Editor and on Editorial Boards of multiple journals. She is a frequent speaker in Domestic and International meetings, symposia, and academic institutions, won multiple awards, elected fellow of several societies, and was twice a highly cited researcher. Her NCI website gives further details. ***https://ccr.cancer.gov/ruth-nussinov****.*

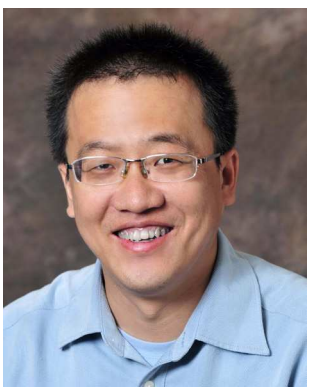

Jie Zheng

Prof. Zheng, a Full Professor of Dept. of Chemical, Biomolecular, and Corrosion Engineering at the University of Akron, earned his PhD from the University of Washington in 2005. His research spans disease-related proteins, biomaterials, and structural biology, incorporating experimental methods, biophysical analysis, molecular simulations, and machine-learning models. He has authored over 290 journal papers, achieving an h-index of 82 and accumulating over 23 300 citations. For further details on his achievements and publications, please visit his profile at ***https://sites.google.com/site/zhengakron/****.*

morphology of classic amyloid fibrils. Similarly, several AMYs, such as Aβ, hIAPP, α-syn, and SAA,[7,14–16] exhibited antibacterial activity against various bacterial strains (*e.g.*, *Candida albicans*, *Escherichia coli*, *Staphylococcus epidermidis*, *etc.*)[17–19] and antiviral activity against different viruses (*e.g.*, influenza virus A, herpes simplex virus, H3N2, H1N1, *etc*).[20,21] AMYs appear to act as a class of innate immune defense molecules, functioning by utilizing toxic amyloid aggregates to eliminate a broad spectrum of pathogens through the disruption of their cell membranes thus crucial functions. The shared functionality between AMYs and AMPs could be attributed to their common β-sheet-rich structures, enabling a strong binding affinity to cell membranes. Such strong membrane-activating interaction allows β-sheet-rich AMYs and AMPs to catalyze toxin-like channel formation and membrane depolarization as the primary mode-of-action of membrane disruption,[22] ultimately leading to the elimination of host target cells and pathogens. Therefore, AMP amyloidogenicity and AMY antimicrobial activity are suggested to originate from their shared innate and conserved characteristics throughout evolution.[6]

More importantly, recent studies revealed intriguing pathological connections between amyloid and antimicrobial peptides, likely arising from their shared structural and functional characteristics. While this area is still relatively less explored, there is emerging evidence that certain pairs of AMYs and AMPs, such as hIAPP and aurein, Aβ and PG1, α-/β-defensin and Aβ/hIAPP/hCT,[23,24] LL-37 and Aβ/hIAPP,[25,26] α-syn and CsgA/CsgC/CsgE,[27–29] can interact with each other, leading to the formation of amyloid fibrils that share similar conformations and pathological properties. This phenomenon, referred to as cross-seeding, highlights the intricate interplay between amyloid and antimicrobial peptides in pathological processes. As a result, the cross-seeding between AMYs and AMPs, likely facilitated by their similar β-sheet structures, often modulates amyloid aggregation through acceleration, inhibition, or modification of amyloid-induced cytotoxicity.[30,31] This dynamic crosstalk between AMYs and AMPs highlights the potential for therapeutic interventions targeting amyloid-related diseases by harnessing the functional properties of antimicrobial peptides.

Pathologically, the cross-seeding between AMYs and AMPs gives rise to the ''microbial infection hypothesis'' and the ''neuroinflammation hypothesis''. Both hypotheses offer insights into the underlying pathological mechanisms of neurodegenerative diseases. Since neuroinflammation is recognized as a significant risk factor in the development of pathological hallmarks of neurodegenerative diseases, both pathogens (including viruses, bacteria, and fungi) and amyloid aggregates (including Aβ, hIAPP, α-syn, and SAA) have been reported to induce persistent neuroinflammation by activating a long-lasting immune response. This chronic neuroinflammation, which arises as the consequence of both amyloid aggregation and microbial infection, contributes to the detrimental effects on neuronal health and leads to the eventual neurodegeneration.[32,33]

Emerging evidence from both experimental and clinical studies revealed a remarkable connection, and even a feedback loop, between amyloid formation and neuroinflammation, in addition to their individual contributions to the pathogenesis of neurodegenerative diseases. This connection is facilitated

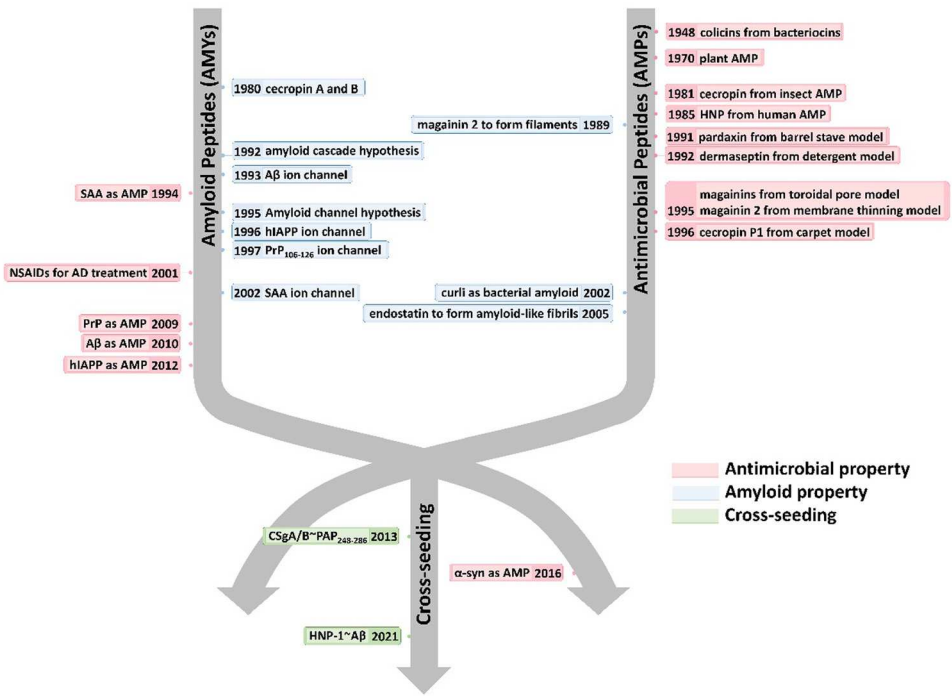

Fig. 1 Historical timeline for discovering the native and alternative functions and cross-seeding of antimicrobial peptides (AMPs) and amyloid peptides (AMYs).

through bidirectional and continuous communication between amyloid proteins and gut microbiota.[34,35] Certain amyloid proteins can influence the activity of gut microbiota, while the gut microbiota, in turn, can modulate amyloid aggregation and its associated toxicity. These findings shed light on the potential involvement of the brain-gut-microbiota axis in neurodegenerative mechanisms.[33,36] The intricate interplay between amyloid formation, neuroinflammation, and the gut microbiota represents a complex and dynamic relationship that underlies the pathogenesis of these diseases, underscoring antimicrobial peptides as promising agents to regulate the detrimental functions of both.

Here, we present a historical timeline tracing the discovery of both native and alternative functions, as well as cross-seeding interactions, between AMPs and AMYs (Fig. 1). Overall, we aim to provide a comprehensive overview of the pathological relationship between AMYs and AMPs, with emphasis on their shared structural/functional characteristics, cross-seeding, and the biological roles of AMPs in the pathogenesis of neurodegeneration. Work on the pathological link between AMYs and AMPs is still at its early stage. We hope that our perspective, which outlines current challenges and future direction, will inspire efforts to exploit the potential of antimicrobial peptides in the development of AMP-based drugs in the treatment of neurodegenerative diseases.

2. Pathological links in sequence, structure, and function similarities between antimicrobial peptides and amyloid peptides

2.1. Sequence and structural similarities between AMPs and AMYs

AMYs and AMPs exhibit distinct sequence and structural characteristics related to their intrinsic antimicrobial activity and peptide aggregation property. As reported in antimicrobial peptides database (APD)[37,38] and collection of anti-microbial peptides (CAMP)[39] database, AMPs contain over 2400 sequences,[40] while AMYs have a much smaller sequence pool, comprising approximately 30 sequences associated with 25 different neurodegenerative diseases. Typically, AMYs demonstrate amphiphilicity with a high hydrophobic residue content,[4] while AMPs of typically 10–40 amino acids long are rich in cationic residues (lysine and arginine) and hydrophobic residues (leucine, valine, and isoleucine) to counterbalance positive charges.[41] A notable commonality between the two peptide classes is the prevalence of hydrophobic residues, crucial for membrane insertion and stabilization through preferential hydrophobic interactions with lipid membranes.[42–44] Both AMYs and AMPs frequently demonstrate a pronounced preference for hydrophobic residues such as Ile, Val, and aromatic amino acids.[40,45] Sequence analysis from AMP databases reveals that the average hydrophobic content of AMPs is 42%. Within this content, Leu, Ala, Cys, Ile, Val, and Phe are frequently occurring residues in AMP sequences, while Met is rarely observed in AMPs ($<1.2\%$).[46] Differently, all AMYs inherently possess the capability to form β-structure-rich aggregates, suggesting that AMY sequences may exhibit a higher tendency for aggregation compared to other peptides. Computational analysis, exploring the aggregation propensity of both amyloidogenic and non-amyloidogenic sequences,[47–49] along with experimental investigations,[50] reveals that amino acids such as Val, Trp, Phe, Cys, Tyr, Ser, and Ile are more favorable for amyloid formation, while charged residues like Asp, Lys, Glu, and Arg are less favored. Aligned with the hydrophobicity indexes of amino acids, these residues play a dual role: strengthening the association force in peptide-cell membrane interactions and providing more robust stabilization of the peptide aggregates. The distinct hydrophobic residue composition among different AMYs and AMPs contributes to the diversity in their structures and functions, which is underscored by the linkage of the hydrophobicity to their hemolytic potential.

While positive charge serves as a distinguishing feature between AMPs and AMYs, however both classes demonstrate stronger interactions with anionic lipid membranes compared to neutral zwitterionic lipid membranes. The prevalence of positively charged residues in AMPs with average net charge of +3.2e promotes selectivity, facilitating the initiation of contacts and the adoption of a surface position on anionic membranes. Typical Arg-rich AMPs (*e.g.*, apidaecin, buforin II, indolicidin) can spontaneously translocate into bacterial cells without membrane perturbationn.[51–54] Upon translocation, these Arg-rich AMPs interact with DNA, RNA, ribosomes, and other intracellular components *via* electrostatic interactions, ultimately leading to cell death. However, the presence of positively charged residues like Arg and Lys appears to discourage their occurrence in amyloid sequences. This may be attributed to electrostatic repulsion, as charge–charge stacking disfavors the self-aggregation of AMYs. On the other hand, the prevalence of negatively charged residues in AMYs enables complex formation with cations, facilitating the transport of cations across the membrane.

The amphiphilic nature of AMPs achieves a balance between polar and nonpolar components, notably featuring a lower prevalence of Gln and Asn in AMPs. Cys is notably abundant ($>14\%$) in β-hairpin AMPs, underscoring the prevalence of disulfide bonds as common structural motifs essential for maintaining a stable amphipathic structure.[40] In contrast, although strong hydrophobicity plays a crucial role in AMY aggregation, the mere bias toward hydrophobicity does not provide a sound explanation for amyloid structures and aggregation. Polar residues are equally essential to facilitate the formation of specific β-sheet organizations. Given that typical, parallel β-sheets in amyloid fibrils are predominantly stabilized by interchain hydrogen bonds between β-sheets, Gln and Asn are highly favored in AMYs. These residues contribute to the formation of a ladder structure crucial for stabilizing amyloid fibrils when Gln/Asn harboring peptides adopt an in-register, parallel β-sheet arrangement, as evidenced by GNNQQNY.

While proline tends to discourage the β-structure in amyloid sequences, it does not exhibit a distinct preference in AMP sequences.

Overall, an amphipathic characteristic is a common sequence feature shared between AMPs and AMYs, although specific attributes may vary to achieve their unique structures and distinct native functions. AMPs commonly exhibit amphipathic structures with an abundance of hydrophobic and cationic residues but fewer polar residues. Key contributors to the positive charge, necessary for membrane interaction, are Arg and Lys, while cysteine residues may form disulfide bonds, enhancing stability. This amphipathicity enables selective interaction with microbial membranes. AMYs feature a propensity for hydrophobic amino acids, presence of aromatic residues, glycine-rich segments for flexibility, and occurrence of charged residues, and these sequence elements contribute to the adoption of β-structure-rich structure in their aggregates. The presence of various residue types contributes to peptide–membrane interactions in distinct ways. Charged residues are known for initiating contacts and membrane adsorption through electrostatic interactions, hydrophobic residues increase the likelihood of the adsorbed peptides to partition into the hydrophobic interior of the membranes, and polar residues achieve their functions by forming hydrogen bonding networks with lipid polar groups and adjusting secondary structures for membrane interactions. Moreover, charged and polar residues play a vital role in determining the correct orientation for peptide adsorption on and insertion into the membrane, with specific tilt angles.[55] A strong correlation in Fig. 2 is evident for 80% of the amino acid residues found in both antimicrobial and amyloid-like regions. The probability of an individual residue being situated in either aggregation-prone or antimicrobial domains is well correlated, with the notable exception of positively charged residues that favors in antimicrobial region, but not aggregation-prone region.[56] Illustratively, AMYs arrange hydrophobic, hydrophilic, and charged residues sequentially, as seen in patterns like CCCHHHPPPPPPPPPPPPPC, while AMPs adopt an alternative sequence, exemplified by PHCPHCPHCPHCPHCPHC (*e.g.*, VKRWKKWRWKWKKWV).[57] Statistical analysis of compositional preferences in naturally occurring AMPs and AMYs may identify specific sequence fragments for membrane binding, transmembrane insertion, and structural transition, which could serve as the basis for engineering specific sequences for AMPs and AMYs, thereby endowing them with new alternative functions.

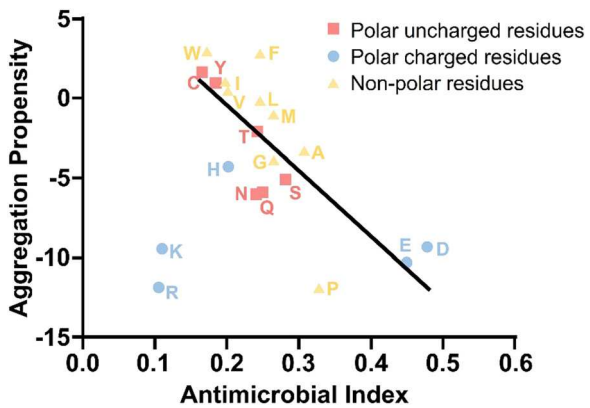

Fig. 2 Functional residue propensity in both amyloid and antimicrobial sequence regions of antimicrobial peptides (AMPs) and amyloid peptides (AMYs). Reproduced with permission from ref. 56.

Structurally, AMPs display four distinctive conformations—α-helical, β-sheet, extended, and disordered states, predominantly determined by solution NMR and X-ray methods. Among these, helical- and β-related structures are the most populated conformations. In many instances, AMPs exhibit distinct structures in solution compared to when they interact with membranes. Upon exposure to cell membranes, they undergo structural transitions or peptide aggregation to facilitate membrane adsorption or insertion. In contrast, AMYs lack defined structures in their native states, however, under pathological conditions, AMYs consistently adopt an in-register, β-sheet organization in their fibrillar aggregates, demonstrating a remarkable independence from both their individual sequences and the cellular environment. Commonly, fibrillar amyloid aggregates exhibit several structural motifs, including (i) the self-complementing polar or non-polar van der Waals (VDW) zippers between (anti)parallel sheets in sequences like GNNQQNY,[58,59] Aβ,[60,61] hIAPP[62] and (ii) chemically-identical amino acid ladders such as Asn and Gln, and π–π stacking.[63] These motifs provide structure-based forces to stabilize β-sheet conformations. Different from AMYs, the presence of cell membranes appears to accelerate amyloid formation, impacting the kinetics of β-sheet structures rather than their thermodynamics. β-structure motifs are present in both AMPs and AMYs (Fig. 3). In AMPs they are often stabilized by disulfide bridges between conserved Cys residues (*e.g.*, protegrin I, tachyplesin, human β-defensin, gomesin)[42,64–66] (Fig. 3a), while those of AMYs (*e.g.*, hIAPP, Aβ, PrP,) are typically stabilized by salt bridges[60,62] (Fig. 3b). Deletion of disulfide bonds in AMPs (*e.g.*, PG-1, α-defensins) leads to loss of β-hairpin and membrane-activated antimicrobial activity,[67–69] emphasizing the essential role of disulfide bonds in the structure and function of AMPs. AMPs without disulfide bonds, including ll37,[70] melittin,[71] magainin,[72,73] cecropin A,[74,75] and dermaseptins,[76] initially adopt a random coil in solution and undergo a random-coil-to-helix transition upon interaction with the membrane. The lengths of these β-sheets typically span the membrane bilayer thickness, in which mismatches between the hydrophobic regions of the β-strands and the lipids significantly influence the peptides lateral and orientational movements within the membranes.

2.2. Common membrane disruption mechanisms of AMPs and AMYs

Antimicrobial peptides (AMPs) and amyloidogenic peptides (AMYs) disrupt cell membranes through both receptor-mediated and nonreceptor-mediated mechanisms. Receptor-mediated mechanisms involve the recognition of target cells

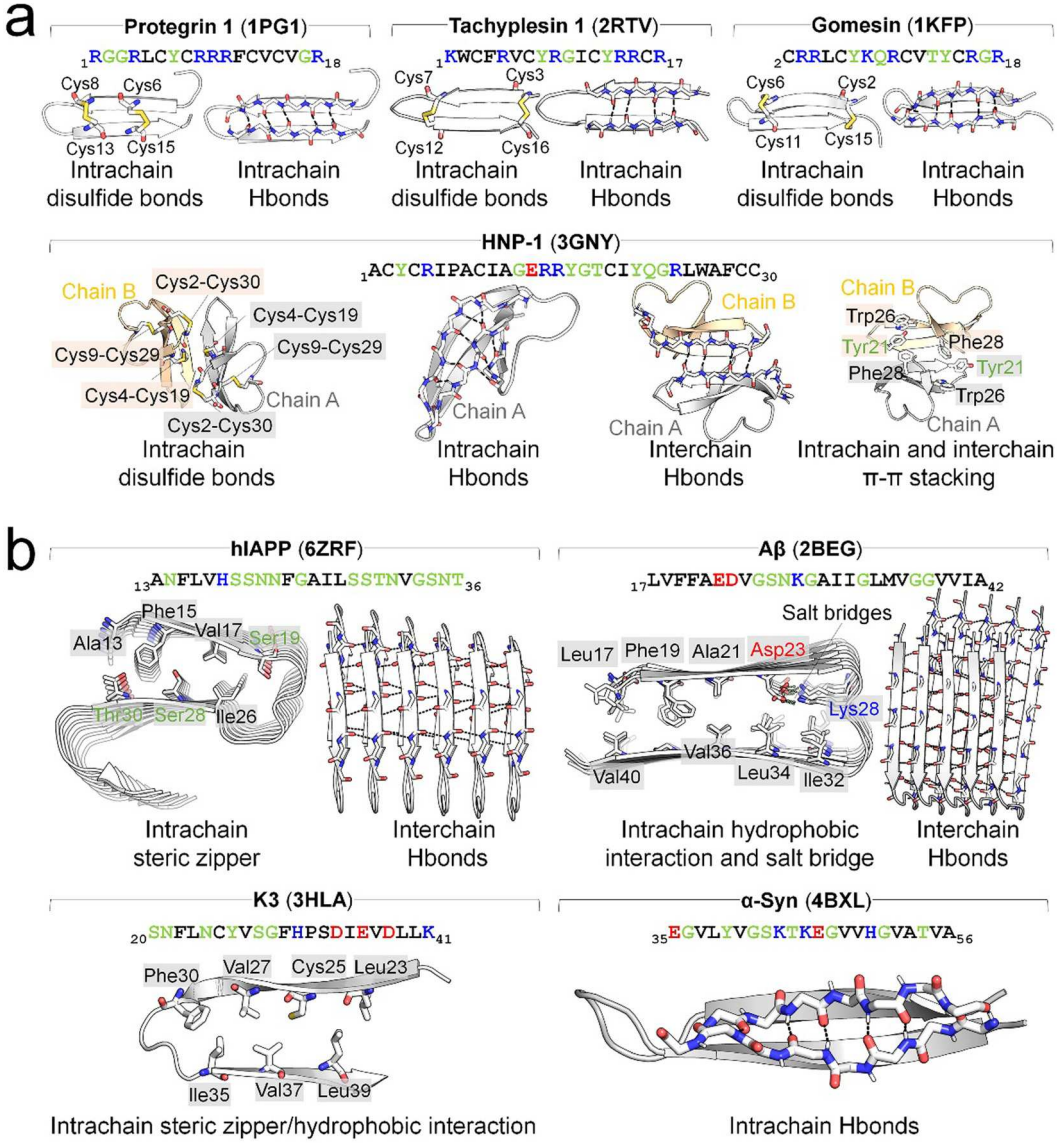

Fig. 3 Overview of typical β-hairpin structure of (a) AMPs of protegrin 1 (PDB: 1PG1), tachyplesin 1 (PDB: 2RTV), gomesin (1KFP), and human β-defensin (HNP-1, PDB: 3GNY) and (b) AMYs of hIAPP (PDB: 6ZRF), Aβ (PDB: 2BEG), K3 of β2-microtubulin (PDB: 3HLA), and α-Syn (PDB: 4BXL). The β-hairpin structures are stabilized by different interactions, specifically, with disulfide bonds between Cys residues in AMPs, and steric zippers (*e.g.*, hIAPP and K3), hydrophobic interactions (*e.g.*, Aβ and K3), and salt bridges between positive and negative residues (*e.g.*, Aβ) in AMYs. Intrachain backbone-backbone hydrogen bonds (H-bonds) are prevalent and crucial for stabilizing the β-hairpin structures of AMPs and are also observed in some AMYs, such as α-Syn. For dimerization or oligomerization of both AMPs and AMYs, interchain backbone-backbone H-bonds serve as the primary interactions. Additional interactions, though sporadic, contribute to maintaining β-hairpin structures. Examples include intrachain and interchain π–π stacking observed in HNP-1. H-bonds and salt bridges are denoted by black and lime dashes, respectively. The text of positively charged, negatively charged, hydrophobic, and hydrophilic residues are drafted in blue, red, black, and green, respectively.

via specific receptors such as sugars, lipids, or proteins, leading to cellular responses including cell necrosis and apoptosis through varied cellular processes.[35,77,78] However, this review primarily addresses nonreceptor-mediated mechanisms, focusing on direct interactions of these peptides with the membrane that lead to increased membrane permeability through various modes (barrel-stave, toroidal-pore, carpet, and detergent models).[79] Such direct membrane interaction process can be generalized into three sequential steps: initial membrane adsorption, deeper peptide insertion, and reorganization within the membrane (Fig. 4a). Although this model simplifies the dynamics, it underscores the critical factors influencing these interactions, including intrinsic physicochemical properties of peptides (size, sequence, secondary structure, net charge, charge distribution, hydrophobicity, and amphiphilic character), dynamic properties of peptides (aggregation, adsorption, orientation, and insertion), characteristics of cell membranes (composition, headgroup size, surface charge, hydrogen bonding capacity, and bilayer elastic properties), and environmental conditions (peptide concentration,

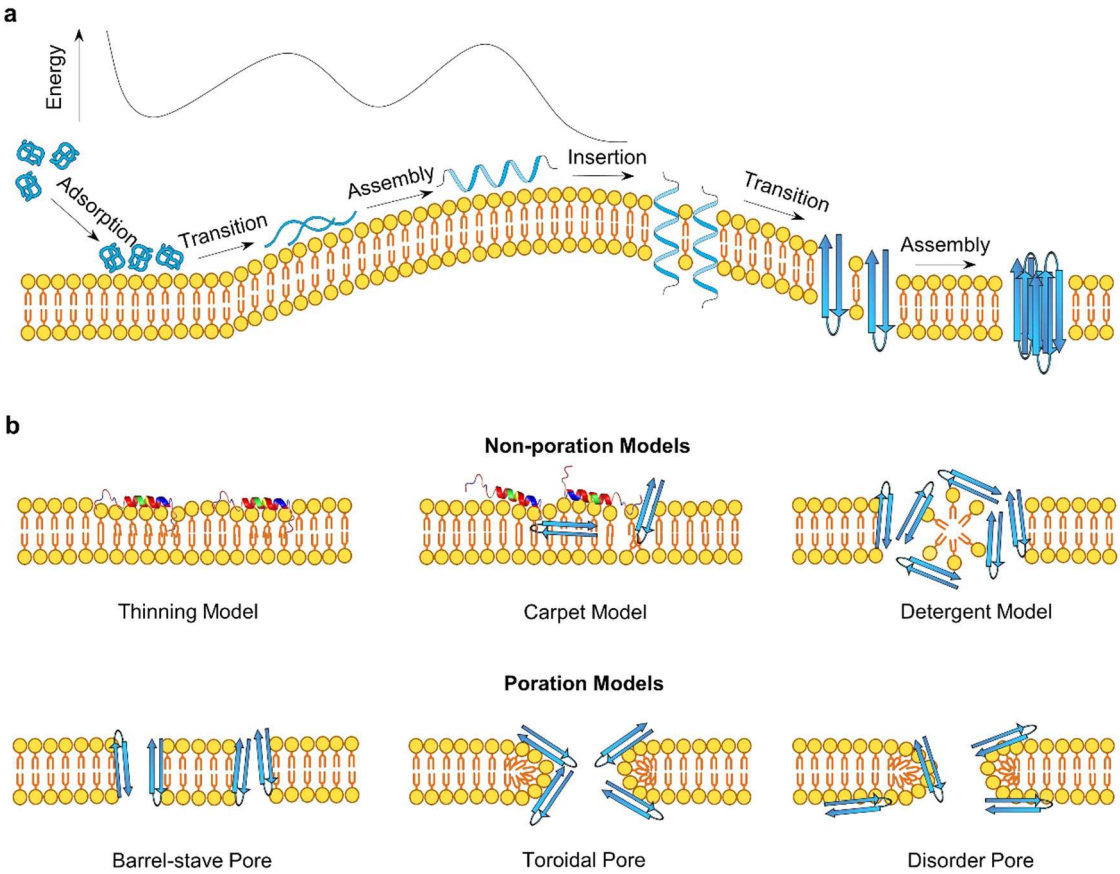

Fig. 4 (a) A general peptide–membrane interaction process in a free energy landscape. It involves initial peptide adsorption, structural transition, self-assembly, insertion pathways, (b) illustrating distinct non-poration (carpet model, detergent model, and membrane thinning model) and poration (barrel-stave pore, toroidal pore, disorder pore) membrane disruption mechanisms of AMPs and AMYs.

temperature, ionic strength, pH).[80,81] Membrane disruption by AMPs and AMYs occurs through two broad mechanisms:[82] non-poration and poration (Fig. 4b). Non-poration does not involve crossing the membrane but can disrupt its integrity. For instance, in the carpet model, peptides disrupt the membrane without forming pores, extracting lipids to create micelles and causing local, transient defects. This mechanism is employed by peptides such as cecropin and melittin, which align parallel to the membrane, disrupting lipid organization and inducing thinning. In contrast, poration involves forming transmembrane pores or channels, typically occurring when peptides insert into the membrane and oligomerize to create structures that facilitate the passage of ions and molecules. The barrel-stave and toroidal models are common scenarios, where monomeric peptides either insert and subsequently form pores, or peptide oligomers directly insert to create pores.

In these non-poration, membrane-disruption events (Fig. 4b), AMP and AMY peptides could function as ''detergents''[83,84] extracting specific lipids from membranes to form peptide/lipid micelles, anchoring themselves in the polar headgroup region to cause lateral membrane expansion and thinning, or triggering lipids clustering and segregation and subsequent lipid phase transitions.[68,69,73,85,86] In the carpet or detergent models, both AMYs and AMPs align parallel to the membrane, with the hydrophilic side of the peptide facing the headgroups through electrostatic interactions, while the hydrophobic portion faces the lipid tails through hydrophobic interactions. These mechanisms have been reported for AMPs such as cecropin,[83] buforin 2,[87] aurein 1.2,[88] Citropin,[88] and melittin[89] to achieve their antimicrobial activity at high peptide densities or peptide-to-lipid ratios, as well as for AMYs like Aβ,[90] hIAPP,[91] α-syn,[92] and PrP[93] to induce cell toxicity and neurodegeneration. Additional evidence for the non-poration models comes from the observation that certain peptides are too short to span the membrane and form a pore. Examples include Mastoparan (14 residues),[94] KLLKLLLKLLLKLLK (15 residues),[95] $(\text{Aib-Lys-Aib-Ala})_{n=1-5}$.[96] These non-poration membrane destabilization events typically involve the membrane interactions of monomeric AMPs or AMYs, resulting in the creation of permeation and leakage pathways that facilitate the crossing of small molecules and ions through lipid bilayers.[97]

Distinct from non-poration actions, AMPs (*e.g.*, PG-1) and AMYs (*e.g.*, Aβ, hIAPP) can form trans-membrane pores or ion channels, generally through two main processes depending on peptide-to-lipid ratios.[98–101] The first process involves monomeric peptides initially inserting into the membrane, followed by reorganization to create pores. In the second scenario,

peptide oligomers directly insert and immediately form pores. Both scenarios require peptide oligomerization, occurring after and before membrane insertion, respectively. Essential to this process is the precise assembly of a specific number of peptides, achieving optimal hydrophobic alignment with lipid chains and reducing exposed hydrophobic and charged residues, crucial for functional transmembrane pore formation. Two primary pore topologies, ''barrel-stave'' and ''toroidal'', derived from α-helices AMPs, are central to understanding peptide-induced pore formation. In barrel-stave pores, peptide chains align vertically and parallel to the membrane lipids, creating stability through hydrophobic interactions. Examples include AMPs such as alamethicin, ceratotoxins, and distinctin,[55,102–104] and AMYs such as Aβ, hIAPP, and α-syn.[105–107] In contrast, toroidal pores form when peptides bind to lipid headgroups, inducing a positive curvature that results in a torus-shaped opening, with peptides arranged circularly. Peptides known to form toroidal pores include magainins,[73] mastoparan-X,[48,49] viroporin, and PG-1[42] among AMPs, as well as Aβ,[108,109] PrP(106–126),[110] and hIAPP[111] among AMYs.

Visualizing is comprehending. While AMP transmembrane pores are directly characterized by X-ray and NMR, amyloid pores – formed by Aβ,[112–115] hIAPP,[116,117] α-synuclein,[118] and serum amyloid A,[116,119,120] and K3 peptides derived from β_2-microglobulin,[114,121,122] ABri, and ADan – are typically analyzed using fluorescence leakage tests in giant vesicles, ionic conductance, confocal microscopy, electrophysiology, cell calcium imaging, and molecular dynamics (MD) simulations. Direct observation of these amyloid pores remains challenging due to difficulties in isolating pure amyloid oligomers for crystallization. Often, their existence is inferred from activities, such as channel conductance, calcium imaging, neuritic degeneration, mitochondrial damage.[81] Alternatively, AFM/SEM images and molecular modeling enables the reconstruction of amyloid pores at low-to-medium resolutions (Fig. 5), showing structural similarities with AMP pores. Both amyloid and AMP pores are characterized by donut-shaped supramolecular arrangements of loosely connected oligomeric aggregates with β-sheet structures,[113,123,124] reminiscent of pore-forming bacterial toxins. Despite variations in pore conformations, types, and subunit interactions with bilayers, these irregularly shaped and dynamic pores, with typical inner diameters of 1–3 nm and outer diameters of 6–10 nm,[125] maintain an open state, allowing the uncontrolled passage of ions and molecules without specific ion selectivity. Unlike traditional gated ion channels, these non-gated ion pores lack mechanisms to regulate their opening and closure, indicating a fundamental difference in their functional properties.

Computational models, utilizing NMR-resolved β-strand-turn-β-strand amyloid monomers, have been employed to reconstruct diverse oligomeric pore structures in amyloids like Aβ, hIAPP, serum amyloid A, β_2-microtublin.[60,142–144] These computational pores feature varied peptide counts (12 to 36 monomers), pore sizes (inner diameters of 2–4 nm and outer diameters of 7–12 nm), and topologies interacting with lipid bilayers.[117] The U-shaped structures of these amyloid pores, consisting of multiple, loosely connected, mobile subunits, are consistent with AFM images and reveal dynamic behaviors,[116] such as multiple conductance, weak cation selectivity, and voltage independence, and responses to inhibitors such as Congo red and zinc.[119,122,145,146] Importantly, computationally constructed pores do not consistently maintain a stable, open pore-like structure, instead factors like lateral bilayer pressure, hydrophobic interactions, and thermal instability can destabilize these pores, leading to pore collapse and reflecting the complex role of amyloid pores in various disorders.

Taken together, AMPs and AMYs, despite their sequence and structural diversity, share common features such as a well-defined β-structure and a hydrophobic, amphipathic region. These attributes support their biological functions, with AMYs displaying antimicrobial activities and AMPs showing self-aggregation properties. Crucially, peptide oligomerization initiates and promotes interactions that lead to the formation of transmembrane pores and curved membranes, both capable of disrupting normal membrane permeability. This oligomerization not only transforms nonamyloidogenic peptides into pathogenic variants,[147] but also enhances the antimicrobial efficacy of AMP monomers,[77] highlighting its essential role in regulating membrane permeability. Moreover, the mechanisms of membrane disruption by AMPs and AMYs are multifaceted, involving various actions like transmembrane pore formation and membrane fusion. These processes are part of a broader phenomenon seen in diverse peptides, including cell-penetrating peptides, pore-forming toxins, glycopeptides, and lipopeptides. Such membrane-activating peptides play crucial roles across biological domains, not only enabling viruses and bacteria to attack host cells but also serving as a defense mechanism in both invertebrates and vertebrates through membrane-disruption strategies.

2.3. Pathological links between antimicrobial peptides and amyloid peptides

The pathological link between antimicrobial peptides (AMPs) and amyloid peptides (AMYs) can be traced back to their common association with microbial contexts. Mechanistically, in addition to the well-established role of amyloid aggregation, microbial infection has emerged as a significant contributor to the pathogenesis of neurodegenerative diseases.[4,35] The ''amyloid aggregation hypothesis'' posits that the formation of toxic amyloid aggregates with β-rich structures is a requirement for the progression of neurodegenerative diseases, leading to cellular degeneration and eventual cell death.[4] Conversely, the ''microbial infection hypothesis'' suggests that neuroinflammation induced by bacteria, viruses, and fungi contributes to the pathology of neurodegenerative diseases through a persistent immune response.[32,33] While these two hypotheses propose distinct mechanisms for neurodegenerative diseases, emerging evidence from experimental and clinical studies has unveiled an intricate relationship between amyloid formation and microbial infection. Bidirectional and continuous communication between amyloid proteins and the gut microbiota (particularly bacterial amyloids) has emerged as a

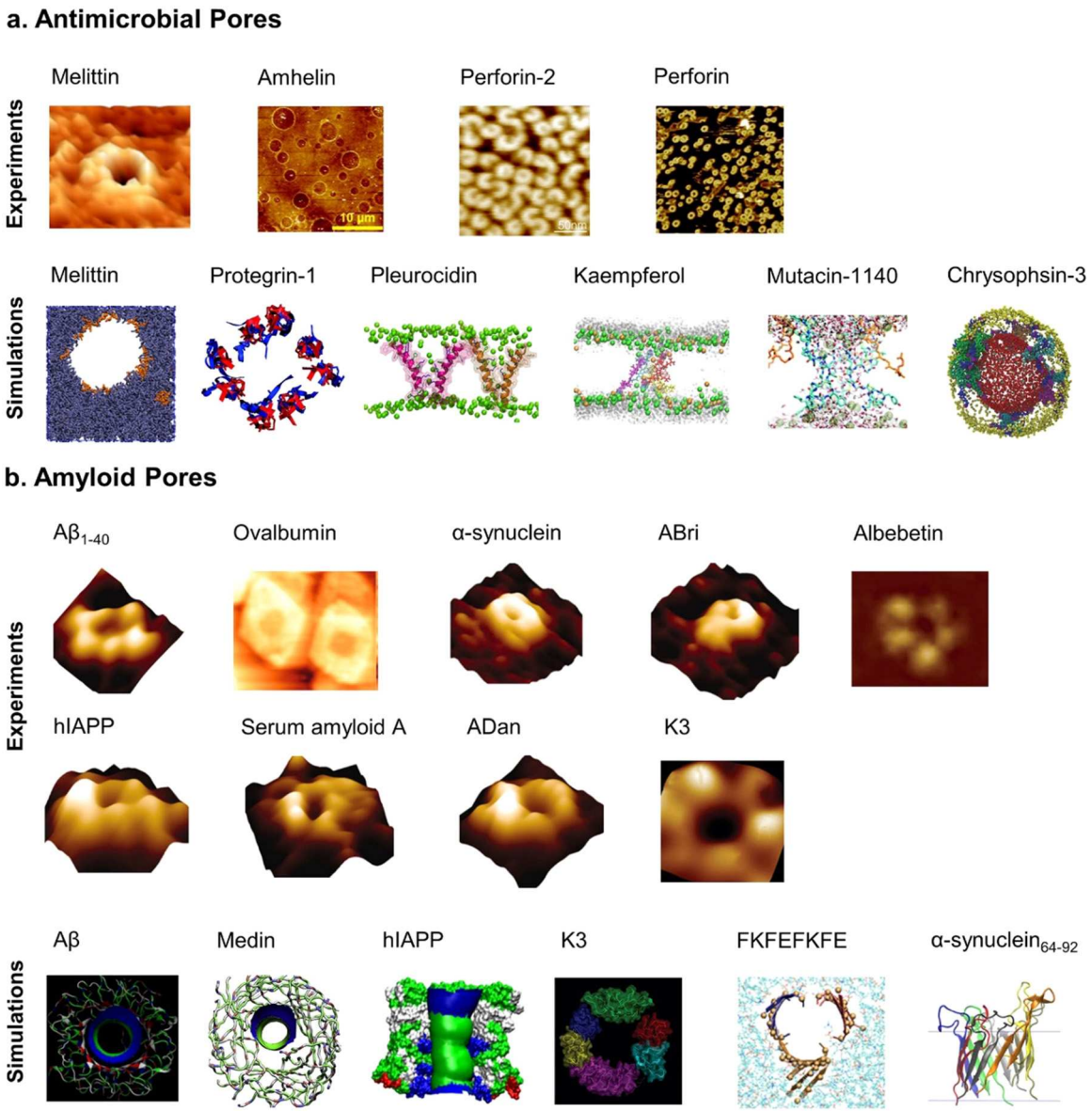

Fig. 5 Comparative characterizations of (a) antimicrobial pores formed by melittin (Reproduced with permission from ref. 126 Copyright © 2015 American Chemical Society), amhelin (Reproduced with permission from ref. 127 Copyright 2013 National Academy of Science), perforin-2 (Reproduced with permission from ref. 128 Copyright © 2022 The Author(s)), perforin (Reproduced with permission from ref. 129 Copyright © 2021 The Royal of Chemistry) by AFM images (upper panel) and melittin (Reproduced with permission from ref. 130 Copyright © 2015 American Chemical Society), protegrin-1 (Reproduced with permission from ref. 131 Copyright © 2008 American Chemical Society), pleurocidin (Reproduced with permission from ref. 132 Copyright © 2021 American Chemical Society), kaempferol (Reproduced with permission from ref. 133 Copyright © 2022 American Chemical Society), mutacin 1140 (Reproduced with permission from ref. 134 Copyright © 2019 the Owner Societies), chrysophsin-3 (Reproduced with permission from ref. 135 Copyright © 2018 The Royal of Chemistry) by molecular simulations (lower panel); (b) amyloid pores formed by $A\beta_{1-40}$ (Reproduced with permission from ref. 116 Copyright © 2005 National Academy of Sciences, U.S.A.), ovalbumin (Reproduced with permission from ref. 136 Copyright © 2013 American Chemical Society), α-synuclein,[116] ABri,[116] albebetin (Reproduced with permission from ref. 137 Copyright © 2004 American Chemical Society), hIAPP,[116] serum amyloid A,[116] ADan,[116] K3 (Reproduced with permission from ref. 121 2009 American Chemical Society) by AFM images (upper panel) and Aβ (Reproduced with permission from ref. 138 Copyright © 2013 American Chemical Society), Medin (Reproduced with permission from ref. 139 Copyright © 2020 Biophysical Society), hIAPP (Reproduced with permission from ref. 106 Copyright © 2012 Elsevier B.V.) K3,[121] FKFEFKFE (Reproduced with permission from ref. 140 Copyright © 2022 American Chemical Society), α-synuclein$_{64-92}$ (Reproduced with permission from ref. 141 Copyright © 2023 American Chemical Society) by molecular simulations (lower panel).

critical factor in the pathogenic connection between these two phenomena.[34,35] This suggests a molecular crosstalk between the amyloid aggregation hypothesis and the microbial infection hypothesis.

Interestingly, recent research has uncovered the convergence of certain features between AMYs and AMPs, adding another layer of complexity to their interplay. Some AMYs, typically associated with disease pathology, exhibit

antimicrobial activity, while certain AMPs, known for their role in host defense, display amyloidogenic potentials. The dual functionality of some AMYs and AMPs provides new evidence for manipulating their sequences, structures, and activities to develop therapeutic intervention strategies for combating both microbial infections and neurodegenerative disorders. The discovery of dual functionality in certain AMYs and AMPs presents compelling evidence for the potential manipulation of these attributes as a basis for developing therapeutic intervention strategies combating both microbial infections and neurodegenerative disorders.

Several AMPs, including phenol-soluble modulin,[148] plantaricin A,[9] longipin,[149] melittin,[150] dermaseptin S9,[76] magainin 2,[12] temporins,[151] aurein,[152,153] uperin,[10,154] LL-37,[155] protegrin-1,[156] defensins,[23,24] and AMC-K9 conjugate,[157] have been observed to exhibit self-assembly into amyloid-like fibrils with β-rich structures, either in buffer solutions or on lipid membranes. These self-assembled AMP fibrils bear similarity to pathological amyloid fibrils associated with human disease. The identification of AMPs as capable of forming amyloid-like structures highlights an intriguing aspect of their biological activity beyond their well-known antimicrobial properties. The resemblance between these self-assembled AMP fibrils and disease-related amyloid fibrils raises important questions regarding their functional implications and the underlying mechanisms governing their assembly. Considering that AMPs are implicated in the pathogenesis of neurodegenerative diseases associated with ''microbial infection hypothesis'', further investigations focusing on cross-seeding interactions between these AMPs and different amyloid proteins may lead to the identification of dual-functional, multiple-target inhibitors. Such AMP inhibitors would have the potential to simultaneously impede pathology-associated amyloid aggregation and microbial infection pathways.

In parallel, recent studies have challenged the conventional perception of AMYs as exclusively pathogenic and useless substances. Instead, emerging evidence reveals the diverse biological functions of AMYs, encompassing their beneficial roles as reservoirs for certain polypeptide hormones storage,[158] participation in cell adhesion,[159] contribution to the development of functionalized biomaterials and nanomaterials,[160,161] and demonstration of antibacterial activity.[7,162] Unlike some AMPs that possess amyloidogenic properties, AMYs are increasingly recognized as ancient and highly conserved innate immune effectors involved in the prevention of microbial infections. Since the initial discovery in 2002 that serum amyloid A (SAA) can cause significant damage to various bacteria cells through the formation of voltage-independent and poorly selective ion channels,[119] numerous other AMYs have been found to possess antimicrobial activity against common bacteria and fungi, including PrP_{23-231} and its truncated variants,[163] Aβ,[17] hIAPP,[18] hCT,[23,24] α-syn,[15] and SAA.[164] In some cases, the antimicrobial potency of these AMYs is equivalent to or even greater than that of LL-37 antimicrobial peptide. These findings provide compelling evidence that AMYs exert their antimicrobial and cytotoxic activities through a shared mechanism involving the formation of ion-permeable channels in the cell membranes of pathogens. Also, these findings not only expand our understanding of the biological roles of AMYs in relation to the ''microbial infection hypothesis'', but also challenge the simplistic notion that they are solely deleterious, as commonly associated with the ''amyloid aggregation hypothesis.''

Emerging but limited studies have revealed the occurrence of cross-seeding between bacterial amyloids and AMYs, as well as between AMPs and AMYs. This is likely due to the presence of these peptides in the blood circulation and cerebrospinal fluid, which raises the possibility of their co-aggregation or cross-seeding with other amyloidogenic proteins.[165–167] The former cross-seeding between bacterial amyloids and AMYs seems to establish a pathogenic link, possibly creating a loop that contributes to disease propagation from microbial/virus infection to amyloid pathogenies through the brain-gut-microbiota.[33–35] Unlike the cross-seeding between bacterial amyloids and AMYs, the cross-seeding observed in certain AMPs-AMYs pair systems, such as human β-defensin and Aβ/hIAPP/hCT,[23] human α-defensin and Aβ/hIAPP/hCT,[23] LL-37 and Aβ/hIAPP,[25,26] α-syn and CsgA/CsgC/CsgE,[27–29] presents a more intricate scenario. This cross-seeding enables AMPs to modulate the aggregation and misfolding of different AMYs. However, the changes in amyloid aggregation induced by AMPs do not necessarily lead to a reduction in amyloid-induced cell toxicity and the preservation of AMPs's antimicrobial activity, presumably due to the formation of AMP-AMY complexes and alterations in the distribution of AMY aggregates. On a positive note, recent studies have identified specific AMPs as dual-functional, multiple-target inhibitors capable of simultaneously blocking amyloid aggregation and microbial infection pathways. These AMPs show the potential to interrupt the interlinked pathological processes and bidirectional communication between amyloid aggregation and microbial infection. This discovery introduces an innovative approach to explore and repurpose a diverse range of antimicrobial peptides that inherently possess both bacterial-killing and amyloid inhibition functions, so as to effectively reconcile the ''amyloid cascade hypothesis'' and the ''microbial infection hypothesis''. Additionally, the occurrence of amyloid cross-seeding, where various disease-related amyloid proteins form structurally similar amyloid fibrils, has been frequently observed.[30,31,168] This phenomenon poses an additional risk factor for the initiation and progression of other neurodegenerative diseases. Surprisingly, seemingly unrelated amyloid proteins can trigger pathological events in different neurodegenerative diseases through amyloid cross-seeding. This further complicates the understanding of the amyloid aggregation hypothesis and its association with microbial infection.[36]

The COVID-19 pandemic has prompted researchers to investigate a potential connection between SARS-CoV-2 infection and amyloidosis. Preliminary studies have reported some interesting findings. It has been observed that the spike protein (S-protein) of the SARS-CoV-2 virus contains aggregation-prone heparin-binding sequences, and this characteristic enables the

S-protein to aggregate into amyloid-like fibrils at a faster rate compared to Aβ and α-synuclein.[169] In another study, S-protein does not affect α-synuclein aggregation, while the SARS-CoV-2 nucleocapsid protein (N-protein) significantly accelerates the aggregation process.[170] Additionally, molecular dynamics simulations have indicated that the SK9 fragment from the E-protein of SARS-CoV-2 promotes the formation of amyloid structures in serum amyloid A.[171] These findings highlight the potential involvement of SARS-CoV-2 viral proteins in amyloid formation but require further investigation to explore the cross-seeding interactions between specific SARS-CoV-2 proteins (*e.g.*, S-protein, N-protein, E-protein) and different amyloid peptides (*e.g.*, Aβ, α-synuclein, tau, and prions), as well as reveal the potential impact of these interactions on disease pathology.

These findings highlight the intricate and multifaceted nature of the pathological links between antimicrobial peptides and amyloid peptides. The bidirectional communication between amyloid proteins and the gut microbiota, coupled with the phenomenon of amyloid cross-seeding, provides new insights into the complex interplay between amyloid formation and microbial infection in the development and progression of neurodegenerative diseases. Further exploration of these pathological links holds promise for advancing our understanding of neurodegenerative diseases and may open avenues for the development of novel therapeutic strategies targeting both amyloid aggregation and microbial infection.

3. Amyloid property of antimicrobial peptides

Antimicrobial peptides (AMPs), also known as host defense peptides (HDPs), are abundant in the brain and other immune-privileged tissues and function as innate defense mechanisms against a variety of microorganisms and pathogens. AMPs, typically comprising 50–100 amino acids, show significant sequence and structural diversity, but mainly fall into two categories based on their secondary structures: α-helical and β-sheet peptides. These peptides disrupt bacterial cell walls, protein and nucleic acid synthesis, enzymatic activities, and membrane integrity, and possess antiviral, antifungal, antitumor, and immunomodulatory properties. The structural and functional similarities between AMPs and amyloids (AMYs) highlight fundamental biological connections, with emerging evidence of amyloidogenic properties in certain AMPs across various organisms, including animals, amphibians, insects, plants, and microbes, suggesting a more universally conserved role for AMPs linked to their amyloid properties.

Mechanistically, the neuroinflammation seen in neurodegenerative diseases[35] is closely linked to microbial infections caused by viruses (such as HSV-1,[172] HIV,[173] HHV-6A[174]), bacteria (such as gut bacteria,[175] liver bacteria *Helicobacter pylori*,[176] *Chlamydia pneumoniae*[177]), fungi (such as *Candida* species, *Cladosporium*, *Cryptococcus*[178]), and SEVI.[179] These infections can compromise the blood–brain barrier (BBB), trigger persistent immune responses, and ultimately contribute to neurodegeneration.[32,33] Bacterial amyloid proteins, found in the gut microbiota, share structural similarities with amyloid proteins in the central nervous system (CNS). Both bacterial and amyloid aggregates are targeted by the immune system, leading to prolonged inflammation[180,181] and activation of microglia,[182] which exacerbate neurodegeneration. Exposure to bacterial amyloids can enhance immune responses against neuronal amyloids, potentially crossing the compromised BBB and disrupting brain function in individuals with infections. Below, Table 1 presents a range of antimicrobial peptides (AMPs), including natural AMPs from various sources and synthetic or engineered AMPs with amyloid-like properties.

3.1. Natural AMPs from mammals

Numerous studies were conducted to unravel the relationship between the self-association of AMPs and membrane disruption. Several models have been proposed, similar to those describing the membrane disruption of AMYs.[83,210,211] The identification of a distorted antiparallel β-sheet structure in bovine lactoferricin B, a 25-residue AMP, suggests a potentially beneficial α-to-β secondary structure transition in antimicrobial activity. This observation implies a resemblance to the pathological amyloid formation (Fig. 6a).[183] Subsequently, several AMPs from various animals have been recognized for their amyloid-like properties.

Cathelicidins, along with defensins, constitute a significant category of cationic AMPs and represent a pivotal component of the immune system in diverse vertebrates, including humans and other animals. This cationic AMP family is featured by a highly conserved N-terminal cathelin domain and a diverse C-terminal antimicrobial domain exhibiting α-helical, β-hairpin, or proline/arginine-rich characteristics. Within the extensive family of over 30 cathelicidin members found in mammals, numerous AMPs have been identified as amyloidogenic peptides. For instance, the 13-residue AMP indolicidin, derived from bovine species, demonstrates the ability to form amyloid-like fibers in the presence of liposomes containing phosphatidylserine (Fig. 6b).[184] The protegrin group of cathelicidin AMPs, isolated from porcine leukocytes, exhibits a distinctive cysteine-rich β-sheet structure.[212] The unique conformation of protegrins, featuring a two-stranded antiparallel β-sheet stabilized by two cysteine bridges with strands connected by a β-turn, suggests potential self-interactions similar to those of AMYs. The amyloidogenic property of protegrins is evident, particularly in the case of PG-1, which exhibits rapid kinetics in forming amyloid fibrils (Fig. 6c).[8] Moreover, LL-37, as the only human cathelicidin, has been extensively studied for its amyloid-like property. LL-37, an α-helical AMP essential in the first line of defense against local infections and systemic pathogen invasions,[213] exhibits initial evidence suggesting that its antimicrobial effects arise from compromising the microbe's membrane barrier through the formation of cytotoxic amyloid-like fibers in the presence of acidic phospholipids.[214] These amyloid-like structures have been studied for their role in immune responses and interactions with host cells. The fibrillation of LL-37 is critical for DNA

Table 1 Summary of different types of AMPs with amyloid-like property

Category	Name	Source	Sub-category	Target microbes			Secondary structure	Amyloid-like fibrils	Other key findings	Ref.
				Anti-Gram (+)	Anti-Gram (−)	Anti-fungal				
Mammal AMPs	Bovine lactoferricin	Bovine	N/A	*Enterococcus sp*, *Staphylococcus sp*	*E. coli*, *P. aeruginosa*, *Shigella Jexneri*	*C. albicans*	Distorted antiparallel β-sheet (2D NMR)	N/A	N/A	183
	Indolicidin	Bovine	Cathelicidin	*S. aureus*	*E. coli*	*Aspergillus fumigatus*	N/A	Yes (Congo red)	Form amyloid-like fibers in the presence of phosphatidylserine containing liposomes	184
	PG-1	Porcine	Cathelicidin	*MRSA*, *vancomycin-resistant Enterococcus*	*E. coli*, *P. aeruginosa*	*C. albicans*	β-hairpin (NMR)	Yes (ThT, AFM)	N/A	8
	LL-37	Human	Cathelicidin	*Enterococcus hirae*, *S. aureus*	*E. coli*, *P. aeruginosa*	*C. albicans*	α-helix (NMR)	Yes (ThT, TEM, Cryo-EM)	Human LL-37 active core (residues 17–29) can form into a protein fibril of densely packed helices	155
	HD-6	Human	Defensin	*B. breve*, *L. acidophilus*, *B. adolescentis*, *B. longum*	*S. Typhimurium*, *Y. enterocolitica*	*C. albicans*	Triple-stranded β-sheet (XRD)	Yes (SEM)	N/A	185
	Eosinophil cationic protein	Human	Ribonuclease A	*S. aureus*	*E. coli*	N/A	α + β folding (XRD)	Yes (Congo red, ThT, TEM)	N/A	186
Amphibian AMPs	Magainin 2	African clawed frog	Magainin	*S. aureus*	*E. coli*, *A. calcoaceticus*, *P. vulgaris*, *H. pylori*	*T. basicola*	α-helix (NMR)	Yes (TEM)	N/A	11
	Dermaseptin S9	South American hylid frog	Dermaseptin	*B. megaterium*, *L. monocytogenes*	*E. coli*, *S. typhimurium*	N/A	β-sheet (CD, FTIR)	Yes (TEM, Congo red)	N/A	13 and 76
	Dermaseptin PD-3-7	South American hylid frog	Dermaseptin	*B. subtilis*	*E. coli*	N/A	Amphipathic α-helix (CD)	Yes (Congo red, ThT, TEM)	Monomeric PD-3-7 displayed no antibiotic action, whereas amorphous aggregates of PD-3-7 release from the amyloid depot mediating a strong cytotoxic effect	187 and 188
	Uperin 3.5	Australian toadlet	Uperin	*M. luteus*, *S. aureus*, *S. hominis*, *S. epidermidis*	N/A	N/A	Cross-α	Yes (ThT, CD, TEM, XRD, cryo-EM)	Antibacterial activity is induced by a chameleon cross-α/cross-β secondary structure switch of uperin 3.5 fibrils	189 and 190
Arthropod AMPs	cupiennin-1	Spider	N/A	*M. luteus*, *S. aureus*	*K. pneumoniae*	*C. parapsilosis*	α-helix/cross-β (XRD)	Yes (TEM)	N/A	190
	Lasioglossin LL-I	Eusocial bee	N/A	*M. luteus*, *S. aureus*, *B. subtilis*	*E. coli*, *P. aeruginosa*	N/A	α-helix/cross-β (XRD)	Yes (TEM)	N/A	190
	Cecropin-C	Mosquitoes	Cecropin	*M. luteus*	*P. carotovorum*	*M. rileyi*	α-helix/cross-β (XRD)	Yes (TEM)	N/A	190
	Melittin	Honeybee	N/A	*S. haemoliticus*	*K. pneumoniae*, *P. aeruginosa*	*Aspergillus*, *Botrytis*, *Candida*, *Colletotrichum*, *Fusarium*, *Malassezia*, *Neurospora*, *Penicillium*, *Saccharomyces*, *Trichoderma*, *Trichophyton*, *Trichosporon.*	α-helix (NMR)	Yes (ThT, Congo red, TEM)	Amyloid-like aggregates formed by melittin in the presence of SDS	150

Table 1 (*continued*)

Category	Name	Source	Sub-category	Target microbes			Secondary structure	Amyloid-like fibrils	Other key findings	Ref.
				Anti-Gram (+)	Anti-Gram (−)	Anti-fungal				
	Longipin	Opiliones	N/A	*M. luteus*	*E. coli*, *S. marcescens*	*Candida*	β-sheet (CD, FTIR)	Yes (ThT)	Fold into β-sheet structure and form into amyloid-like fibril in the presence of a lipid bilayer	149
Microbe AMPs	Microcin B17	Gram (−) *E.coli*	Ribosomally bacteriocins (microcins)	N/A	*E. coli*	N/A	N/A	Yes (TEM)	N/A	191
	Microcin E492	Gram (−) *K. pneumoniae* RYC492	Ribosomally bacteriocins (microcins)	N/A	*Escherichia*, *Klebsiella*, *Salmonella*, *Citrobacter*, *Enterobacter*	N/A	β-sheet (CD)	Yes (Congo red, ThT, TEM)	Loss of toxicity after *in vivo* MccE492 amyloid formation.	192
	Plantaricin A	Gram (+) *L. plantarum* C11	Ribosomally bacteriocins (class IIa)	*S. aureus*, *L. Monocytogenes*, *Bacillus*	*E. coli*, *Salmonella*	N/A	N/A	Yes (phase contrast microscopy)	The formation of amyloid-like fibrils is induced by PS-containing liposomes.	9
	Plantaricin J	Gram (+) *L. plantarum* C11	Ribosomally bacteriocins (class IIb)	*M. luteus*	N/A	N/A	Cross-β (XRD)	Yes (TEM)	N/A	190
	Plantaricin K	Gram (+) *L. plantarum* C11		*M. luteus*	N/A	N/A	Cross-β (XRD)	Yes (ThT, TEM)	N/A	
	cOB1	Gram (+) *E. faecalis*	Sex pheromone	*E. faecalis*	N/A	N/A	β-sheet (CD)	Yes (Congo red, ThT, TEM)	Antibacterial ability of cOB1 is not affected by the formation of cOB1 aggregates	193
	sakacin P	Gram (+) *L. sakei*	Ribosomally bacteriocins (class IIa)	*L. sake*, *L. corynеformis*, *E. faecalis*, *C. piscicola*	N/A	N/A	S shaped antiparallel β-sheet (*in silico*)	N/A	N/A	194
	Gramicidin S	Gram (+) *B. brevis*	Non ribosomally	*A. aureus*, *B. subtilis*	*E. coli*	*C. Albicans*	β-helix (NMR)	N/A	N/A	195
	Tyrocidines	Gram (+) *B. aneurinolyticus*	Non ribosomally	*L. monocytogenes*	N/A	N/A	S shaped antiparallel β-sheet (CD, *in silico*)	N/A	Different dimer models are studied.	196
Plant AMPs	RsAFP-19	Radish seed	Defensin	N/A	N/A	*Candida*, *Aspergillus*, *Fusarium*, *B. cinerea*, *N. crassa*	Cross-β (XRD)	Yes (ThT, TEM, AFM)	loss of the antifungal ability after ''gel-like'' RsAFP-19 fibrils formation.	197
	Cn-AMP2	Cocos nucifera	Defensin	*B. subtilis*, *S. aureus*	*E. coli*, *P. aeruginosa*	N/A	N/A	Yes (Congo red, ThT, TEM)	N/A	198
Synthetic or Engineered AMPs	C16-Gn(IIKK)nI-NH2	N/A	N/A	*S. mutans*	N/A	N/A	β-sheet (CD)	Yes (ThT, CD, AFM, TEM)	β-sheet lipidated AMPs exhibit either comparable or diminished antimicrobial acitivity	199
	FF8	N/A	N/A	N/A	*E. coli*	N/A	β-sheet and β-turn (CD, FTIR)	Yes (AFM)	FF8 remains random coil structure under physiological conditions, but specifically triggered by the negatively charged lipid membrane and self-aggregate into nanofibrils	200
	HPRP-A1 isomers	Gram (+) *H. pylori*	Sequence shuffling	N/A	*E. coli*, *P. aeruginosa*, *K. pneumoniae*	N/A	α-helix, β-sheet, random coil (CD)	N/A	Reduction of antibacterial ability after the formation of HRPR-A1 amyloid aggregates antibacterial efficiency: α-helix > β-sheet > random coil	201

Table 1 (*continued*)

Category	Name	Source	Sub-category	Target microbes			Secondary structure	Amyloid-like fibrils	Other key findings	Ref.
				Anti-Gram (+)	Anti-Gram (−)	Anti-fungal				
	(KIAGKIA)3-NH2	PGLa derivative (α-helix)	Residues substitution	*S. aureus*	*E. coli*, *P aeruginosa*	N/A	β-sheet (CD, FTIR)	N/A	(KIGAKI)3-NH2 is highly selective to bacterial membranes as compared to mammalian membranes	202
	GL13K	Salivary protein BPIFA2 (α-helix)	Residues substitution	*S. aureus*	*E. coli*	N/A	β-sheets (CD, NMR)	No (AFM)	GL13K is highly selective for anionic bacterial model membranes (DOPG) compared to zwitterionic (neutral) eukaryotic model membranes (DOPC).	203 and 204
	Pardaxin diasteromer	Pardaxin fragment (α-helix)	Stereoisomer substitution	*B. subtilis*, *B. megaterium*	*E. coli*, *A. calcoaceticus*	N/A	β-sheet (FTIR)	N/A	The diastereomer retain potent antimicrobial activity, while the hemolytic activity was abolished.	205
	GS14K4	GS14 (β-sheet)	Stereoisomer substitution	*S.epidermidis*, *E. faecalis*, *C. xerosis*	*E. coli*, *P. aeruginosa*, *S.typhimurium*	*C. Albicans*	Non β-sheets (CD, NMR)	N/A	GS14K4 shows high specificity for microbial cells than human cells.	206
	Temporin L analogue	Temporin L (α-helix)	Residues and stereoisomer substitution	*S. aureus*, *S. epidermidis*, *B. megaterium*	*E. coli*, *P. aeruginosa*, *A. baumannii*, *K. pneumoniae*	N/A	β-sheet (CD)	N/A	Temporin L analogue remians unstructured in water, while forms β-aggregates in liposome mimikcing bacterial membranes	207
	(IRIK)2-NH2	N/A	N/A	*S. epidermidis* *S. aureus*	*E. coli* *P. aeruginosa*	*C. Albicans*	β-sheet (CD)	N/A	N/A	208
	(IRVK)3-NH2	N/A	N/A	*S. epidermidis* *S. aureus*	*E. coli* *P. aeruginosa*	*C. Albicans*	β-sheet (CD)	N/A	N/A	208
	FSKRGY	N/A	N/A	*S. aureus*	N/A	N/A	β-sheet (CD)	N/A	N/A	209

binding and affects receptors in the immune system.[215] Further studies have identified an active core of LL-37 (residues 17–29) that mimics the ability of full-length LL-37 to self-assemble into densely packed helices forming a protein fibril (Fig. 6d).[155] Recent studies on LL-37 suggested a potent inhibitory effect on amyloid aggregation,[25,26] suggesting the complex role that AMPs may play in response to external stimuli.

Defensins, characterized as small cysteine-rich cationic proteins, play a central role in the host defense mechanisms of granulocytic leukocytes, mucosal surfaces, skin, and other epithelia. Three defensin subfamilies—α-defensins, β-defensins, and θ-defensins—are expressed in animals. Typically spanning 18–45 amino acids, defensins feature three or four highly conserved disulfide bonds, and their tertiary structures are dominated by turn-linked β-strands, resulting in compact folded structures with favorable self-assembly properties. Human α-defensin 6 (HD-6) showcases a unique innate immune mechanism, wherein it self-assembles into elongated fibrils that effectively entrap bacteria, preventing microbial invasion (Fig. 6e).[185,216] Notably, certain subgroups of defensins, with their unique β-strand-rich conformations, exhibit a potent inhibitory effect on amyloid peptides. This inhibitory effect has been observed in human α-defensin HNP-1, rabbit α-defensin NP-3A,[24] HD-6, and human β-defensin HBD-1.[23] These defensins can cross-seed with three amyloid peptides—Aβ, hIAPP, and hCT—hindering their aggregation into amyloid fibrils from both monomers and oligomers. These findings suggest a therapeutic potential for AMPs in the context of amyloid-related diseases. This raises an intriguing question about the potential bidirectional communication between microbial infection and amyloid formation and opening avenues for further exploration.

Beyond AMPs derived from the innate immune system, certain basic proteins exhibit potent toxicity against microbes and viruses. The eosinophil cationic protein (ECP), located in the eosinophil primary matrix, belongs to the Ribonuclease A superfamily. Apart from its involvement in tissue-remodeling processes, ECP serves as an AMP with a broad spectrum of action against bacteria, and at higher concentrations, displays cytotoxic activity to eukaryotic cells. Recently, the *in vitro* formation of amyloid-like aggregation of ECP has been reported (Fig. 6f). This discovery may offer new insights into the antimicrobial mechanism of the protein involving amyloid formation, and its potential toxicity to host tissues during inflammation processes.[186] The amyloid-like fibril propensity of ECP suggests a connection to the presence of eosinophil infiltration in AD. These findings imply that amyloidosis in mammals could be a more general outcome potentiated by the immunomodulatory and infection control functions of AMPs.

3.2. Natural AMPs from amphibians

In 1989, the first documentation of an AMP with aggregation properties emerged, revealing the spontaneous polymerization of magainin 2.[11] Magainin 2, a 23-residue AMP derived from the skin of the African clawed frog *Xenopus laevis*, possesses the ability to form filaments with a diameter of 13 nm with a

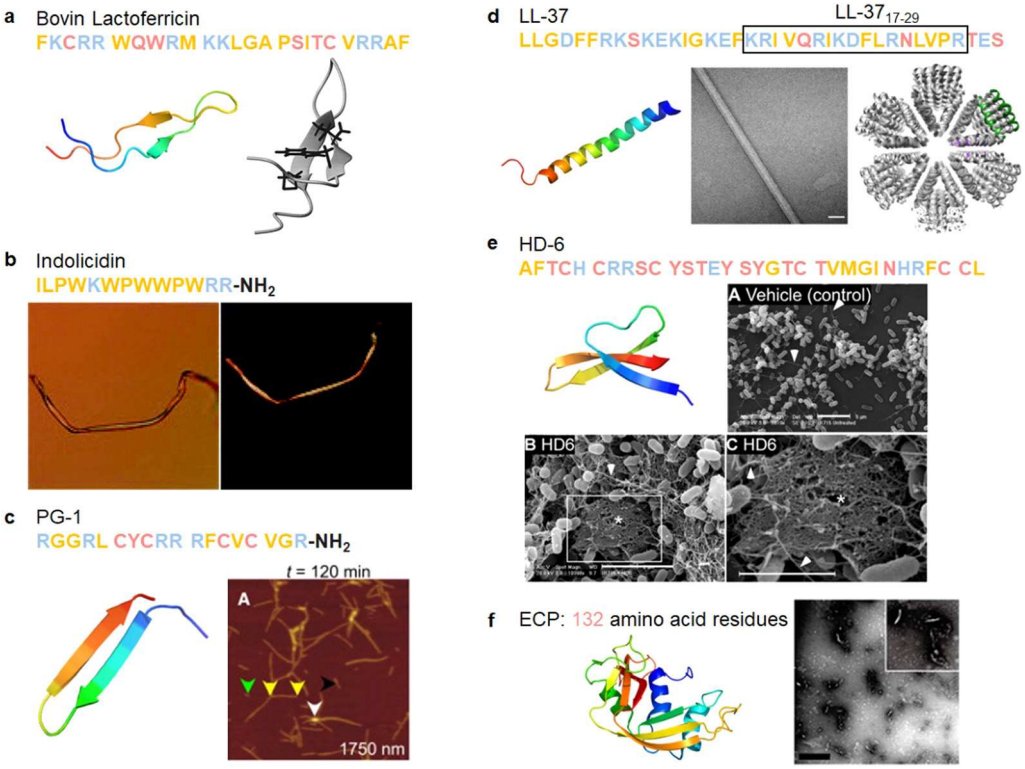

Fig. 6 Illustrations of natural AMPs from mammals with amyloid property. (a) Bovin lactoferricin characterized by a distorted antiparallel β-sheet structure in solution as elucidated by 2D NMR (Reproduced with permission from ref. 183 Copyright © 1998 American Chemical Society.) (PDB: 1LFC). (b) Bovine cathelicidin indolicidin capable of forming amyloid-like fibers induced by acidic phospholipids; a left image displays phase-contrast microscopy, while a right image exhibits a polarizing microscopy after Congo red staining. (Reproduced with permission from ref. 184 Copyright © 2005 American Chemical Society.) (c) Porcine cathelicidin PG-1, featuring a cysteine-rich β-hairpin structure (PDB: 1PG1), spontaneously forming amyloid fibrils within hours in the AFM image. (Reproduced with permission from ref. 8 Copyright © 2014 Elsevier Inc.) (d) Human cathelicidin LL-37 is an α-helical AMP (PDB: 2K6O). The active core of LL-37 (residues 17–29) mimics the ability of the full-length peptide to self-assemble into densely packed helical protein fibrils, as demonstrated by transmission electron microscopy (TEM, middle image) and the resolved crystal structure (right image). (Reproduced with permission from ref. 155 Copyright © 2020 Springer Nature Limited) (e) Human α-defensin HD-6 adopting a triple-stranded β-sheet structure (PDB: 1ZMQ). HD-6 self-assembles into elongated fibrils that entrap bacteria, as evidenced by SEM images of wild-type *S. Typhimurium* incubated with vehicle (upper image) and HD-6 (bottom images); scale bar is 5 μm. (Reproduced with permission from ref. 185 Copyright © 2024 American Association for the advancement of Science) (f) Human ribonuclease ECP is an AMP with an α + β folding topology (PDB: 1DYT). ECP demonstrates amyloid-like aggregation capacity as depicted in the TEM micrograph of ECP aggregates; scale bar is 1 μm. (Reproduced with permission from ref. 186 Copyright © 2010 American Chemical Society.) Amino acid residues of each AMP are color-coded to reflect their properties: polar uncharged residues in rose, polar charged residues in blue, and non-polar residues in yellow.

periodic helical substructure (Fig. 7a). This observation suggests a crucial aspect of peptide–lipid interactions, implicating polymerization in membrane-disrupting antibiotic activities. Following the identification of magainin 2, numerous natural AMPs sourced from amphibians have been reported.[217,218]

Skin secretions of hylid frogs comprise a diverse array of genetically related AMPs, collectively termed dermaseptins. This peptide family forms a superfamily characterized by marked diversity, predominantly exhibiting a cationic nature with an amphipathic α-helical structure. Dermaseptin S9, a representative member of the dermaseptins superfamily, exhibits amyloidogenic properties (Fig. 7b).[76] Mechanistic studies on dermaseptin S9 revealed that its largely hydrophobic middle segment serves as a structural foundation for the formation of β-strand, subsequently facilitating self-assembly into amyloid-like fibrils.[13] The antimicrobial activity of Dermaseptin S9 is attributed to the same hydrophobic segment, which can adopt an α-helical conformation, supported by its cationic N- and C-termini when bound to anionic target membranes.[219] The amyloid-like properties are not exclusive to dermaseptin S9 but extend to other dermaseptins as well. Dermaseptin PD-3-7, for instance, stands out as a unique example within the dermaseptin family, featuring a negative net charge at neutral pH due to the presence of three aspartic acid residues. The peptide can self-assemble into reversible amyloid fibrils in a pH-controlled manner (Fig. 7c). Through the transition from low pH to pH exceeding 5.0, metastable amorphous aggregates of PD-3-7 form and release from the amyloid depot, inducing a robust cytotoxic effect.[187,188] This observation introduces a novel natural defense strategy involving amyloid deposits, wherein a temporary cytotoxic agent can be rapidly generated and released in response to microenvironmental factors such as pH. The dual functionality of dermaseptin peptides suggests a connection between amyloid and antimicrobial characteristics,

prompting the exploration of potential associations between the two properties.

The connection between amyloid and antimicrobial activities gains further support with the discovery that amyloid-like self-assembly serves as a mechanism regulating AMPs. Uperins, representing a family of AMPs, are α-helical peptides consisting of 13 to 19 residues secreted on the skin of *Uperoleia mjobergii* (Australian toadlet). A wide variety of uperin peptides have shown their intriguing aggregation propensity, among which uperin 3.5 exhibits the highest propensity.[220] A simulation study exploring helix-to-coil transitions in individual uperin 3.*x* (x = 4, 5, 6) peptides demonstrates an inverse relationship between the helical stability of peptides and their tendency to form structures rich in β-sheets. These findings underscore the significance of helical intermediates in the amyloidogenesis pathway for uparin AMPs.[154] The crystal structure of uperin 3.5 presents a distinctive helical cross-α amyloid fibril formed on membranes, recapitulating properties of β-sheets and contributing to its antibacterial activity. However, in the absence of lipids, the same peptide primarily forms cross-β fibrils.[189] Cryo-EM further elucidates the amyloid cross-β fibrils, revealing mated β-sheets at atomic resolution (Fig. 7d).[152] These secondary structure transitions suggest a role as structural and functional cross-α/β chameleons. Building on these observations, a recent computational screen successfully identified new sequences of fibril-forming AMPs (ffAMPs) from living

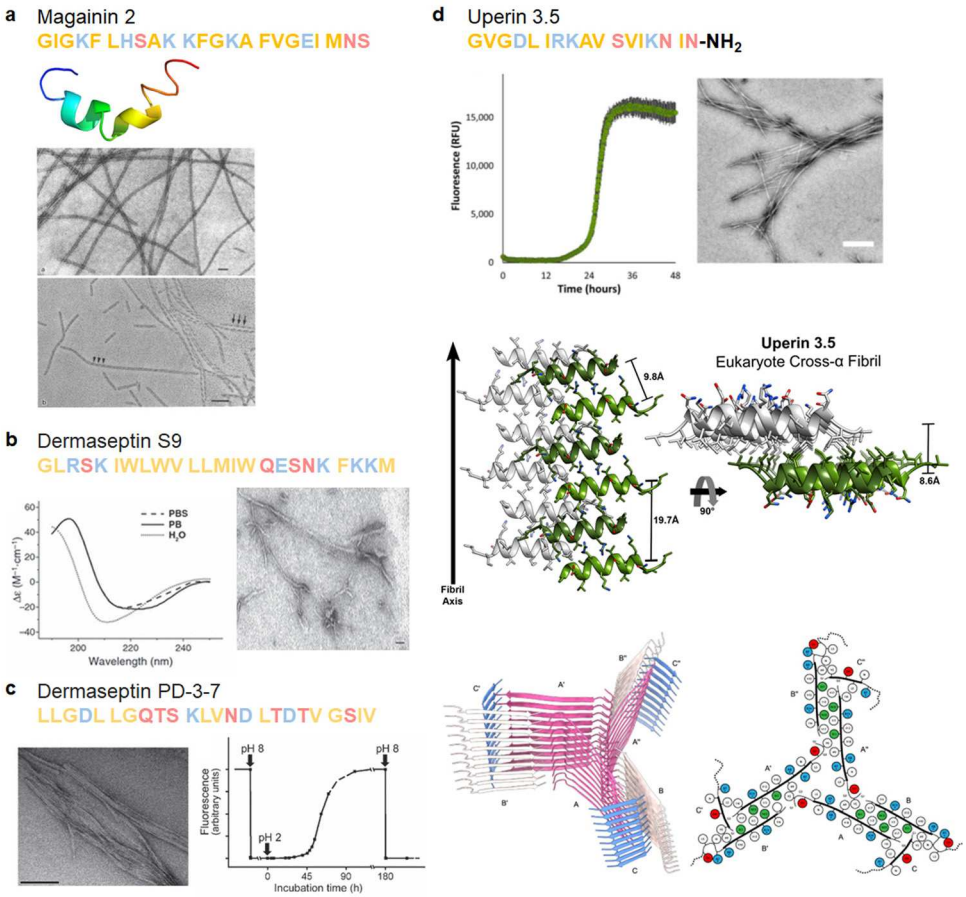

Fig. 7 Illustrations of natural AMPs from amphibians with amyloid property. (a) Magainin 2, a helical AMP derived from the African clawed frog's skin (PDB: 2LSA), can spontaneously polymerize into 13 nm filaments with a periodic helical substructure, revealed by TEM images; scale bar is 100 nm. (Reproduced with permission from ref. 11 Copyright © 1989 John Wiley & Sons, Inc.) (b) Dermaseptin S9, found in hylid frog skin secretions, exhibits a β-sheet-rich conformation with a high aggregation propensity in aqueous environments, as identified by CD spectrum (left image) and TEM (right image); scale bar is 50 nm. (Reproduced with permission from ref. 76 Copyright © 2008 John Wiley & Sons, Inc.) (c) Dermaseptin PD-3-7 with a unique negative net charge opposed to other dermaseptins forms amyloid-like fibrils at acidic pH as observed by TEM (left image; scale bar is 200 nm), while it exhibits reversibly amyloid-like aggregates in a pH-dependent manner as monitored by ThT fluorescence changes (right image). (Reproduced with permission from ref. 188 Copyright © 2009 John Wiley & Sons, Inc.) (d) Uperin 3.5, an α-helical peptide from the Australian toadlet's skin, can self-assemble into elongated amyloid fibrils, as confirmed by ThT (upper left panel) and TEM (upper right panel, scale bar is 300 nm). Crystal structures of uperin 3.5 in the presence of bacterial cells or membrane mimetics reveal a cross-α amyloid fibril architecture (middle panel, PDB: 6GS3), integral to antimicrobial activity. (Reproduced with permission from ref. 189 Copyright © 2021 National Academy of Science) In the absence of lipids, uperin 3.5 forms a 3-blade symmetrical propeller of nine peptides per fibril layer with tight β-sheet interfaces (bottom panel, PDB: 7QV5). (Reproduced with permission from ref. 152 Copyright © 2022 Springer Nature Limited) Amino acid residues of each AMP are color-coded to reflect their properties: polar uncharged residues in rose, polar charged residues in blue, and non-polar residues in yellow.

organisms, particularly in amphibians.[190] Examples from amphibians, including cyanophlyctin secreted on the skin of the amphibian *Euphlyctis cyanophlyctis*, citropin-1.3 secreted from the granular dorsal and submental glands of the Blue Mountains tree frog *Litoria citropa*, brevinin-2SKb isolated from the stream brown frog *Rana sakuraii*, temporin-1CEa extracted from the skin of the Asiatic grass frog *Rana chensinensis*, bombinin H4 secreted on the skin of the yellow-bellied toad *Bombina variegate*, and aurein 3.3 secreted by *Ranoidea raniformis* (Southern bell frog), all exhibit cross-β and cross-α amyloid properties.[190] These findings prompt hypotheses about the prevalent role of fibril secondary structure switching in regulating antimicrobial activities in AMPs, providing a new perspective on the amyloid-antimicrobial link.

3.3. Natural AMPs from arthropods

Insects have evolved a diverse array of AMPs to defend themselves against a broad spectrum of pathogens, often displaying a propensity to form large amyloid-like aggregates. The cross-α/β amyloid properties are notably prevalent in various natural AMPs found in insects, exemplified by cupiennin-1 from the spider venom of *Cupiennius salei*, lasioglossin LL-I isolated from the venom of the eusocial bee *Lasioglossum laticeps*, and cecropin-C produced by *Anopheles gambiae* mosquitoes (Fig. 8a).[190]

Cecropins, initially discovered in the hemolymph of *Hyalophora cecropia*, are AMPs of 31–37 residues and constitute the essential part of the innate immune system of insects. Besides cecropin-C exhibiting cross-α/β amyloid properties, their aggregation tendencies have been demonstrated, closely associated with their antimicrobial activity. Early investigations into the aggregation of cecropin P1 in the presence of membrane proposed the widely cited ''carpet model'' of AMPs' mechanism of action. In this model, cecropin P1 adheres extensively to the pathogen's membrane, causing membrane deformation and eventually destruction when the concentration of cecropin P1 exceeds a critical threshold.[83] Similarly, cecropin A demonstrates concentration-dependent membrane activity, implying

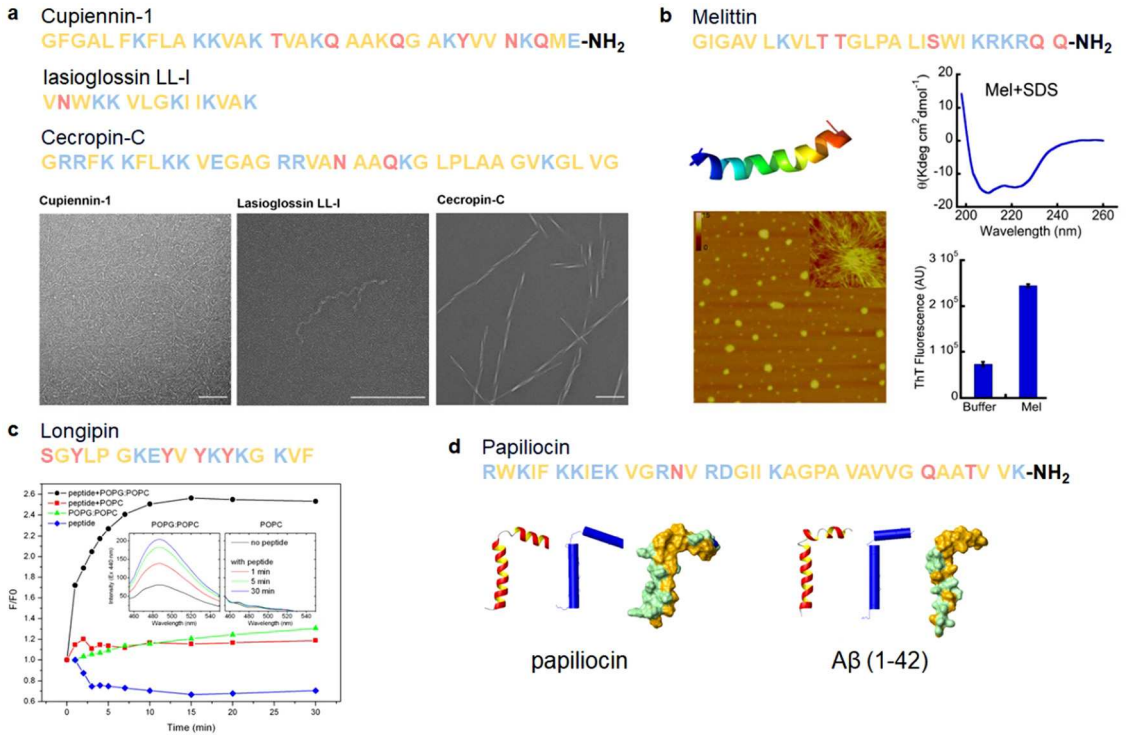

Fig. 8 Illustrations of natural AMPs from arthropods with amyloid property. (a) Cupiennin-1 from the spider venom of *Cupiennius salei*, lasioglossin LL-I from the venom of the eusocial bee *Lasioglossum laticeps*, and cecropin-C from *Anopheles gambiae* mosquitoes can form amyloid-like fibrils, as visualized by TEM; scale bar is 200 nm. (Reproduced with permission from ref. 190 Copyright © 2022 American Chemical Society.) (b) Melittin from the honeybee (PDB: 6DST) adopts a helical conformation (CD spectrum, upper right panel) and forms large globular oligomers and some fibrillar species (AFM, bottom left panel) in the presence of SDS. Melittin aggregates exhibit ThT fluorescence (bottom right panel), indicating the presence of amyloid-like β-sheet structures. (Reproduced with permission from ref. 150 Copyright © 2015 Singh *et al.*) (c) Longipin, derived from the harvestman *Acutisoma longipes*, forms amyloid-like structures in the presence of lipid-vesicles, as evaluated by ThT. The inset shows representative emission spectra of longipin and POPG or POPC vesicles incubated for 1, 5, and 30 minutes. (Reproduced with permission from ref. 149 Copyright © 2016 Sayegh *et al.*) (d) Papiliocin (PDB: 2LA2), a cecropin originally found in the haemolymph of *Hyalophora cecropia*, shares high structural similarity with $A\beta_{42}$. (Reproduced with permission from ref. 221 Copyright © 2020 Springer Nature Limited) All structures are depicted from left to right as a ribbon, a schematic secondary structure with helices shown as cylinders, and a surface representation highlighting the distribution of polar (green) and apolar (orange) residues. Amino acid residues of each AMP are color-coded to reflect their properties: polar uncharged residues in rose, polar charged residues in blue, and non-polar residues in yellow.

that its binding and state of aggregation determine its antimicrobial activity against bacterial membranes.[222] Another study on cecropin AD and POPC/POPG vesicles reveals concentration-dependent positive cooperativity, indicating potential cecropin aggregates formation in the lipid phase.[223] However, more data is required to firmly establish the amyloid-like properties of these cecropins.

Melittin, an extensively studied AMP, is a 26-residue C-terminal amidated peptide derived from the honeybee (*Apis mellifera*). While there is no direct evidence to support the ability of free melittin to form amyloid structures, the peptide has been reported to generate amyloid-like aggregates in the presence of sodium dodecyl sulfate (SDS). Melittin rapidly oligomerizes to form helix-rich oligomers in the presence of SDS, and further aggregation into fibrils has been demonstrated. The amyloid-like aggregates induce ThT fluorescence, indicating the presence of β-sheet structures (Fig. 8b).[150] Additionally, melittin oligomers exhibit cytotoxic and hemolytic activity, likely due to the accumulation of helix-rich oligomers on the cell surface. Similarly, longipin, an unstructured AMP consisting of 18 residues derived from the harvestman *Acutisoma longipes*, has been shown to fold into a β-sheet structure and form amyloid-like fibril in the presence of a lipid bilayer (Fig. 8c).[149]

In addition to the observed amyloid formation properties of natural AMPs from arthropods, the connection between AMYs and AMPs is further underscored by structural similarities shared between representative amyloid peptide Aβ and natural AMPs from various organisms. Papiliocin, a cecropin-like peptide discovered in the Asian butterfly *Papilio Xuthus*, exhibits the highest structural resemblance to Aβ among the analyzed AMPs. In a comparative analysis between Aβ and papiliocin, it was observed that both peptides display a similar tilt angle between helices, and their surfaces, particularly in the C-terminus, exhibit a comparable distribution of apolar residues (Fig. 8d).[221] Such structural and sequence similarity highlights an emerging connection between AMYs and AMPs based on shared structural characteristics.

3.4. Natural AMPs from microbes

Based on biosynthesis pathways, microbial AMPs can be categorized into ribosome- and nonribosome-synthesized AMPs,[224] constituting a diverse group of antibacterial proteins found in various bacterial strains. Similar to their eukaryotic counterparts, microbial AMPs are small in size, cationic, and amphiphilic or hydrophobic. However, a significant distinction lies in their antibacterial efficiency; eukaryotic AMPs are typically active at micro-molar concentrations, while microbial AMPs are highly potent, acting at pico- to nano-molar concentrations.[225] Despite their potency, bacterial AMPs often exhibit a relatively narrow killing spectrum, specifically affecting bacteria closely related to the producing strain.[226] This limitation is attributed to their specific modes of action. Bacterial AMPs kill or inhibit the growth of closely related species by binding to specific cell surface receptors, inducing pore formation in the cytoplasmic membrane, DNA/RNA degradation, and inhibition of transcription, translation, or DNA replication.[227]

Ribosome-synthesized AMPs, commonly known as bacteriocins, are prevalent in Gram-negative bacteria, particularly within the *Enterobacteriaceae* family (*e.g.*, Escherichia and Klebsiella). These bacteriocins are commonly categorized into microcins (small peptides, $<10\,000$ Da) or colicins (large proteins, 25–80 000 Da). A representative example of microcin is Microcin B17 (MccB17), a 43-residue peptide produced by *E. coli*. MccB17 showcases antibacterial activity by inhibiting DNA replication and inducing the SOS response in susceptible bacteria.[228] MccB17 was the first bacterial AMP discovered to exhibit amyloid-forming capabilities. This groundbreaking discovery, dating back to 1986, was captured by electron microscopy, revealing highly ordered and conspicuously long filaments reminiscent of amyloid fibrils[191] (Fig. 9a). Microcin E492 (MccE492), a peptide naturally produced by *Klebsiella pneumoniae* RYC492, exhibits activity against various *Enterobacteriaceae* strains, including *Escherichia*, *Klebsiella*, *Citrobacter*, *Salmonella*, *and Enterobacter*.[229] Unlike other bacteriocins, MccE492 employs a mechanism involving the formation of ion-permeable pores, leading to the depolarization and permeabilization of the bacterial cytoplasmic membrane, ultimately resulting in a lethal loss of membrane potential.[230,231] Additionally, MccE492 demonstrates the capability to form amyloid-like fibrils *in vitro*, sharing structural, morphological, biochemical, and kinetic properties with disease-related AMYs.[192] This aligns with the observation that Mcc E492 extends beyond antibacterial activity and has been found to induce eukaryotic cell apoptosis and necrosis.[232] Computational analysis using different algorithms (such as AGGRESCAN, AmyloidMutants, *etc.*) identified the region $\mathrm{MccE492}_{54-63}$ (VNVPIPVLIG) as the pro-amyloidogenic stretch. Consistently, a mutant of MccE492 lacking residues 54–63 exhibited a significantly reduced tendency for intracellular aggregation and displayed slower kinetics in *in vitro* polymerization.[233] However, similar to other amyloid-like AMPs, *in vivo* MccE492 amyloid-like aggregation is associated with the loss of antibacterial capability[192] (Fig. 9b), supporting the emerging perspective that mature amyloid fibrils may not be inherently harmful; rather, they might serve as inert end products or play a protective role by isolating toxic intermediates.

In Gram-positive bacteria, bacteriocins are classified into two main classes: lantibiotics (class I) and nonlantibiotics (class II).[234] Class II bacteriocins can be further divided into four subclasses: pediocin-like bacteriocins (class IIa), two-component bacteriocins (class IIb), circular bacteriocins (class IIc), and unmodified, linear, non-pediocin-like bacteriocins (class IId).[235] Notably, bacteriocins produced by lactic acid bacteria (LAB), covering diverse types from class I to class IIa-d, have garnered significant attention due to their unique attributes such as food-grade safety and heat stability. As a result, LAB-produced bacteriocins find widespread use in the food industry as natural biopreservatives. In comparison to bacteriocins from Gram-negative bacteria, those originating from LAB exhibit a broader spectrum of activity, extending

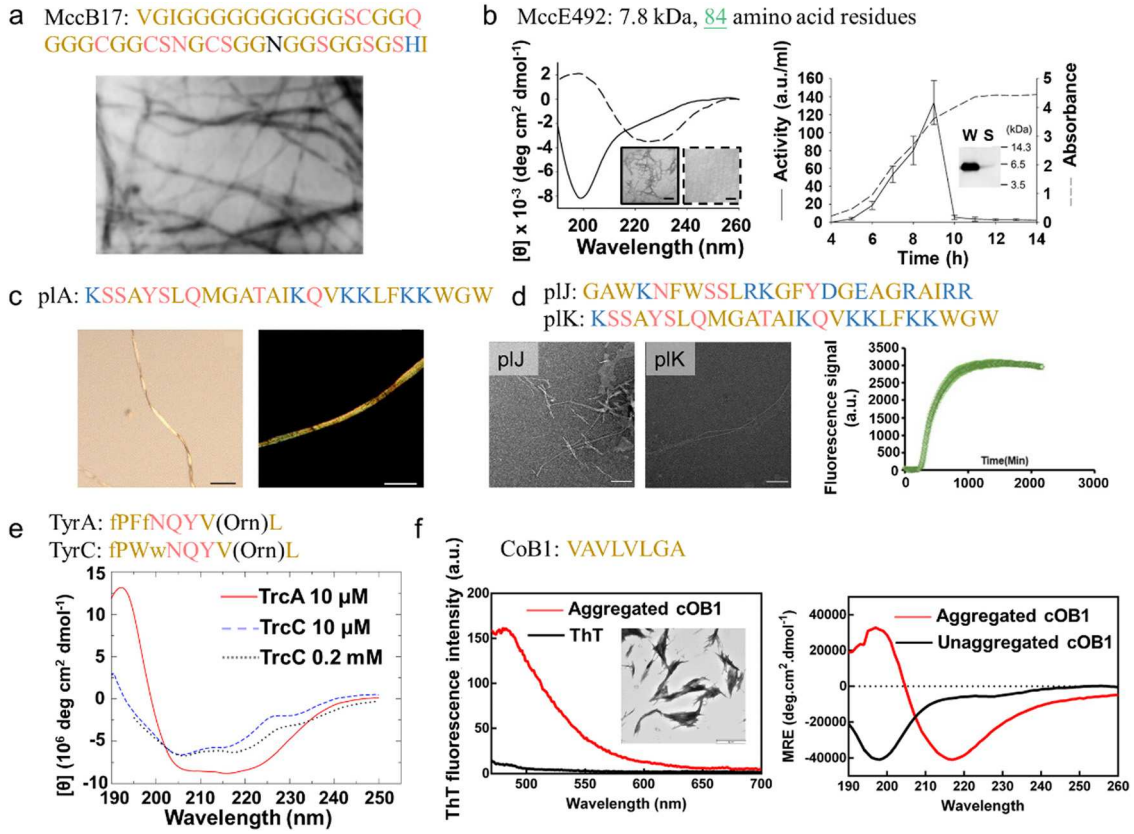

Fig. 9 Illustrations of natural AMPs from microbes with amyloid property. (a) MccB17 produced from *E. coli* can form amyloid-like fibrils, as visualized by EM. (Reproduced with permission from ref. 191 Copyright © 1986 John Wiley & Sons, Inc.) (b) MccE492 produced by *Klebsiella pneumoniae* RYC492 possesses the capability to form β-sheet-rich, amyloid-like fibrils, as evidenced by CD spectrum and TEM (left images). Scale bars are 200 nm. The occurrence of amyloid-like fibril formation, verified by the immunoblot in the right inset image, is correlated with the diminished antibacterial activity. (Reproduced with permission from ref. 192 Copyright © 2005 Elsevier Inc.) (c) Plantaricin A (plA) generated from *L. plantarum* C11 exhibits the ability to form amyloid-like fibrils in the presence of PS-containing liposomes, as demonstrated through phase-contrast microscopy (left image) and Congo red staining observed *via* fluorescent microscopy (right image). Scale bars are 10 μm (left) and 15 (right). (Reproduced with permission from ref. 9 Copyright © 2005 Elsevier B.V.) (d) Plantaricin J (plJ) and Plantaricin K (plK) derived from *L. plantarum* C11 exhibit the ability to form amyloid-like fibrils, as observed by TEM (left image) and ThT fluorescence (right image). Scale bars are 200 nm. (Reproduced with permission from ref. 190 Copyright © 2022 American Chemical Society.) (e) Tyrocidines (TyrA and TyrC) derived from *B. aneurinolyticus* adopt an antiparallel β-sheet confirmation, as indicated by CD spectrum. (Reproduced with permission from ref. 196 Copyright © 2013 American Chemical Society.) (f) cOB1 produced from *E. faecalis* shows amyloid-like properties, as demonstrated by the enhanced ThT fluorescence (left image), the presence of amyloid-like fibrils by TEM (left inset image), and β-sheet confirmation by CD spectrum (right image). (Reproduced with permission from ref. 193 Copyright © 2019 John Wiley & Sons, Inc.) Amino acid residues of each AMP are color-coded to reflect their properties: polar uncharged residues in rose, polar charged residues in blue, and non-polar residues in yellow.

their antibacterial efficacy beyond closely related species. These LAB-produced bacteriocins have demonstrated effectiveness against various food spoilage and pathogenic bacteria, including Gram-positive strains such as *Listeria monocytogenes*, *Clostridium perfringens*, *Bacillus cereus*, and Gram-negative strains like *Salmonella enteritidis and Escherichia coli*, contributing to the extension of the shelf life of food products.[236]

Plantaricin A (plA), a 26-residue peptide produced by *Lactobacillus plantarum* C11, a strain of LAB found in the human microbial flora, exhibits membrane-permeabilizing antimicrobial activity. The interaction of plA with membranes is highly dependent on the lipid composition of the membrane. Intriguingly, plA has been observed to form supramolecular protein-lipid amyloid-like fibrils upon binding to negatively charged phospholipid-containing membranes (Fig. 9c). This suggests a potential mechanistic link between fibril formation and the cytotoxicity of plA.[9] Another bacteriocin produced by *Lactobacillus plantarum* C11, plantaricin J (plJ), and plantaricin K (plK), are two synergistic peptides with little sequence similarity, measuring 25 and 32 residues, respectively. Typically, they are used in equal amounts to achieve optimal antibacterial activity, potentially by forming an active complex. When considered separately, both plJ and plK can individually form amyloid-like fibrils, as observed by TEM. Distinctively, plJ displayed a typical cross-β pattern in fiber X-ray diffraction, whereas plK formed a mixed population with the major polymorph being of cross-β content, along with the ability to induce ThT fluorescence (Fig. 9d).[190] However, the amyloid-forming capability of the mixture of plJ and plK remains unclear. The wild-type and G6A-substituted N-terminal domain of pediocin-like bacteriocins of sakacin P (class IIa), obtained from *Lactobacillus sakei*, have been identified as an S-shaped three-stranded antiparallel

β-sheet-like domain.[194] It remains to be investigated in future studies whether this β-sheet conformation is associated with an amyloid-like structure and whether it contributes to the antibacterial activity of sakacin P.

Unlike conventional ribosomal protein synthesis, nonribosome synthesized peptides are secondary metabolites produced by intricate enzymatic machinery, typically categorized by the linearity or cyclization of the molecule. Among these, a group of nonribosomal AMPs (*e.g.*, gramicidin S (GS), tyrocidines (Tyr), loloatins, and laterocidin) originating from Gram-positive Bacillus strains share structural similarities, notably featuring a cyclic decapeptide. Structurally, GS demonstrates 50% identity with Tyr, specifically sharing the conserved pentapeptide unit of FPV(Orn)L. Additionally, GS[195] and Tyr[196] also share a similar secondary structure of β-sheets in solution. To delve into specifics, the β-sheet conformations of tyrocidines and gramicidin S are distinct, *i.e.*, tyrocidines have an S-shaped, three-stranded antiparallel β-sheet-like domain (Fig. 9e), whereas gramicidin S adopts a β-helix structure. More recently, a new antimicrobial innate immune peptide called cOB1 has been identified. Originating from *Enterococcus faecalis*, cOB1 (VAVLVLGA) operates as a sex pheromone, exerting its natural antimicrobial effects to restrict the growth of multidrug-resistant *Enterococcus faecalis* in the gut at a picomolar concentration.[237] Experimental evidence indicates that cOB1 forms amyloid-like structures, as supported by both *in silico* predictions and *in vitro* assays involving Congo red, ThT staining, CD, and TEM morphology (Fig. 9f).[193] These structures are postulated to serve as the nucleating core, potentially facilitating enhanced biofilm formation.

3.5. Natural AMPs from plants

Plant AMPs exhibit several shared characteristics with those from animals, amphibians, and insects, such as (i) small peptides ranging from 10 to 54 amino acids in length; (ii) positive charges to interact with negatively charged microbial membranes; (iii) amphipathic structure for interacting with and disrupting the lipid membranes of microorganisms, all of which make them effective in broad-spectrum antibacterial, antifungal, and antiviral activities. However, plant AMPs are distinguished by their high cysteine content, playing a pivotal role in stabilizing, and maintaining the structural integrity of these peptides. The presence of cysteine residues enables the formation of 3–5 intramolecular disulfide bridges, contributing to the stabilization of the secondary structure, enhancing resistance to degradation by proteolytic enzymes and environmental factors, and thereby maintaining bioactivity. Plant AMPs are categorized into distinct subgroups, such as thionins, defensins, cyclotides, hevein, knottin, α-hairpinin, lipid transfer proteins, and snakins, based on their sequence similarity, number of cysteine residues, disulfide bond patterns, and tertiary structure.[238,239]

While diverse plant AMPs have been extensively studied for their antimicrobial activities, the connection between these peptides and amyloidogenicity remains poorly understood. To date, only two peptides within the defensin category have been reported to exhibit a high propensity for amyloid fibril formation, suggesting that amyloidogenicity is not a generic feature of plant AMPs. One example is RsAFP-19, a 19 amino acid C-terminal fragment derived from the radish seed (*Raphanus sativus*) antifungal protein (RsAFP). RsAFP-19 has been demonstrated to possess amyloid fibril-forming properties by a synergistic approach combing computational methods (*i.e.*, TANGO) and experimental techniques (*i.e.*, fluorescent-binding, morphology, and secondary structures). Evidently, RsAFP-19 exhibits characteristics typical of classical amyloid fibrils, including ThT assay fluorophore-binding intensity, narrow protofilaments observed by AFM and TEM, and a cross-β structure from X-ray fiber diffraction analysis. In contrast, NaD1-19, a plant defensin peptide structurally and functionally related to RsAFP-19, derived from the ornamental tobacco plant *Nicotiana alata*, does not show any propensity for amyloid fibril formation,[197] highlighting the specificity and diversity of amyloidogenic properties in plant AMPs. Interestingly, challenging the assumption that amyloid formation is intricately linked to antimicrobial properties, the "gel-like" RsAFP-19 amyloid fibrils formed after 1-month storage (freezing and thawing) completely lost their anti-fungal activity (Fig. 10a), suggesting the irrelevance of fibril formation to the biological functions of RsAFP.[197] The other example is Cn-AMP2, a plant defensin derived from the liquid endosperm of coconut (Cocos nucifera), which is rich in hydrophobic residues (a characteristic shared with AMYs) and exhibits a natural tendency to form amyloid-like fibrillary structures comparable to Aβ (Fig. 10b). However, the antibacterial effect of fibrillar Cn-AMP2 remains unstudied, creating uncertainty about the link between the amyloidogenic structure and its biological functions.[198]

3.6. Synthetic or engineered AMPs

Most naturally occurring antimicrobial peptides are characterized by cationic linear sequences that tend to fold into amphipathic α-helices. This structural feature plays a crucial role in inducing membrane leakage, contributing to their broad-spectrum antimicrobial activity and rapid action against microbial membranes. Despite these advantages, AMPs with amphipathic α-helices face certain limitations, including the requirement for high concentrations to effectively eliminate target organisms, susceptibility to proteolytic degradation by enzymes, high toxicity to host cells, and limited selectivity that may lead to unintended interactions with host cells. To address these challenges and enhance the antimicrobial efficacy of AMPs, rational design strategies to explore AMPs with stable β-sheet structures are essential. However, there is ongoing debate about the preference for the development of β-sheet species into amyloid-like aggregates.

The interaction between amyloid aggregates and antimicrobial properties is complex and multifaceted. Although formation of amyloid-like fibrils can create pores or channels in microbial membranes, exhibiting potential antimicrobial capabilities, the prevailing consensus is that self-assembly is detrimental to antibacterial potency. On one hand, a simple and straightforward approach to increase the folding ability of

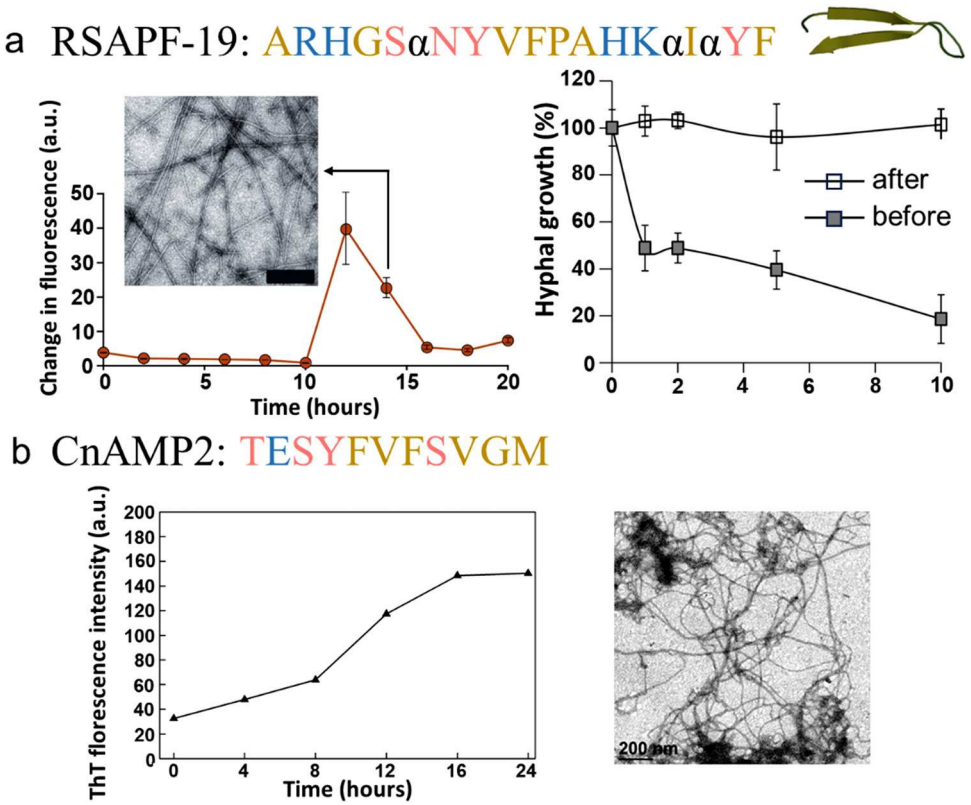

Fig. 10 Illustrations of natural AMPs from plants with amyloid property. (a) RsAFP-19 produced from Radish seed shows amyloid-like properties, as indicated by the enhanced ThT fluorescence and the presence of amyloid-like fibrils by TEM (left images). The scale bar is 200 nm. The occurrence of amyloid-like fibril formation correlates with the reduction in antibacterial activity (right image). (Reproduced with permission from ref. 197 Copyright © 2013 Elsevier B.V.) (b) Cn-AMP2 generated from Cocos nucifera exhibits amyloid-like properties, as evidenced by the enhanced ThT fluorescence (left image) and the presence of amyloid-like fibrils by TEM (right image). The scale bar is 200 nm. (Reproduced with permission from ref. 198 Copyright © 2016 John Wiley & Sons, Inc.) Amino acid residues of each AMP are color-coded to reflect their properties: polar uncharged residues in rose, polar charged residues in blue, and non-polar residues in yellow.

short peptides is acylation with long-chain fatty acids (*i.e.*, lipidation). In the design of lipidated peptides, palmitic acid was conjugated to the N-terminus of $(IIKK)_n$I-NH_2 (n = 2–3). This lipidation enhanced the hydrophobic interaction and induced the formation of β-sheet-rich nanofibrils resembling amyloid fibrils, as confirmed by ThT, CD, and TEM analyses[199] (Fig. 11a). However, the antimicrobial activity of these lipidated AMPs was either comparable or diminished. This reduction was primarily attributed to stronger homo-interactions (*i.e.*, self-aggregation) compared to hetero-interactions, resulting in limited interaction with bacteria.[199] On the other hand, the delivery of such large, self-assembled AMPs to infectious locations poses challenges, resulting in reduced efficiency. The critical aspect lies in understanding when and where these amyloid-like fibrils form. As proof of concept, a designed peptide, KRRFFRRK (FF8), remains in a random coil structure under physiological conditions but is specifically triggered by the negatively charged lipid membrane to self-aggregate into nanofibrils (Fig. 11b). This structure exhibits enhanced antimicrobial capability compared to a control peptide, GG8 (KRRGGRRK), without the ability to self-assemble,[200] implying that formation of amyloid-like fibrils occurs subsequent to FF8 being transported to the membrane, reducing the transportation pressure of self-assembling AMPs.

To date, there has been only limited research exploring the self-assembly capabilities of newly designed AMPs into larger amyloid aggregates. Several studies suggested a tendency for these peptides to fold into β-sheets. Further investigation is necessary to explore the potential transformation of β-sheets into amyloid-like fibrils. To this end, a number of approaches aimed at re-engineering naturally occurring AMPs, such as sequence shuffling, residue or stereoisomer substitution, guided by the structure–activity relationship. These modifications aim to bring about changes in charge, conformation, sequence, length, amphipathicity, hydrophobicity, self-aggregation, and other key properties. These efforts are geared towards engineered AMPs to enhance their properties and overcome inherent limitations.

In this regard, a significant area of investigation involves transforming α-helical AMPs into β-sheet AMPs, representing a current focal point in the field. One illustrative instance is HPRP-A1, a 15-residue α-helical AMP derived from the N-terminus of the *Helicobacter pylori* ribosomal protein L1. HPRP-A1 served as the foundational peptide for designing

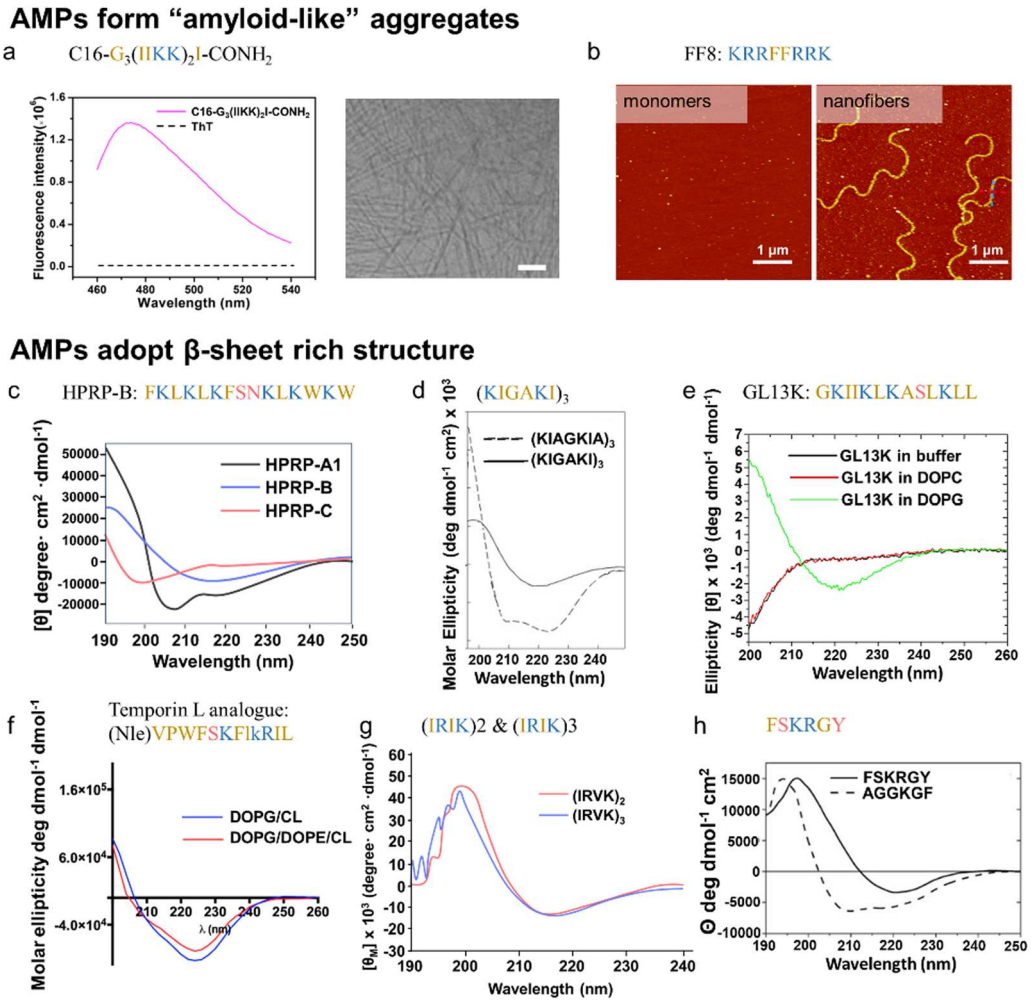

Fig. 11 Illustrations of synthetic or engineered AMPs with amyloid-forming or β-sheet formation properties. (a) C16-G_3(IIKK)$_2$I-$CONH_2$, an engineered AMPs *via* terminal alkylation, forms amyloid-like aggregates, as indicated by the enhanced ThT fluorescence (left image) and the presence of amyloid-like fibrils by cryo-TEM (right image). The scale bar is 100 nm. (Adapted with permission from ref. 199 Copyright © 2020 American Chemical Society). (b) FF8 (b) FF8 demonstrates the ability to form amyloid-like nanofibrils under pH 9.4, while maintaining a monomeric state at pH 7.4, as visualized by AFM. (Reproduced with permission from ref. 200 Copyright © 2020 The Royal Society of Chemistry.) (c) HPRP-A1 isomers are designed to adopt different conformations, where HPRPA1 assumes an α-helix, HPRPB adopts a β-sheet, and HPRPB adopts a random coil conformation, as confirmed by the CD spectrum. (Adapted with permission from ref. 201 Copyright © 2015 John Wiley & Sons, Inc.). (d) (KIGAKI)$_3$, designed from α-helical (KIAGKIA)$_3$, adopts β-sheet structure in the presence of POPG LUV, as indicated by CD spectrum. (Adapted with permission from ref. 202 Copyright © 2001 Elsevier Inc.). (e) GL13K folds into β-sheet structure in the presence of anionic DOPG liposomes, while retaining unstructured in the presence of neutral DOPC liposomes and PBS buffer, as confirmed by CD spectrum (Reproduced with permission from ref. 204 Copyright © 2013 Elsevier B.V.) (f) Temporin L analogue adopts a β-type conformation when exposed to liposomes mimicking bacterial membranes, as evidenced by CD spectrum. (Reproduced with permission from ref. 207 Copyright © 2022 MDPI (Basel, Switzerland).) (g) (IRIK)$_2$ and (IRIK)$_3$ demonstrate β-sheet folding in the presence of membrane-mimicking environment, specifically in a 25 mM SDS micelles solution. (Adapted with permission from ref. 208 Copyright © 2013 John Wiley & Sons, Inc.). (h) FSGRGY – a pore-forming peptide – adopts β-sheet structure, in contrast to non-pore-forming AGGKGF that exhibits some α-helical secondary structure, as depicted by CD spectrum. (Reproduced with permission from ref. 209 Copyright © 2005 National Academy of Science.) Amino acid residues of each AMP are color-coded to reflect their properties: polar uncharged residues in rose, polar charged residues in blue, and non-polar residues in yellow.

isomers with distinct secondary structures (*i.e.*, α-helical structure with different helicity, β-sheet structure, and random coil structure, Fig. 11c). This was achieved by reshuffling the peptide sequence while maintaining an identical amino acid composition to eliminate the influence of other properties, such as peptide length, charge, and hydrophobicity. A comparative analysis of HPRP-A1 isomers with different secondary structures revealed a hierarchy in antibacterial efficacy, with the order being α-helix > β-sheet > random coil.[201] This aligns with the prevailing consensus indicating that a decline in antibacterial capability occurs following the formation of amyloid aggregates.

Inspired by a derivative of PGLa, (KIAGKIA)$_3$-NH_2, known for its amphipathic α-helix structure, (KIGAKI)$_3$-NH_2 was engineered to adopt an amphipathic β-sheet structure (Fig. 11d). A direct comparison reveals that the β-sheet variant,

$(KIGAKI)_3$-NH_2, exhibits antimicrobial activity comparable to that of its α-helical counterpart, $(KIAGKIA)_3$-NH_2, but with higher selectivity toward bacterial membranes over mammalian membranes.[202] Notably, $(KIGAKI)_3$-NH_2 exhibits higher selectivity in binding to and inducing leakage in membranes rich in phosphatidylethanolamine, a neutral phospholipid prevalent in bacterial plasma membranes, compared to those rich in phosphatidylcholine, a major neutral lipid in mammalian plasma membranes.[240] Furthermore, a single substitution of Ile (I) with Trp (W) in $(KIGAKI)_3$-NH_2, while preserving the β-sheet structure, enhances its binding affinity to membranes containing acidic phospholipids (characteristic of bacterial membranes) over zwitterionic phospholipids (characteristic of mammalian membranes), underscoring the specificity of β-sheet $(KIGAKI)_3$-NH_2 and its analogs for targeting bacterial membranes.[241] Similarly, GL13K, engineered from the salivary protein BPIFA2 by substituting charged residues with Lys (K), gained a newfound antibacterial capacity and a preference for folding into β-sheets in anionic DOPG membranes, as opposed to zwitterionic (neutral) eukaryotic DOPC membranes[203,204] (Fig. 11e). However, it is crucial to note that the adoption of a β-sheet structure in GL13K does not necessarily lead to the formation of amyloid-like fibrils. Subsequent investigations have revealed that GL13K does not form fibrils under physiological conditions, effectively dispelling the possibility of pathological amyloid presence.[242]

Beyond residue substitution, the incorporation of stereoisomers, specifically substituting L-amino acids with their D-enantiomers, offers advantages in enhancing resistance to enzymatic degradation and improving stability. An illustrative example involves the substitution of D-amino acids into a cytolytic α-helical pardaxin fragment, inducing a structural transition to a β-sheet conformation. This modification not only leads to a structural shift but also results in a functional transition, transforming from high toxicity towards both bacteria and erythrocytes to specific cytolytic activity targeted at bacteria while sparing erythrocytes.[205] Similarly, the gramicidin S analogue (GS14) with a β-sheet structure demonstrates broad-spectrum antimicrobial capability against both Gram-positive/negative bacteria and fungi, but it poses a toxicity risk to red blood cells. To address this concern, GS14 was modified by substituting D-amino acids with L-amino acids, disrupting the β-sheet structure and significantly reducing toxicity to red blood cells.[206] Furthermore, the combination of residue and stereoisomer substitution/addition has been investigated in the modification of Temporin L, an antimicrobial peptide with the ability to form α-helical aggregates, aiming to enhance peptide stability and effectiveness. These modifications encompass the addition of a norleucine residue at the N-terminus, the substitution of Q3 to P3 and G10 to K10, as well as the replacement of L9 and K10 with l9 and k10. This tailored modification strategy ensures that the Temporin L analogue remains unstructured in an aqueous environment but adopts a β-type conformation when exposed to liposomes mimicking bacterial membranes (Fig. 11f), resulting in improved antibacterial efficacy.[207] These findings underscore the promising advantage of β-sheet-forming AMPs in selectively targeting and disrupting bacterial membranes while minimizing the impact on host cell membranes.

While employing wild-type AMPs as templates for chemical modifications to design new AMPs has its drawbacks, such as the potential for increased immunogenicity due to extended sequences which may elevate manufacturing costs, and a high similarity to host defense AMPs that could trigger resistance, recent research by Novabiotics Ltd demonstrates promising advancements in this area. Utilizing HDP templates, they have developed new antimicrobial and immunomodulatory compounds, with several products currently undergoing clinical trials. This underscores the potential of such strategies, although optimizing efficacy and safety profiles remains a challenge.[243] Hence, the strategic development of short synthetic peptides that bear minimal resemblance to naturally occurring AMP sequences is anticipated to be a promising approach for creating safe and effective AMPs for clinical applications. Pursuing this objective, a series of short synthetic β-sheet folding AMPs, consisting of short recurring $(X_1Y_1X_2Y_2)_{n=2-3}$-NH_2, have been designed. Here, X and Y represent hydrophobic (*i.e.*, V, I, F, W) and cationic (R, K) residues, respectively, which facilitate interaction with microbial membranes. These designed β-sheet folding AMPs (confirmed by CD, Fig. 11g) demonstrate wide-ranging antimicrobial efficacy against Gram-positive bacteria such as *S. epidermidis* and *S. aureus*, Gram-negative bacteria like *E. coli* and *P. aeruginosa*, and the yeast *C. albicans*. Among these AMPs, $(IRIK)_2$-NH_2 and $(IRVK)_3$-NH_2 emerge as the most potent, inhibiting sessile biofilm bacteria growth and inducing biomass reduction.[208]

The D-amino acid-substituted β-sheet-forming peptides, $(IRIK)_2$-NH_2-all-D and $(IRVK)_3$-NH_2-all-D, demonstrate enhanced antimicrobial activities, extending to a series of clinically relevant antibiotic-resistant bacteria (*i.e.*, methicillin-resistant *S. aureus*, vancomycin-resistant *Enterococci*, *A. baumannii*, *M. tuberculosis*, *etc.*). Additionally, these peptides exhibit improved protease stability, making them promising candidates for therapeutic applications in the fight against antibiotic resistance.[244,245] However, the limitations in the number of rational designs for AMPs may stem from a poor understanding of the fundamental principles governing the correlation between self-assembly and action mechanisms, as well as the complex nature of diverse AMPs. In contrast to trial-and-error attempts, the utilization of rational combinatorial libraries offers a potent method for the selection and engineering of novel pore-forming sequences. Construction of the combinatorial library involved employing β-sheets as a foundational framework and subsequent screening to obtain good hits. One example is FSKRGY, a novel AMP that self-assembles into β-sheet pores in membranes to exhibit antimicrobial properties[209] (Fig. 11h).

4. Antimicrobial activity of amyloid peptides

Amyloid aggregation involves the transition from unstructured soluble monomers to β-sheet-rich amyloid fibrils, hallmark features of protein misfolding diseases like AD, PD, and T2D.[246,247]

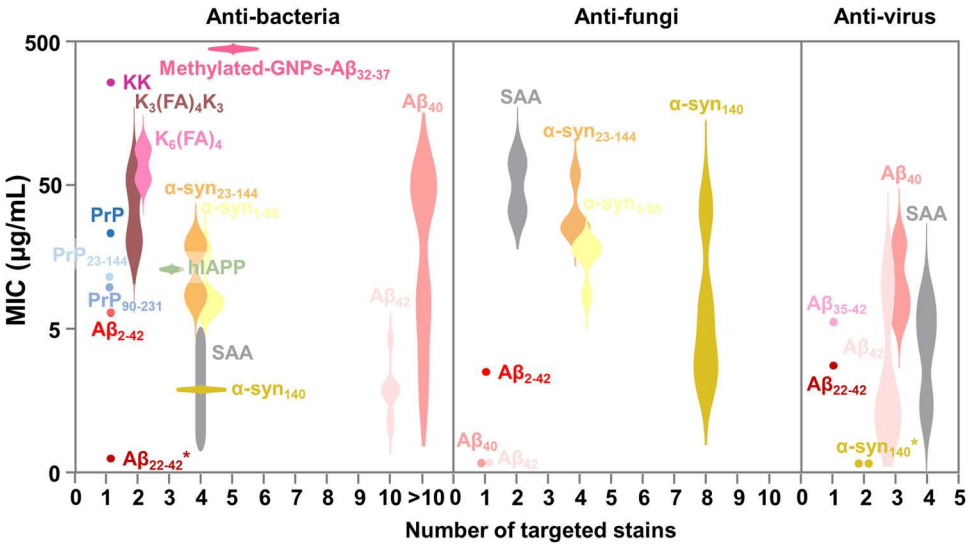

Fig. 12 Summary of amyloid peptides with anti-bacterial, anti-fungal, and anti-viral activity in terms of minimal inhibitory concentrations (MIC) and the number of targeted stains. *MIC data are not available in the references.

The abnormal accumulation of these fibrils leads to deposits in organs, causing cellular dysfunction and tissue damage. Recently, "functional amyloid fibrils" have gained recognition for their positive biological roles,[248] such as curli fibrils in bacteria and silk proteins in insects, which aid in biofilm formation and structural support.[249,250] Despite belonging to different peptide families, AMYs and AMPs share notable similarities. Both involve hydrophobic residues crucial for aggregation in AMYs and microbial membrane interactions in AMPs.[22] As discussed in Section 3, many AMPs, like AMYs adopt β-sheet structures and can self-assemble into aggregates, particularly during microbial interactions. Both AMYs and AMPs disrupt lipid bilayers, causing cell or bacterial death.[7,18] This section presents a range of AMYs (Fig. 12 and Table 2), such as Aβ (red, Alzheimer's disease), hIAPP (green, type 2 diabetes), α-syn (yellow, Parkinson's disease), PrP (blue, prion disease), and SAA (grey, systemic amyloid A), which exhibit antimicrobial properties.

4.1. Amyloid-β peptide (associated with Alzheimer disease)

Aβ, an inadvertent byproduct of amyloid protein precursor (APP) catabolism in the brain and peripheral tissues, is widely recognized as a crucial pathological hallmark of AD. Aβ is generated in both AD and healthy individuals through extracellular and intramembrane endoproteolytic cleavage of APP *via* β-secretase/γ-secretase pathways.[265] The degradation of Aβ is facilitated by the Aβ-degrading enzyme neutral endopeptidase (NEP).[266] Under normal circumstances, Aβ maintains a dynamic equilibrium between production and degradation, with a steady low level (approximately nanomolar concentration) of soluble Aβ.[267] However, an imbalance in this equilibrium leads to elevated Aβ deposition in the brain, contributing to the onset and progression of AD. Despite extensive efforts to develop therapeutic strategies targeting Aβ inhibition, none have received approval due to limited efficacy or adverse side effects.[268,269] For instance, clinical studies on Aβ immunotherapy with AN1792 showed that AD patients experienced a higher incidence of subacute meningoencephalitis—a brain inflammatory disease caused by infection—resulting in the termination of the trial.[270,271] Similar challenges have been encountered in other Aβ-related inhibition therapies, such as AD02[272] and CAD106.[273] These observations suggest a potential physiological role of Aβ beyond its pathological implications, prompting the consideration of maintaining normal Aβ doses and forms rather than pursuing complete clearance.

Recently, a novel model for AD amyloidogenesis, known as the "antimicrobial protection hypothesis" has emerged, complementing the traditional "amyloid cascade hypothesis".[274] According to this hypothesis, Aβ is not a functionless peptide released into the cell by accident or genetic predisposition. Instead, akin to AMPs, Aβ production is stimulated as part of an innate immune response to activate neuroinflammatory pathways (*e.g.*, microglia and proinflammatory cytokines) and eliminate foreign threats. As a byproduct, Aβ subsequently plays a secondary role in AD pathology by inducing chronic activation of these pathways, leading to sustained inflammation and neurodegeneration.[32] Notably, Aβ has been identified as an AMP *in vitro*, exhibiting activity against 8 of 16 common and clinically relevant pathogens (*e.g.*, Gram-positive bacteria, Gram-negative bacteria, fungi), with antimicrobial capacity equivalent to or greater than LL-37, a human innate AMP[17,253] (Fig. 13a). Recent findings from the same group indicate that the expression of Aβ is associated with an increased survival rate in different bacterial and fungal infection models, such as *in vitro* mammalian cells, *in vivo* nematodes, and mice. Conversely, APP knockout mice, exhibiting immunodeficiency associated with low Aβ expression, showed higher mortality than wild-type mice after infection, further highlighting the protective role of Aβ as an AMP in innate immunity.[275] Brain tissues from AD patients exhibit higher

Table 2 Summary of different types of AMYs with antimicrobial capability

		Targeted bacteria				Targeted fungi			Targeted virus			
AMD	Sequence	# of strains	Anti-Gram (+)	Anti-Gram (−)	MIC (μg mL^{-1})	# of strains	Anti-fungal	MIC (μg mL^{-1})	# of strains	Anti-viral	MIC (μg mL^{-1})	Ref.
Aβ	$A\beta_{40}$	12	*S. epidermidis*, *S. aureus*, *S. pneumoniae*, *L. monocytogenes*, *E. faecalis*, *S. agalactiae*, *S. mitis*, *L. acidophilus*	*E. coli*, *P. gingivalis*, *A. actinomycetemcomitans*, *F. nucleatum*	1.56–50	1	*C. albicans*	0.78	3	HSV-1, H3N2, H1N1	7.5–>20	17 and 251–253
	$A\beta_{42}$	10	*S. epidermidis*, *S. aureus*, *S. pneumoniae*, *L. monocytogenes*, *E. faecalis*, *S. agalactiae*, *L. acidophilus*	*E. coli*, *P. gingivalis*, *A. actinomycetemcomitans*	1.56–12.5	1	*C. albicans*	0.78	3	HSV-1, H3N2, H1N1	1–>20	17, 23, 24, 153, 157 and 251–253
	$A\beta_{35-42}$	N/A	N/A	N/A	N/A	N/A	N/A	N/A	1	H3N2	6	254
	$A\beta_{22-42}$	1	N/A	*E. coli*	N/A	N/A	N/A	N/A	N/A	N/A	N/A	254 and 255
	$A\beta_{2-42}$	1	*E. faecalis*	N/A	6.25	N/A	N/A	N/A	N/A	N/A	N/A	254 and 255
	Methylated-GNPs-$A\beta_{32-37}$	5	*S. aureus*, *E. faecalis*	*E. coli*, *P. aeruginosa*, *K. pneumoniae*	>500	N/A	N/A	N/A	N/A	N/A	N/A	256
	KK	1	N/A	*E. coli*	375	N/A	N/A	N/A	N/A	N/A	N/A	257
	$K_3(FA)_4K_3$	2	N/A	*Salmonella*, *E. coli*	32–63	N/A	N/A	N/A	N/A	N/A	N/A	258
	$K_6(FA)_4$	2	N/A	*Salmonella*, *E. coli*	63–125	N/A	N/A	N/A	N/A	N/A	N/A	258
hIAPP	$hIAPP_{37}$	3	*S. aureus S. epidermidis*	*E. coli*	>20	N/A	N/A	N/A	N/A	N/A	N/A	14, 23, 24, 153 and 157
α-syn	$\alpha\text{-syn}_{140}$	4	*S. aureus*, *S. epidermidis*	*E. coli*, *P. aeruginosa*	2.8	8	*C. albicans*, *C. tropicalis*, *F. neoformans*, *A. flavus*, *A. fumigatus*, *A. parasiticus*, *R. solani*, *T. harzianum*	5.6–44.8	2	WNV, VEEV	N/A	15 and 259
	$\alpha\text{-syn}_{1-60}$	4	*S. aureus*, *S. epidermidis*	*E. coli*, *P. aeruginosa*	9.6–19.2	4	*C. albicans*, *F. neoformans*, *A. flavus*, *R. solani*	38.4–76.8	N/A	N/A	N/A	15
	$\alpha\text{-syn}_{1-95}$	4	*S. aureus*, *S. epidermidis*	*E. coli*, *P. aeruginosa*	7.6–15.2	4	*C. albicans*, *F. neoformans*, *A. flavus*, *R. solani*	15.2–30.4	N/A	N/A	N/A	15
PrP	PrP_{23-231}	1	N/A	*E. coli*	35	1	*C. parapsilosis*	70	N/A	N/A	N/A	163
	PrP_{23-144}	1	N/A	*E. coli*	<12	N/A	N/A	N/A	N/A	N/A	N/A	163
	PrP_{90-231}	1	N/A	*E. coli*	<15	N/A	N/A	N/A	N/A	N/A	N/A	163
SAA	SAA_{104}	4	*S. aureus*	*E. coli*, UTI89, F11	1–5	2	*C. albicans*, *C. dubliniensis*	40–>100	4	HCV, Phil, PR-8	<2–8	16, 164 and 260–264

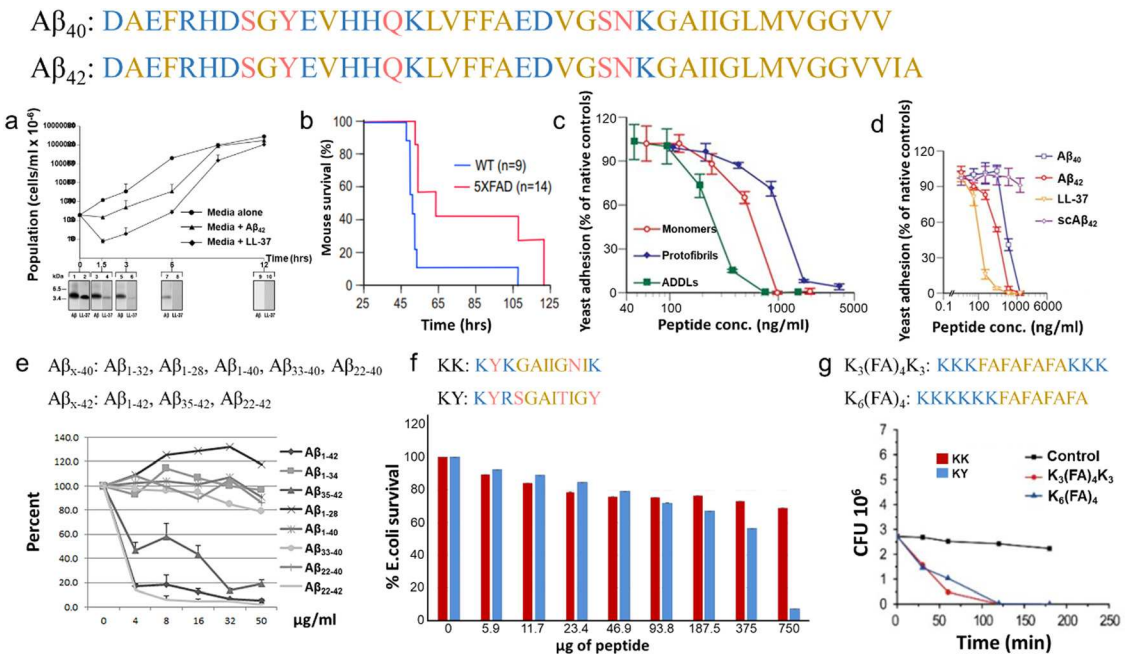

Fig. 13 Antimicrobial activity of Aβ. (a) Antibacterial efficacy of $Aβ_{42}$ against *E. faecalis* growth, in comparison to untreated and LL-37-treated bacteria, through colony forming unit (CFU) counting and western blot analyses using mAβ 6E10 or anti-LL-37 antibodies to further evaluate the impact on bacterial cultures. (Reproduced with permission from ref. 17 Copyright © 2010 Soscia *et al.*) (b) Antiviral ability of $Aβ_{42}$ in an HSV1 Encephalitis 5XFAD Mouse Model. 5XFAD mice exhibit an extended survival rate compared to wild-type mice after the injection of HSV1 into the hippocampal region of each brain hemisphere. (Reproduced with permission from ref. 251 Copyright © 2018 Elsevier Inc.) (c) Comparative analysis of the antifungal efficacy of monomeric $Aβ_{42}$, amyloid-β-derived diffusible oligomeric ligands (ADDLs), and protofibrillar $Aβ_{42}$ against *C. albicans*, with the descending order of anti-fungal efficiency: oligomers > monomers > protofibrils. (Reproduced with permission from ref. 275 Copyright © 2016 American Association for the Advancement of Science.) (d) Comparative analysis of the antifungal activity of cell-derived $Aβ_{42}$, $Aβ_{40}$, LL-37, and synthetic $Aβ_{42}$ against *C. albicans*, with the descending order of anti-fungal efficiency: LL-37 > cell-derived $Aβ_{42}$ > cell-derived $Aβ_{40}$ > synthetic $Aβ_{42}$. (Adapted with permission from ref. 275 Copyright © 2016 American Association for the Advancement of Science). (e) Comparative analysis of the antiviral ability (neutralization) of $Aβ_{42}$ fragments lacking C-terminals (*i.e.*, $Aβ_{x-40}$) *versus* those retaining C-terminals (*i.e.*, $Aβ_{x-42}$) on Phil IAV H3N2-infected MDCK cells, emphasizing the crucial role of C-terminals in $Aβ_{42}$ in antiviral ability. (Reproduced with permission from ref. 254 Copyright © 2018 White *et al.*) (f) Antibacterial efficacy of peptides KK (red) and KY (blue) against *E. coli*. (Reproduced with permission from ref. 257 Copyright © 2019 MDPI (Basel, Switzerland).) (g) Antibacterial efficacy of peptides $K_3(FA)_4K_3$ and $K_6(FA)_4$ against *E. coli*. (Reproduced with permission from ref. 258 Copyright © 2020 American Chemical Society.) Amino acid residues of each AMP are color-coded to reflect their properties: polar uncharged residues in rose, polar charged residues in blue, and non-polar residues in yellow.

antimicrobial activity than samples from age-matched non-AD individuals, correlating with Aβ levels in the brain.[17]

In addition to microbial infection, there is growing evidence suggesting the potential involvement of viral infection in the development of AD.[276,277] Members of the herpes virus family, specifically HSV-1, HSV-2, CMV, and HHV-6, are frequently identified in the brains of AD patients, where they colocalize within Aβ plaques.[278,279] Intriguingly, direct interactions between Aβ and HSV-1 have been demonstrated both *in vitro* and *in vivo*. In these studies, Aβ was shown to bind to the surface glycoproteins of HSV-1, triggering a general protective viral entrapment response in various cell lines challenged with HSV-1. This response inhibited HSV-1 replication and upregulated miRNA-146.[21,280] Similarly, 5xFAD mice (a transgenic AD mouse model overexpressing human Aβ) subjected to hippocampal HSV-1 inoculation exhibited an improved survival rate compared to wild-type counterparts[251] (Fig. 13b). Beyond HSV-1, Aβ has demonstrated its ability to prevent infection of cultured cells by other viruses, including HHV-6,[251] as well as seasonal and pandemic strains of H1N1 and H3N2 of the influenza virus.[252]

The inherent oligomerization and fibrillization behavior observed in AMP function (as discussed in Section 2.2) suggests that the form of Aβ oligomers may not be inherently abnormal in the context of AD pathophysiology. Instead, Aβ oligomerization may occur as an adaptive response to optimize antimicrobial activities, akin to established AMPs. As illustrated in Fig. 13c, synthetic Aβ oligomers (referred to as amyloid-β-derived diffusible oligomeric ligands, ADDLs) exhibit higher potency against *Candida* compared to non-oligomerized peptides (*i.e.*, monomers and protofibrils).[275] In a separate comparative analysis, cell-derived Aβ, encompassing diverse polymorphic molecular forms, demonstrates superior antimicrobial and antiviral activity compared to homogenous synthetic Aβ[251,275] (Fig. 13d). Various hypotheses regarding the mechanism have been proposed, including (i) enhanced binding of soluble Aβ oligomers to microbial cell wall carbohydrates *via* a heparin-binding domain (VHHQKL);[275]

(ii) amyloidogenic-induced microbial agglutination, entrapping microbes in a network of β-amyloid;[281,282] (iii) insertion of Aβ oligomers into the lipid bilayer cell membrane;[283] and (iv) pore-forming ability of β-sheet-rich Aβ oligomers on the plasma membrane *via* toxic ion channels.[7] Considering the intrinsic properties of oligomeric Aβ, they are relatively unstable and can exist in various aggregation states, morphologies, and sizes,[284] thereby creating a diverse and polymorphic oligomer pool capable of targeting a broader spectrum of pathogens.

To date, over 40 distinct variants/isoforms of the Aβ peptide, featuring N- and C-terminal truncations, have been identified in secretory compartments and peripheral blood, forming a complex mixture with lengths ranging from 37 to 43 amino acids.[285,286] Among these, $A\beta_{1-40}$ is the most prevalent, while $A\beta_{1-42}$ is recognized as the most amyloidogenic and neurotoxic form.[287,288] Efforts to pinpoint the crucial antimicrobial domains of Aβ have involved extensive comparisons between full-length and truncated $A\beta_{x-40}$/$A\beta_{x-42}$. Regardless of the origin (synthetic or cell-derived), $A\beta_{1-42}$ consistently exhibits more robust antibacterial and antiviral activity than $A\beta_{1-40}$.[17,275] This is evident in lower minimum inhibitory concentration (MIC) values against the same types of microorganisms (Fig. 13d), emphasizing the significance of Ile41 and Ala42 located at the C-terminus of $A\beta_{1-42}$. The pivotal role of these domains is reinforced by observations that truncated $A\beta_{x-42}$ variants (*e.g.*, $A\beta_{22-42}$, $A\beta_{35-42}$) retain antimicrobial activities, while fragments lacking C-terminals (*e.g.*, $A\beta_{1-34}$, $A\beta_{1-28}$, $A\beta_{22-40}$, $A\beta_{33-40}$) lose such capabilities[254,255] (Fig. 13e). These differences likely arise from (i) the higher amyloidogenicity of $A\beta_{x-42}$, inducing agglutination and mediating oligomerization through a loop between Met35 and Ala42;[289] (ii) the heightened neurotoxicity of $A\beta_{x-42}$, directly inducing bacterial death;[287] (iii) the increased hydrophobicity of $A\beta_{x-42}$, leading to higher binding to the surface of microorganisms; and (iv) the enhanced uptake of bacteria by neutrophils for $A\beta_{x-42}$. Studies suggest an increased tendency for aggregation in N-terminal truncated $A\beta_{x-42}$ variants.[290,291] Accordingly, $A\beta_{22-42}$ demonstrates a notable ability to enhance neutrophil uptake of IAV and *E. coli*, surpassing that of the full-length $A\beta_{1-42}$.[254] However, further truncation to $A\beta_{35-42}$ decreases *E. coli* uptake, likely attributed to the absence of the β-turn-β confirmation formed by a salt bridge between Lys28 and Asp23.[254]

Given the robust anti-microorganism behavior of Aβ, numerous studies have explored variations inspired by its core motif. In one such investigation, two variables were introduced: N-methylation modification and the functionalization of gold nanoparticles (GNPs). These modifications were assessed for their anti-bacterial capabilities in comparison to fragments containing naked $A\beta_{32-37}$ (*i.e.*, CGGIGLMVG and CGGGGGIGLMVG). The results demonstrated a significant enhancement in antimicrobial efficacy with N-methylated peptides, further amplified when conjugated with GNPs.[256] Additionally, specific Aβ segments, namely GAIIG ($A\beta_{29-33}$) and KLVFFA ($A\beta_{16-21}$), have been identified as self-assembling building blocks capable of spontaneously forming a β-sheet amyloid core.[292,293] This intrinsic ability suggests potential fibrillization-mediated antimicrobial properties. Consequently, these segments were utilized as starting sequences for designing experimental functional scaffolds, including KYK-GAIIGNIK, KYRSGAITIGY, $K_3(FA)_4K_3$, and $K_6(FA)_4$. As anticipated, all these peptides demonstrated the capacity to self-assemble into amyloid fibrils, exhibiting a potent bactericidal effect against *E. coli*[257,258] (Fig. 13f and g).

4.2. Human islet amyloid polypeptide (associated with type 2 diabetes)

Presently, it is clear that type 2 diabetes (T2D) arises from a combination of factors, encompassing inadequate response to insulin (insulin resistance) and impaired insulin secretion by the pancreatic islet β cells. This culminates the elevated blood glucose level.[294,295] However, the precise pathological mechanisms underlying these processes remain elusive. On one hand, a pathological correlation exists between aggregated human islet amyloid polypeptide (hIAPP) and type 2 diabetes (T2D), evident in clinical observations where over 90% of T2D patients exhibit the presence of hIAPP deposits in the form of extracellular fibrillar aggregates within their pancreatic tissue.[296] It was postulated that alterations in the local microenvironment, particularly changes in the hydrophobicity of hIAPP, play a pivotal role in amyloid formation.[297] This, in turn, contributes to pancreatic β dysfunction, cell death, and ultimately triggers the onset of T2D.

On the other hand, recent studies have investigated into the connection between T2D and microbial infection/inflammation. Similar to the speculation in AD, hIAPP might also be produced as a form of inflammatory response to high levels of blood glucose or external pathogens. Clinically, the onset of T2D often coincides with or follows a pathogen infection, especially pancreatitis.[298] The microbiome plays a crucial role in both indirect and direct contributions to T2D development. Numerous studies have highlighted that gut microbial dysbiosis can indirectly contribute to the onset of T2D. When microbial dysbiosis occurs, it can lead to changes in the function and permeability of the intestinal barrier. This, in turn, has the potential to activate the innate immune system and modify signaling pathways, triggering low-grade inflammation, ultimately leading to insulin resistance and possibly T2D.[299,300] Moreover, direct infections by viruses (hepatitis C, cytomegalovirus),[301,302] bacteria (*H. pylori*, *Lactobacillus*, *C. pneumoniae*),[303–305] and fungi (*C. albicans*)[306] are also linked to an increased risk of developing T2D or worsening its symptoms. In this context, an elevated number of immune cells are detected in the pancreatic islets, accompanied by heightened levels of cytokines, chemokines, and IL-1.[307,308] These seem to be part of an immune response aimed at eliminating foreign intruders. This observation prompts consideration of whether hIAPP production might be a consequence of this inflammatory response, akin to the antimicrobial role of Aβ in AD.

Structurally, both hIAPP and AMPs share a net positive charge and exhibit amphipathic characteristics, crucial features enabling their interactions with negatively charged lipid

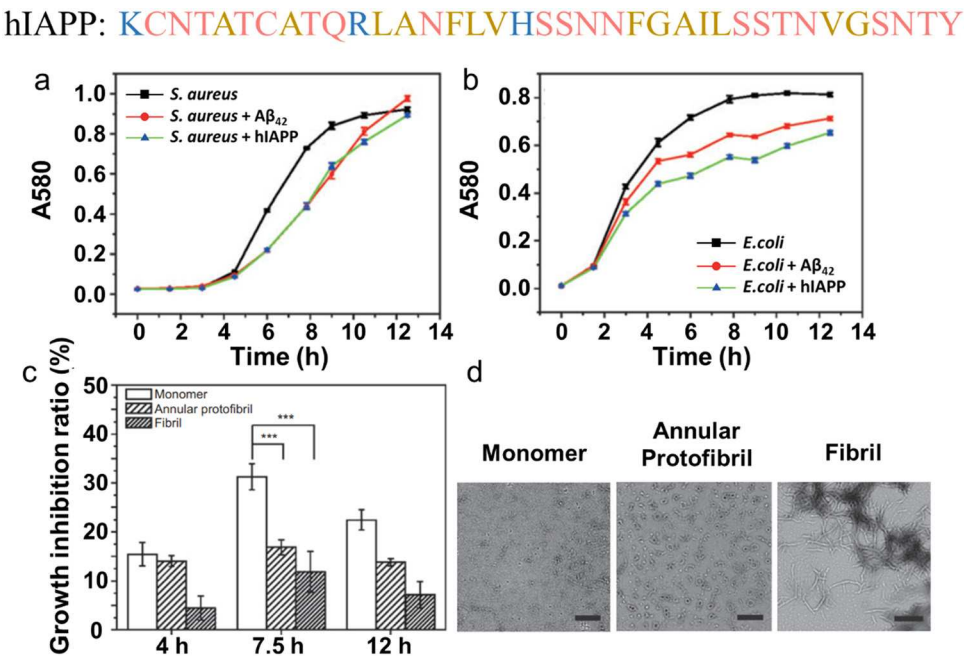

Fig. 14 Antimicrobial activity of hIAPP. Antibacterial efficacy of hIAPP against (a) *S. aureus* and (b) *E. coli*, in comparison to untreated and $A\beta_{42}$-treated bacteria, monitored by the turbidimetry method. A comparative analysis of (c) antibacterial activity and (d) morphology by TEM of monomeric, annular protofibrillar, and fibrillar hIAPP against *S. aureus*, with a decreasing order of antibacterial efficiency: monomers > annular protofibrils > fibrils. All scale bars represent lengths of 500 nm. (Reproduced with permission from ref. 14 Copyright © 2012 by Walter de Gruyter Berlin Boston.) Amino acid residues of each AMP are color-coded to reflect their properties: polar uncharged residues in rose, polar charged residues in blue, and non-polar residues in yellow.

membranes. Notably, hIAPP demonstrates antimicrobial activity against clinically relevant bacteria such as *S. aureus* and *E. coli* (Fig. 14a and b). Certainly, hIAPP demonstrated a significant inhibition of bacteria growth during the incubation period, particularly evident from 5 hours for *S. aureus* and 2 hours for *E. coli.* However, these differences gradually diminished as the incubation progressed, nearly disappearing at the end, possibly due to peptide degradation. In comparison to the extensively discussed $A\beta_{42}$ as a potent AMP (Section 4.1), hIAPP exhibited greater potency in inhibiting the growth of *E. coli*. Furthermore, the antimicrobial efficacy of hIAPP varied based on its amyloid states, with the ascending order of antimicrobial capacity being freshly-prepared hIAPP monomers > protofibrillar hIAPP > fibrillar hIAPP (Fig. 14c and d) at incubation timepoints of 4, 7.5, and 12 hours.[14] Our series of studies342 further confirmed hIAPP's antimicrobial properties against *S. aureus*, *S. epidermidis*, and *E. coli*. Due to variations in batches and concentrations of hIAPP tailored for distinct projects, the antimicrobial efficacy exhibited variability, with growth inhibition ranging from 14% to 36% for *S. aureus*, 8% to 53% for *S. epidermidis*, and 26% to 32% for *E. coli*. Overall, it is essential to emphasize that research focused on the antimicrobial properties of hIAPP is limited and ongoing. The exact mechanisms linking hIAPP aggregation, microbial infection, and T2D are still under exploration.

4.3. α-Synuclein (associated with Parkinson disease)

α-Synuclein (α-syn), a widespread protein prominently found in the brain, is linked to Parkinson's disease (PD) and other neurodegenerative conditions.[309] It has been established that the characteristic proteinaceous deposits of α-syn constitute the primary component of Lewy bodies and Lewy neurites, hallmark pathologies in PD, cortical Lewy body dementia (LBD), and multiple system atrophy (MSA).[310,311] Recently, α-syn and its fragment $\alpha\text{-syn}_{61-95}$ (also known as non-Aβ component, NAC) were identified in association with AD, accumulating with Aβ in senile plaques.[312] Consequently, strategies targeting the production, aggregation, spread, and degradation of α-syn have been actively pursued to combat these diseases.[313] Unfortunately, none of these approaches has successfully advanced to the clinical stage, reflecting the challenge of balancing the inhibition of α-syn pathological activities with the preservation of its physiological function. While the precise functions of α-syn remain elusive, compelling evidence suggests its role as a membrane protein in its physiological state. This is evident through (i) the localization of α-syn at pre-synaptic terminals of neurons, implying an association with membranes as synaptic vesicles are membrane-bound structures,[314] and (ii) the binding interaction between α-syn and synaptic membranes, facilitating its various cellular functions such as neurotransmitter release, synaptic vesicle trafficking, and cellular membrane fusion.[315–317] The affinity of α-syn for membranes can be attributed to favorable electrostatic interactions, particularly with the numerous positively charged lysine residues in the N-terminus of α-syn and the negatively charged phospholipid membranes. This binding mechanism closely resembles the working principle of AMPs, prompting further exploration of potential physiological functions of α-syn as an AMP through membrane-targeting models.[318,319]

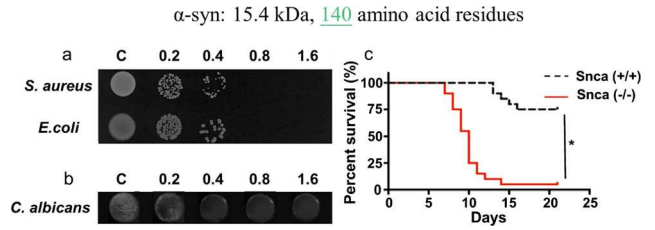

Fig. 15 Antimicrobial activity of α-synuclein. (a) Antibacterial efficacy of α-syn at 0.2–1.6 μM against *S. aureus* and *E. coli*, compared to untreated bacteria (control, C). (Reproduced with permission from ref. 15 Copyright © 2016 Elsevier Inc.) (b) Antifungal efficacy of α-syn at 0.2–1.6 μM against *C. albicans*, compared to untreated fungal (Ccntrol, C) (Adapted with permission from ref. 15 Copyright © 2016 Elsevier Inc.). (c) Antiviral efficacy of α-syn in inhibiting WNV growth, as indicated by the lower mortality rate in $Snca^{+/+}$ mice (wild type) than $Snca^{-/-}$ mice (homozygous knockout lack α-syn). (Reproduced with permission from ref. 259 Copyright © 2016 American Society for Microbiology.) Amino acid residues of each AMP are color-coded to reflect their properties: polar uncharged residues in rose, polar charged residues in blue, and non-polar residues in yellow.

Clearly, clinical observations suggest that patients undergoing antiviral therapy for hepatitis C virus (HCV) are less prone to developing PD,[320] indicating a potential link between pathogen exposure and PD risk. Similar implications arise regarding an elevated PD risk in patients with bacterial infections (*e.g.*, *Helicobacter pylori*) or fungal infections (*e.g.*, *Malassezia*).[321] While epidemiological studies have yet to establish direct associations between microbial infections and PD risk, let alone determine their sequential occurrence, at the molecular level, it is evident that full length $\alpha\text{-syn}_{1-140}$ can directly inhibit the growth of bacteria (*e.g.*, *Staphylococcus aureus* and *E. coli*, *etc.*, Fig. 15a), yeast (*e.g.*, *Candida albicans*, *Candida troppicalis*, *etc.*, Fig. 15b),[15] and mold (*e.g.*, *Aspergillus flavus*, *Aspergillus fumigatus*, and *Rhizoctonia solani*, *etc.*) with extremely high efficiency, as indicated by low MIC values ranging from 0.2 to 3.2 μM. When comparing different α-syn fragments with the full-length α-syn, an antimicrobial activity ranks as follows: $\alpha\text{-syn}_{1-140} > \alpha\text{-syn}_{1-95}$ (MIC = 0.8–3.2 μM) > $\alpha\text{-syn}_{1-60}$ (MIC = 1.6–12.8 μM) > $\alpha\text{-syn}_{61-140}$ (MIC > 25.6 μM) ≈ $\alpha\text{-syn}_{96-140}$ (MIC > 25.6 μM). This ranking highlights the crucial roles of highly conserved N-terminal region (1–65) compared to less conserved C-terminal region (96–140). Further investigation into the targeted sites of α-syn demonstrated that rhodamine-labeled α-syn accumulated on the cell surface of *E. coli*, while it accumulates in the cytoplasm of *C. albicans*. This suggests that α-syn interacts with bacterial membranes and fungal cytoplasmic compounds in microbial cells, leading to membrane leakage and inhibition of cell growth. Moreover, the endogenous neuronal expression of α-syn in a mice model has been demonstrated to inhibit the replication of viruses, such as West Nile virus (WNV) and Venezuelan equine encephalitis virus (VEEV).[259] This inhibition reduces the likelihood of viral infection, injury, and disease in the central nervous system, as evidenced by lower WNV viral titers and loads, along with a higher survival rate among mice (Fig. 15c).

A plausible deduction is that monomeric α-syn is produced as an AMP in response to immune activation, serving to protect and eliminate external threats. Once the threats are neutralized or eradicated, the body ideally returns to a state of equilibrium, and any remaining antimicrobial agents (*i.e.*, α-syn) are degraded or recycled. However, during this process, α-syn monomers may undergo aggregation before complete degradation, a phenomenon triggered by bacteria.[322] Consequently, all forms of α-syn, including monomeric, oligomeric, and aggregated forms, collectively contribute to inducing neuroinflammation. In this scenario, α-syn and immune responses appear to occur synchronously during infections, forming a self-reinforcing cycle. Any dysregulation of this coordination may transform the virtuous cycle of infection defense into a vicious cycle of neuroinflammation and neurodegeneration.

4.4. Prion protein (associated with prion disease)

Prion diseases, also referred to as transmissible spongiform encephalopathies (TSEs), constitute a spectrum of neurodegenerative disorders. This group includes Creutzfeldt–Jakob disease (CJD), fatal familial insomnia (FFI), kuru, Gerstmann-Sträussler-Scheinker disease (GSS), and variably protease-sensitive prionopathy (VPSPr) in humans.[323] Similar to other amyloid-forming peptides, the soluble cellular prion-related protein (PrP^{c}) undergoes a conformational change from α-helix to β-sheet during pathogenesis. This results in the formation of an insoluble protease-resistant isoform (PrP^{sc}), which further aggregates in the brain, forming deposits that contribute to the onset of neurodegenerative diseases. Importantly, PrPsc can act as a seed or template, binding with PrP^{c} and facilitating the PrP^{c}-to-PrP^{sc} conversion, thereby intensifying the progression of neurodegenerative diseases.[324] Unlike other amyloid diseases with uncertain transmissibility and infections, prion diseases are well-established to be transmissible between individuals, inducing chronic infection and/or disease in different species—presenting an additional potential pathological route for disease induction. Prnp-knockout mice lacking PrP expression are not susceptible to prion infection, emphasizing the inflammatory role of PrP in prion pathogenesis.[325] Increasing evidence suggests that the most infectious particles are PrP-folding intermediates, specifically small oligomers consisting of 12–24 monomers.[326,327] This aligns with the widely accepted notion that small oligomers of the misfolded protein are primarily responsible for neurotoxicity.[246]

In addition to the putative neurotoxicity attributed to misfolded amyloids, the loss of normal PrP^{C} function is considered integral to neurodegenerative processes. PrP serves diverse physiological functions, including cellular differentiation, neuronal excitability, myelin maintenance, and metal ion homeostasis.[328–331] Other studies have demonstrated an increase in PrP expression during bacterial infection[332] and inflammatory wounding/diseases,[163,333] suggesting that PrP may play a crucial role in inducing innate immune responses. PrP has been identified as an antimicrobial agent against both Gram-negative (*e.g.*, *E. coli*, *P. aeruginosa*) and Gram-positive

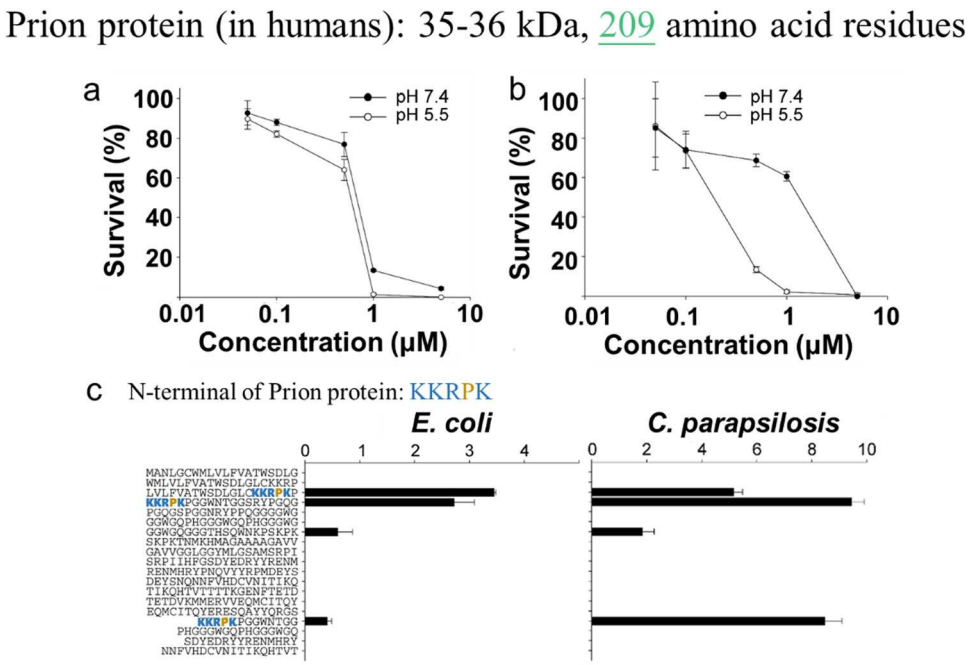

Fig. 16 Antimicrobial activity of prion protein. (a) Antibacterial efficacy of prion protein aginst *E. coli* in a concentration-dependent manner. (b) Antifungal efficacy of prion protein aginst *C. parapsilosis* in a concentration-dependent manner. (c) Antimicrobial efficacy of prion protein fragments, with and without KKRPK motif, agsinst *E. coli* and *C. parapsilosis*. (Reproduced with permission from ref. 163 Copyright © 2009 Pasupuleti *et al.*) Amino acid residues of each AMP are color-coded to reflect their properties: polar uncharged residues in rose, polar charged residues in blue, and non-polar residues in yellow.

bacteria (*B. subtilis*, *S. aureus*) (Fig. 16a), as well as fungi (*e.g.*, *C. parapsilosis*, Fig. 16b) under normal (pH = 7.4) and low pH (pH = 5.5) conditions.[163] When comparing the antibacterial effects of PrP with its truncated variants, a descending antimicrobial ability is observed in the order of $PrP_{23–231}$ > $PrP_{23–144}$ > $PrP_{90–231}$, highlighting the significance of the N-terminal region. A more detailed comparison between full-length and a series overlapping peptide sequences comprising 20 amino acids, as well as shorter variants, further emphasizes the importance of the N-terminal part of PrP, especially the unstructured N-terminal (KKRPK) region of the protein (Fig. 16c), which is mainly attributed to (i) the highly positive sequence of KKRPK interacting with negatively charged microbial membranes, (ii) the heparin-binding site enhancing the binding and disruption of microbial membranes, and (iii) the histidine-rich region coordinating interactions with metal ions (*e.g.*, Zn^{2+} and Cu^{2+}).[110,163] Substantial evidence suggests that the antimicrobial activity primarily depends on the formation of unstable oligomers, rather than mature amyloid fibrils, to disrupt bacterial membranes *via* a carpet or detergent model.[110] Despite significant efforts over the past two decades to investigate the pathological (infectious and neurotoxic) and physiological (antimicrobial) nature of prion proteins, a major gap persists in our understanding of the vicious loop involving PrP^{c}–PrP^{sc}-infections-PrP^{c}. Here, we propose two potential scenarios, with the hope that they prove useful for future research and validation: (i) the conversion of PrP^{c} to PrP^{sc} induces inflammatory infection and upregulation of antimicrobial PrP^{c} and (ii) external microbial threats induce PrP^{c} upregulation, leading to PrP^{c}–PrP^{sc} conversion.

4.5. Serum amyloid A (associated with systemic amyloid A)

Serum amyloid A (SAA), a highly conserved acute-phase protein present in nearly all mammalian species, is primarily synthesized by hepatocytes in the liver.[334] However, its production is not exclusive to hepatocytes, as various cells in extrahepatic tissues also contribute to its synthesis. The SAA family comprises four protein isoforms, each consisting of 104 amino acids. In humans, the acute-phase isoforms SAA1 and SAA2 (collectively referred to as SAA in this review) are prominently induced by inflammatory signals, particularly interleukin-1 beta (IL-1β), interleukin-6 (IL-6), and lipopolysaccharide (LPS) during the acute-phase response (APR). SAA3 is a pseudogene in humans. Human SAA4, identified as a constitutive isoform, is presumed to play a housekeeping role rather than serving as a responsive element to inflammation, constituting the most abundant serum SAA form in healthy individuals. Similarly, in mice, SAA1 and SAA2 are the major forms of SAA proteins produced by hepatocytes, while SAA4 is constitutively expressed. A notable distinction between human and mouse SAA lies in the SAA3 isoform, which codes for a functional SAA protein and emerges as the primary form in mouse inflammatory tissues.[335,336]

Originally identified as a major component of amyloid A (AA) fibrillar deposits associated with reactive systemic amyloidosis,[337] SAA has since been recognized for its dual role.

SAA primarily functions as an apolipoprotein of high-density lipoproteins (HDL), the principal carrier of SAA in the bloodstream, and acts as a secondary (reactive) precursor inducing pathological AA amyloidosis. In the absence of the acute-phase response (APR), SAA is constitutively produced at relatively low levels, contributing to the maintenance of lipid metabolism balance. APR process involves displacing apolipoprotein A1 (apoA1) *via* its N-terminal lipid binding sites (SAA1–15) to form acute-phase HDL. This modified HDL participates in various functions, including (i) regulating lipid metabolism and cholesterol efflux regulation;[338] (ii) recruiting immune cells (*e.g.*, monocytes and polymorphonuclear leukocytes) to sites of inflammation;[339] (iii) promoting the expression of several proinflammatory cytokines, such as TNF-α, IL-6, IL-8, IL-1β, and the growth-promoting granulocyte-macrophage colony-stimulating factor;[340] (iv) inducing directional migration of human mast cells;[341] and (vi) serving as an immune opsonin for Gram-negative bacteria, including *E. coli* and P. aeruginosa.[342] In normal cases, elevated SAA levels decline rapidly as inflammation resolves. However, any abnormal prolonged or excessive inflammation or infectious diseases can lead to pathological conditions, including secondary amyloidosis, where SAA contributes to the formation of amyloid deposits.

While a clear clinical association between SAA and inflammatory infections exists, the precise physiological role of SAA during microbial infection remains elusive. The bacteriotoxicity of SAA was initially observed in 1992 during an investigation utilizing *E. coli* to express recombinant SAA at high production levels. This expression led to a notable decrease in the volume of cells, reaching 70–80% of the initial volume within 2 hours, indicative of cell lysis[260] (Fig. 17a). Subsequent studies confirmed that SAA toxicity is connected to the formation of ion channels in the bacterial membrane,[119] resembling the behavior observed in other amyloid peptides.[117,343,344] The formation of such channels is attributed to both host cell damage and antimicrobial activity. On one hand, it particularly affects cells in the kidney, liver, and spleen, which require electrically tight membranes for their ionic exchange functions. This is supported by clinical evidence that renal dysfunction is the most common symptom at the onset of AA amyloidosis.[345] On the other hand, amyloid-forming SAA variants (*e.g.*, human

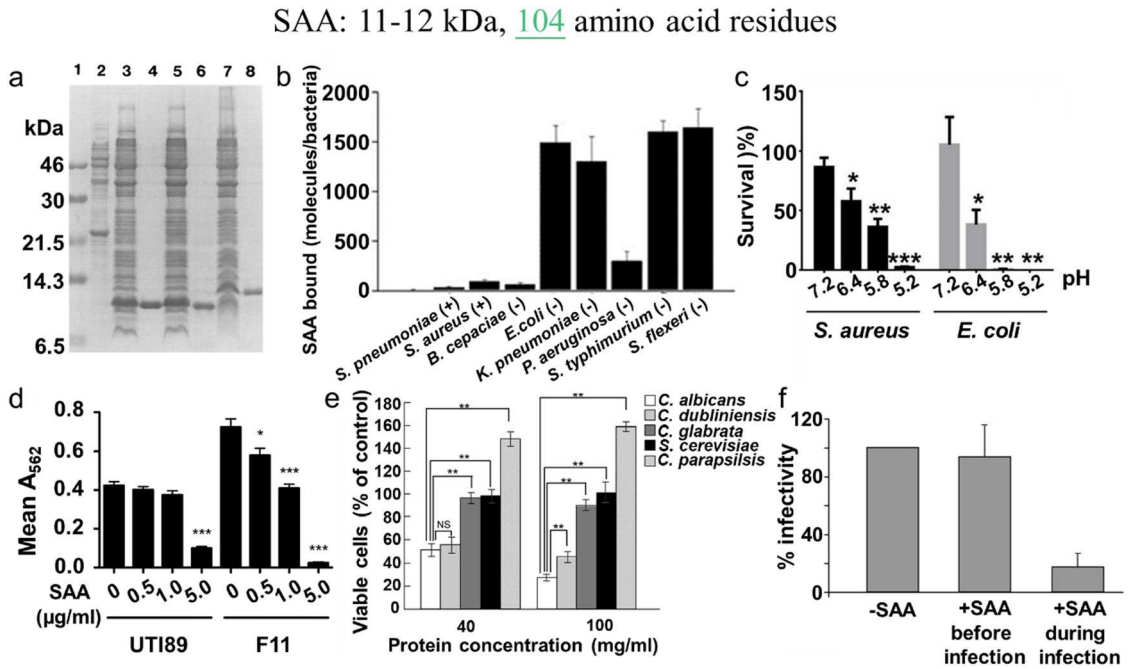

Fig. 17 Antimicrobial activity of serum amyloid A (SAA). (a) Antibacterial efficacy of recombinant SAA against *E. coli*, as indicated by the presence of *E. coli* lysates subsequent to SAA expression in *E. coli*. Lane 1: molecular weight markers. Lane 2: lysates of non-induced *E. coli*. Lane 3,5,7: lysates of *E. coli* expressing SAA1, SAA2, SAA4. Lane 4,6,8: purified rSAA1, rSAA2, rSAA4. (Reproduced with permission from ref. 260 Copyright © 1994 Published by Elsevier B.V.) (b) Stain-selective antibacterial efficacy of SAA. Where SAA binds to Gram-negative bacteria while not interacting with Gram-positive bacteria. (Reproduced with permission from ref. 164 Copyright © 2005 Elsevier Inc.) (c) pH-dependent antibacterial efficacy of SAA against *S. aureus* and *E. coli*., highlighting its enhanced antibacterial activity under acidic conditions. (Reproduced with permission from ref. 16 Copyright © 2020 Elsevier Inc.) (d) Antibacterial efficacy of SAA against uropathogenic *E. coli* (UPEC, *e.g.*, UTI89 and F11) through the inhibition of their biofilm formation. Biofilm levels were quantified by measuring A_{562}. (Reproduced with permission from ref. 261 Copyright © 2012 Erman *et al.*) (e) Stain-selective antifungal efficacy of rhSAA, where rhSAA exhibits anti-fungal activity specifically against *C. albicans* or closely related species of *C. dubliniensis*, excluding other fungal species. (Reproduced with permission from ref. 262 Copyright © 2019 American Society for Microbiology.) (f) Antiviral efficacy of SAA against Huh-7 cells infected by HCVpp. (Reproduced with permission from ref. 263 and 264 Copyright © 2016 American Association for the Study of Liver Diseases.) Amino acid residues of each AMP are color-coded to reflect their properties: polar uncharged residues in rose, polar charged residues in blue, and non-polar residues in yellow.

SAA1, mouse SAA2) can effectively induce bacterial lysis, a capability not shared by SAA4. This distinction highlights the essential requirements of a β-pleated sheet confirmation and the hydrophobicity of the N-terminus to interact with the hydrophobic component of the bacterial cell.[119] This interaction occurs with high affinity (K_D = 10^{-7}–10^{-8} M) and in a rapid manner (~15 minutes).[164] In addition to *E. coli*, SAA exhibits binding affinity with a diverse array of Gram-negative bacteria, including *S. typhimurium*, *S. flexneri*, *K. pneumoniae*, *V. cholerae*, and *P. aeruginosa*, while showing no binding affinity for Gram-positive bacteria such as *S. pneumoniae* and *S. aureus* (Fig. 17b). This strain-specific binding capability is closely linked to the outer membrane protein A (OmpA)/OprF family conserved ligands, present in nearly all Gram-negative bacteria. These ligands act as opsonins, enhancing bacterial clearance by modulating macrophages and neutrophils.[164,342] OmpA-deficient *E. coli* or OprF-deficient *P. aeruginosa* did not bind to SAA, underscoring the role of SAA as a pattern-recognition innate immune protein.[164]

Clinically, investigations into the bactericidal activity of SAA have systematically explored different microenvironments and utilized distinct gene knockout mouse models to understand its efficacy in various infectious diseases. In comparison to physiological neutral conditions, SAA has demonstrated heightened bactericidal activity under acidic conditions, particularly at pH 5.2 (Fig. 17c). This suggests its potential as an effective antibacterial agent in addressing cutaneous infections, a characteristic environment of the skin surface. This effectiveness was further demonstrated using SAA1/2 double knockout mice (SAA1/2 DKO), which exhibited impaired clearance of *S. aureus* during cutaneous infections.[16] Similarly, SAA1/2 DKO mice proved to be more susceptible to dextran sodium sulfate (DSS)-induced colitis, showcasing increased weight and blood loss, along with higher histological disease scores compared to wild-type controls.[346] A robust mouse urinary tract infections (UTI) model utilized the introduction of uropathogenic *E. coli* (UPEC, *e.g.*, UTI89 and F11) into the urinary tract to induce SAA expression. The results revealed heightened levels of SAA1/2 in response to UTI, demonstrating its role in blocking biofilm formation by uropathogens[261] (Fig. 17d).

In addition to its antibacterial function, SAA also exhibits anti-fungal activity against Candida albicans. The potential anti-fungal properties of recombinant SAA were initially demonstrated in 1990, showcasing its role as a potent activator that enhances calcium mobilization, cell-surface antigen expression, lactoferrin secretion, phagocytosis, and the anti-Candida activity of polymorphonuclear cells.[347] However, direct evidence of SAA's anti-fungal capabilities became clearer in 2019 when a systemic infection model was employed. In this model, mouse SAA1 was upregulated following the induction of *C. albicans* infection. During the infection, both human and mouse recombinantly expressed SAA1 exhibited species-specific anti-fungal activity by binding to the surface of *C. albicans* or closely related species of *C. dubliniensis* (but not *C. glabrata*, *S. cerevisiae*, and *C. parapsilsis*) cells (Fig. 17e). This binding disrupted the integrity of the fungal cell membrane, leading to cell death.[262] Further investigation by the same research group delved into the molecular mechanisms of SAA1's anti-fungal activity and indicated that SAA1 mainly targets Als3 (agglutinin-like sequence 3), a cell wall adhesin of *C. albicans*, inducing rapid cell aggregation and subsequent death.[348]

Upregulated expression of SAA has been observed in various viral infections affecting both animals and humans. For instance, SAA levels were notably elevated in COVID-19 patients at the onset of hospitalization, even in cases with mild respiratory symptoms. This highlights SAA's potential as an effective predictive factor for severe COVID-19, demonstrating an accuracy of 89%.[349,350] Additionally, SAA has been reported to exhibit antiviral activity against the hepatitis C virus (HCV) by inhibiting its entry into cells. However, this antiviral activity is limited to the timing of SAA addition and virus adsorption (*i.e.*, SAA addition during infection > SAA addition before infection)[263,264] (Fig. 17f). Another study demonstrates the antiviral effect of SAA by directly binding to the influenza A virus (IAV) and enhancing the uptake of the virus by neutrophils.[351] SAA has demonstrated the capacity to block HIV-1 infection of host cells through CCR5 receptors. Notably, SAA emerges as one of the initial systemic antiviral responses to HIV-1, detected as early as 5–7 days before the first detection of plasma viral RNA and significantly earlier than other systemic cytokines.[352]

5. Cross-seeding between antimicrobial, bacterial-secreted, and amyloid peptides

The concept of cross-seeding between AMPs, bacterial-secreted peptides, and amyloid peptides is supported by several lines of indirect evidence. Firstly, the co-existence and often co-localization of these peptides in various tissues, blood vessels, and spinal fluids have led to conceptual frameworks proposing molecular interactions and cross-seeding among these diverse peptide aggregates. Secondly, additional evidence from previous sections has demonstrated the alternative antimicrobial activity of certain AMPs (AMPs) and the amyloid-like aggregation property of specific amyloids (AMYs), as well as some shared sequential and structural features in both AMPs and AMYs. Thirdly, some investigations into cross-seeding among amyloid peptides, particularly in cases where (i) multiple neuropathologies co-occur in patients with two or more forms of dementia and (ii) both amyloid aggregation and microbial infection are observed, confirm that such co-occurrences can be key pathological causes of neurodegenerative diseases.[353] Building on the aforementioned findings and logical connections, the cross-seeding concept appears to offer a plausible explanation for both direct and indirect molecular crosstalk and spreading mechanisms between neurodegenerative diseases and microbial infections. These cross-seeding interactions involve the mutual modulation of peptide aggregations in a transmissible manner, both *in vitro* and *in vivo*. The identified

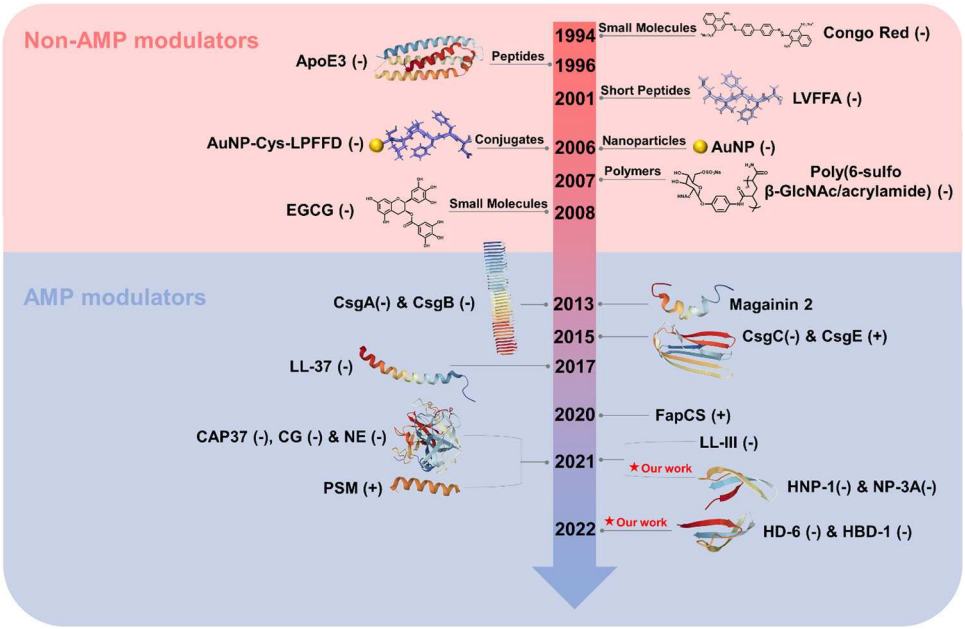

Fig. 18 Historical literature review of the first-discovered or important amyloid modulators including both non-AMPs and AMPs. The inclusion of a negative (−) or positive (+) sign in brackets denotes the amyloid inhibition or promotion effect by these modulators.

cross-seeding systems between antimicrobial peptides, bacterial-secreted peptides, and amyloid peptides are still limited. However, antimicrobial peptides, owing to their intrinsic antimicrobial activity, represent a vast and native resource that has been relatively underexplored for repurposing as potential and effective amyloid inhibitors (Fig. 18). Hence, gaining a comprehensive understanding of the new functions of AMYs and AMPs, along with the molecular events that underlie their cross-seeding, spreading, and crosstalk in mixed pathologies, is of paramount importance for the development of new therapeutic strategies.

5.1. Cross-seeding between antimicrobial peptides and amyloid peptides

Amyloid peptides (AMYs), traditionally associated with neurodegenerative diseases, have a strong tendency to aggregate into fibrillar formation, contributing to pathological processes. Conversely, antimicrobial peptides play a crucial role in the innate immune response, targeting and neutralizing microbial invaders. However, emerging research has unveiled unexpected intersections between these two peptide classes through a phenomenon known as cross-seeding. This cross-seeding interaction showcases how amyloid peptides can impact the behavior of antimicrobial peptides and *vice versa*. This underscores the intricate nature of peptide-peptide interactions, offering a rich avenue for exploring novel mechanisms, implications, and potential applications in the realms of health and diseases within the context of this cross-seeding phenomenon.

5.1.1. Defensins and Aβ, hIAPP, hCT. Recently, four defensins—human neutrophil peptide (HNP-1), rabbit neutrophil peptide (NP-3A), human α-defensin 6 (HD-6), and human β-defensin 1 (HBD-1)—have demonstrated multi-targeting, dual-functional properties.[23,24] These defensins exhibit the ability to not only prevent the aggregation of three amyloid peptides associated with various conditions; Aβ (linked to Alzheimer's disease), hIAPP (linked to Type 2 Diabetes), and hCT (linked to medullary thyroid cancer), but also retain their original antimicrobial activity to kill four common microorganisms. Both HNP-1 and NP-3A, α-defensins featuring β-sheet structures, effectively inhibited the aggregation of Aβ, hIAPP, and hCT at sub-stoichiometric concentrations ($\leq$equimolar ratio) in a dose-dependent manner over 24–30 hours at 37 °C.[24] The ThT data presented in Fig. 19a clearly indicate that at an equal molar ratio, both HNP-1 and NP-3A enabled to completely suppress the amyloid fibril formation of the three different Aβ, hIAPP, and hCT, as evidenced by nearly 0% relative ThT intensity, instead of formation of the less-fibrillar, amorphous-like aggregates with disordered secondary structures. Consistently, another α-defensin, HD-6, demonstrated a comparable dose-dependent inhibition effect on the three amyloid aggregations. The increase of the HD-6 : amyloid molar ratio from 0.005 to 1 resulted in a significant reduction in ThT signals for Aβ from 11 to 94%, hIAPP from 16 to 49%, and hCT from 35 to 93% (Fig. 19b).[23] This HD-6-induced amyloid inhibition effect led to the formation of less-fibrillar, amorphous-like aggregates, while retaining the original disordered structures. In the HBD-1:amyloid systems across various molar ratios (1 : 0.005–1 : 1), HBD-1 notably decreased ThT fluorescence (a marker for amyloid fibril presence) by 44–93%, reduced the rate of aggregation (halving the aggregation time) by 71–96%, postponed the shift towards β-structures, lowered β-structure content by 4–28%, and broke down mature, larger, and thicker fibrils into smaller, thinner forms. Comprehensive evaluations using ThT, CD, AFM, and SPR methods

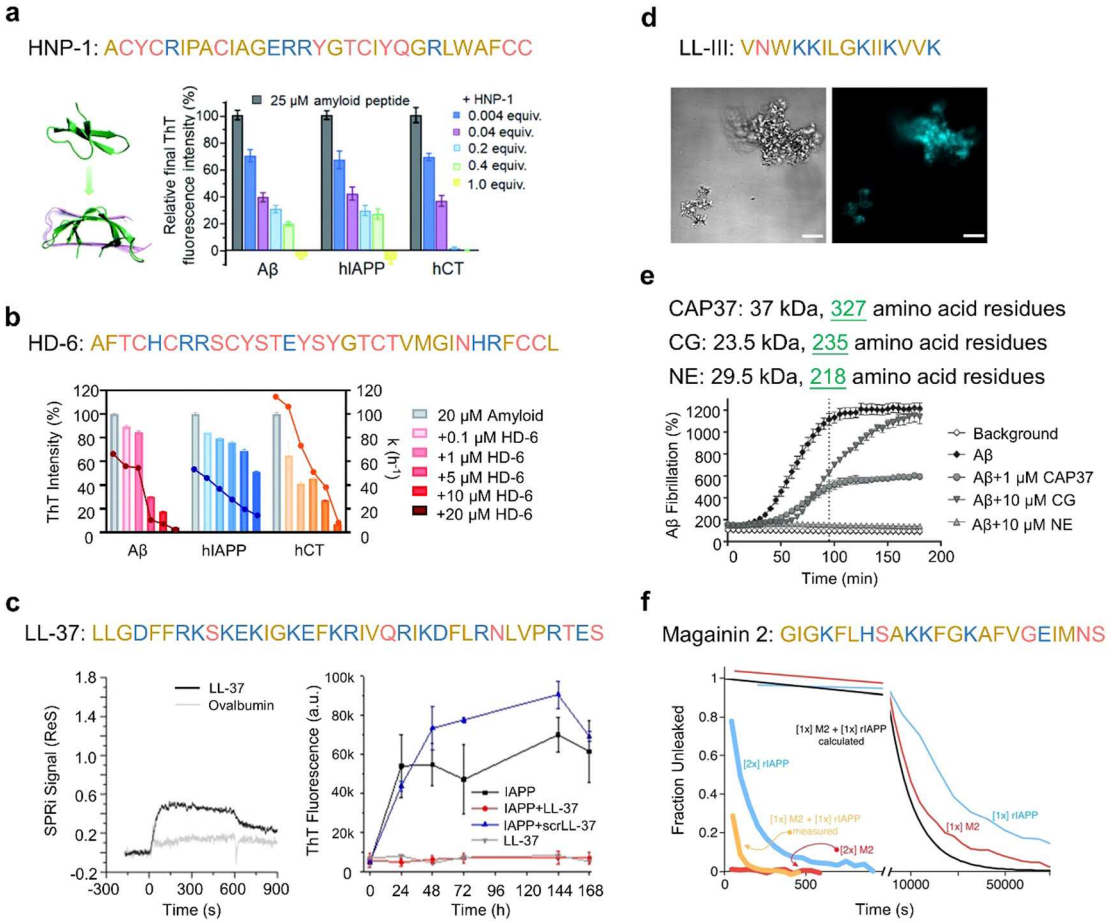

Fig. 19 Identified cross-seeding systems between antimicrobial peptides and amyloid peptides, including (a) HNP-1 and Aβ, hIAPP, hCT by ThT, (Reproduced with permission from ref. 24 Copyright © 2021 The Royal of Chemistry) (b) HD-6 and Aβ, hIAPP, hCT by ThT, (Reproduced with permission from ref. 23 Copyright © 2022 The Royal of Chemistry) where both HNP-1 and HD-6 exhibit a general inhibition property against the fibrillization of different amyloid peptides. (c) LL-37 and $Aβ_{42}$ by SPR imaging (Reproduced with permission from ref. 25 Copyright © 2017 IOS Press) and LL-37 and hIAPP by ThT, (Reproduced with permission from ref. 26 Copyright © 2020 John Wiley & Sons, Inc.) where LL-37 acts as a nanomolar inhibitor to prevent the fibril formation of both Aβ and hIAPP and their associated cell toxicity; (d) LL-III and α-synuclein by phase-contrast light and fluorescence microscopy, (Reproduced with permission from ref. 354 Copyright © 2021 MDPI (Basel, Switzerland)) where the addition of LL-III to a monomeric α-synuclein solution facilitates the formation of LL-III-enriched droplet clusters, effectively preventing the conversion of α-synuclein into mature fibrils; (e) CAP37, CG, NE and Aβ by ThT, (Reproduced with permission from ref. 355 Copyright © 2021 Bentham Science Publishers) where CAP37 (circles), CG (inverted triangles), and NE (triangles) inhibit the kinetic aggregation of Aβ through different pathways, with varied inhibition efficiencies ranked in a decreasing order of NE > CAP37 > CG. (f) Magainin 2 and rIAPP by liposome leakage assay, (Reproduced with permission from ref. 18 Copyright © 2013 National Academy of Science) where magainin 2 and rIAPP exhibit full cross-cooperativity, leading to equilibrium membrane leakage that is 100 times greater than the simple sum of the activities of individual peptides. Amino acid residues of each AMP are color-coded to reflect their properties: polar uncharged residues in rose, polar charged residues in blue, and non-polar residues in yellow.

across different amyloid–defensin systems highlight that the defensins amyloid aggregation inhibitory effects depend on both dosage and peptide sequence. Significant observations include: (i) HD-6 and HBD-1 exhibit sequence-specific effectiveness in inhibiting amyloid aggregation, ranked as Aβ > hCT > hIAPP for HBD-1 and in the order hCT > Aβ > hIAPP for HNP-1 and NP-3A. (ii) At lower concentrations, α-defensins more effectively slow the expansion of amyloids from smaller to larger aggregates, while at higher doses, they primarily prevent the formation of amyloid nuclei during the lag phase. These differences indicate the existence of interspecies energy barriers that influence the interactions between different α-defensins and amyloid proteins.

The four defensins also exhibited a dose-dependent protective role in rescuing cells from amyloid-induced toxicity to varying extents. Specifically, in the presence of three amyloid peptides, HNP-1 improved cell viability by 23–28%, NP-3A by 12–35%, HD-6 by 7–55%, and HBD-1 by 32–51%, while reducing cell toxicity by 9–31%, 10–31%, 11–33%, and 16–25%, respectively. The aggregated cellular data indicate various potential mechanisms through which defensins could reduce amyloid-induced toxicity. Potent interactions between defensins and amyloid peptides may lessen the creation of harmful amyloid aggregates known to disrupt cell membranes, resulting in the formation of defensin–amyloid complexes that are either less toxic or non-toxic and relatively harmless to cell

membranes. Additionally, defensins may competitively decrease the binding propensity of amyloids to cell membranes, collectively endowing defensins with an improved cell protection function. On the other hand, cross-seeds of defensins with the three different amyloid peptides generally demonstrated comparable or even higher antimicrobial efficiency than the corresponding pure amyloid peptides or defensins.

Considering that β-rich configurations are prevalent in amyloid aggregates independent of sequence, the ability of α-defensins to inhibit amyloids in a sequence-independent manner mainly stems from their interaction with amyloid proteins *via* β-structure engagements. This interaction is explained by the ''conformational selection binding'' mechanism, which suggests that defensins with β-structures, or any peptides capable of forming β-structures, are predisposed to engage with amyloids that share similar β-structural features. This mechanism competitively reduces amyloid–amyloid interactions, thereby preventing amyloid aggregation of Aβ, hIAPP, and hCT, along with the resultant amyloid-induced toxicity. Additionally, it contributes to antimicrobial protection.

5.1.2. LL-37 and $A\beta_{42}$, hIAPP. The human cathelicidin peptide LL-37, functioning as both an innate immune effector and modulator, demonstrates a wide-ranging antimicrobial and immunomodulatory activity. LL-37 was discovered to interact with Aβ at nanomolar affinity,[42] and it also demonstrated the ability to effectively inhibit the formation of $A\beta_{42}$ oligomers and fibrils by impeding β-structure formation.[25] The cross-seeding phenomenon between LL-37 and Aβ is likely attributed to their evident sequence complementarity. $A\beta_{42}$ carries a net negative charge of -3, in contrast to a net positive charge of +6 in LL-37, fostering robust electrostatic attraction. $A\beta_{42}$ comprises 11 hydrophobic residues, including 4 aromatic residues (F or Y), while LL-37 possesses nine hydrophobic residues with 4 aromatic residues, thereby introducing additional hydrophobic associations and π–π interactions for cross-seeding. Furthermore, while both LL-37 and $A\beta_{42}$ display individual toxicity and proinflammatory effects on the neuroblastoma cell line SH-SY5Y through the stimulation of microglial production of inflammatory cytokines, co-incubation of LL-37 and $A\beta_{42}$ leads to cross-seeding, which significantly reduces their cytotoxic impact on neurons. Although there is no direct correlation observed between cathelicidin expression levels and AD, *in vitro* cross-seeding of Aβ and LL-37 serves a foundational exploration to investigate common factors related to both peptides and their impact on biophysical activities and signaling functions. Notably, both Aβ and LL-37 have been reported to regulate the same Formyl-like Peptide Receptor 1 (FPRL1). This receptor plays a role in phagocyte responses within the inflammatory aspects of AD, particularly influenced by the reduced presence of LL-37.[356]

Similarly, considering the presence of both LL-37 and hIAPP in the pancreas and their notable (42%) sequence similarity, LL-37 has been identified to interact with hIAPP with nanomolar affinity. This cross-seeding mechanism proves effective in preventing hIAPP aggregation and associated pancreatic β-cell damage and neuroinflammation in vitro.[26] The inhibitory action of LL-37 is achieved by its attachment to (1) initial hIAPP species, encapsulating them into soluble, non-fibrillar mixed complexes, and (2) established hIAPP fibrils, transforming them into assemblies that cannot seed further aggregation (Fig. 19c). LL-37 emerges as having a significant connection to the pathogenesis of T2D through various pathways, *e.g.*, LL-37 has been observed to suppress pancreatic β-cell inflammation in a mouse model, while concurrently promoting insulin and glucagon secretion, ultimately enhancing islet function.[357] These studies suggest a potential protective role for LL-37, acting as a molecular inhibitor of both Aβ and hIAPP, in the pathogenesis of both AD and T2D. Particularly noteworthy is the resemblance of sporadic AD to what is often termed as 'type 3 diabetes' occurring in brain tissue.[358]

5.1.3. LL-III and α-synuclein. LL-III, which is extracted from the venom of the eusocial bee *Lasioglossum laticeps*, exhibited remarkable interactions with both monomers and condensates of α-synuclein in the droplet phase, effectively stabilizing the condensate and inhibiting its maturation to the fibrillar state.[354] As illustrated in Fig. 19d, the co-incubation of LL-III (50 μM) and monomeric α-synuclein (100 μM) facilitated the formation of droplet condensates, likely through significant partitioning within the droplet phase. The increase in LL-III concentrations to 200 or 500 μM further enhanced the association of more droplets, with both the size and quantity of the droplets increasing with higher LL-III concentrations. During the period of droplet formation, only random conformations were detected in the mixed solution of LL-III and α-synuclein. This clearly indicates that LL-III interacts efficiently with monomeric α-Syn within the droplet phase, stabilizing the condensate and preventing the amyloid fibril formation of α-synuclein. The cross-seeding interaction between LL-III and α-synuclein is primarily governed by a combination of electrostatic interactions in the unstructured N-terminal domain and hydrophobic interactions in the NAC region. LL-III showcases its anti-aggregation activity in a cellular model by mitigating α-synuclein aggregation in neuronal cells and related cell death, in addition to its intrinsic activities against various bacterial strains, fungi, and cancer cells. Such dual functionality of antimicrobial peptide LL-III enables it to target and neutralize various cell types by preventing their transition into the fibrillar amyloid state associated with the pathologies of Parkinson's disease.

5.1.4. CAP37, CG, NE and Aβ. Three neutrophil granule peptides—cationic antimicrobial protein of 37 kDa (CAP37), cathepsin G (CG), and neutrophil elastase (NE)—demonstrate the ability to interact with $A\beta_{42}$ and inhibit $A\beta_{42}$ fibrillation through distinct pathways. ThT results showed that CAP37 and NE predominantly inhibit the elongation phase, while CG primarily inhibits the nucleation phase during the $A\beta_{42}$ fibrillation process (Fig. 19e). ELISA assays further revealed that $A\beta_{42}$ exhibited similar binding to both CAP37 and CG in the presence and absence of protease inhibitors, but $A\beta_{42}$ appeared to bind to NE only in the presence of protease inhibitors. This suggests that the cleavage of $A\beta_{42}$ by these three peptides is correlated with their subsequent inhibition efficiency. NE and

CG efficiently cleaved $A\beta_{42}$, impeding its aggregation into fibrils. In contrast, CAP37, while not efficiently cleaving $A\beta_{42}$, exerted its inhibition effect most likely through a quenching mechanism. Moreover, only CG and NE showed significant inhibition of Aβ neurotoxicity, with CG being more efficient than NE. The varied inhibition efficiencies of these peptides in a decreasing order of NE > CAP37 > CG are likely attributed to their ability to cleave Aβ and bind to Aβ, suggesting distinct mechanisms of action in their anti-amyloid activities.[355]

5.1.5. Magainin 2-rIAPP. Magainin 2 (M2), a 23-residue broad-spectrum antimicrobial peptide initially identified in Xenopus laevis, exhibits its bactericidal activity through membrane leakage. M2 and rIAPP share structural and functional features in the context of cell membranes, undergoing a structural transition from random coils to amphipathic α-helix upon binding to the cell membrane. Both peptides also display common membrane permeation characteristics, including stochastic initiation of leakage, a subsequent evolution of leakage, and the formation of equilibrium pores. The cross-seeding of rIAPP and magainin 2 leads to the formation of stable pores in liposome membranes,[18] causing a significant >100-fold increase in liposome leakage beyond the sum of their activities of hIAPP and magainin 2 alone (Fig. 19f). This cross-seeding also results in >2000-fold growth inhibition of the Gram-negative bacterium Paracoccus denitrificans.

The limited studies on AMPs-AMYs systems indicate that cross-seeding can cooperatively induce membrane leakage and bacterial cell death through different mechanisms. In some cases, both AMPs and AMYs show strong antimicrobial activity. The discovery of antimicrobial peptides with β-structure, which can simultaneously inhibit microbial infection and amyloid aggregation, expands their potential as multi-target amyloid inhibitors. These AMPs, while existing in limited quantities, provide a molecular foundation for further engineering and designing new variants. These variants could combine antimicrobial, anti-amyloid, and immunomodulatory functions, making them promising candidates for multifunctional drugs in combating both microbial infections and amyloid-related issues. These multiple-functional AMPs introduce a novel concept, resembling ''killing two birds with one stone.'' This concept successfully integrates the ''amyloid cascade hypothesis'' with the ''microbial infection hypothesis''. The functional and structural links between antimicrobial peptides and amyloid proteins illustrate their natural abilities in both bacterial elimination and amyloid suppression functions.

5.2. Cross-seeding between bacterial-secreted peptides and amyloid peptides

The gut-brain axis, involving bidirectional communication between the gut and the brain, has garnered significant interest due to its potential relevance in human disease and health. Throughout this axis, the gut and the brain are interconnected systems that can influence each other's functioning, thus representing a possible connection between the gut microbiome, their metabolites, and neurological disorders. Recent research presented compelling evidence supporting the notion that symptoms of Alzheimer can be transferred to a healthy young organism through the gut microbiota, establishing a causative role that gut microbiota may have in the disease.[359] A growing body of symptomatic, physiological, and pathological data suggest that cross-seeding occurs between microbial amyloid curli presented in the gut and amyloid peptides found in the brain.[27,360–362] Curli fibrils are assembled through bacterial secretion of unfolded amyloid proteins (*e.g.*, CsgA, CsgC, CsgE, FapCS) (Fig. 20a). Interestingly, these curli fibrils exhibit some similarities to amyloid fibrils, including self-aggregation into β-rich fibrils, surface adhesion to epithelial cells, and participation in bacteriophage defense mechanisms. Biochemical studies have provided compelling evidence that the native bacterial chaperones of curli possess the ability to interact with diverse human amyloid proteins, thereby influencing their aggregation pathways *in vitro* and *in vivo*, including αSyn,[27–29,322] Aβ,[29] Tau,[363] hIAPP,[364,365] and cellular prion protein (PrP^C).[366] Specifically, In the *in vivo* study of curli-producing *Escherichia coli* (CsgA) in mice[27] and in worm,[367] a promotion of αSyn aggregation and inflammation was observed in both the gut and the brain, leading to a worsening of motor impairment and gastrointestinal (GI) dysfunction. However, in the two cases of variants of CsgA that were incapable of forming amyloids and the introduction of an amyloid inhibitor that prevented CsgA expression in the gut, they both did not affect αSyn aggregation in the brain of mice. Different from the cross-β amyloid conformation characteristic of curli fibrils, phenol-soluble modulins (PSM) are amyloidogenic proteins originating from *Staphylococcus aureus* that adopt a cross-α fibrillar structure.[368] Both CsgE and PSMα have been observed to accelerate αSyn amyloidogenesis in vitro[28,369] (Fig. 20b). The higher cross-α content observed in PSMα3 has been associated with an augmented promotional effect on the aggregation of $A\beta_{40}$,[370] implying a highly diverse conformational interplay in cross-seeding interaction (Fig. 20c). Remarkably, pre-formed CsgA seeds have also been identified as accelerators of Aβ aggregation, and it is noteworthy that fibrillation inhibitors are shared between CsgA and Aβ.[371] Similarly, Aβ displayed favorable binding with FapC amyloid fragments (FapCS) of *Pseudomonas aeruginosa*, leading to the acceleration of cross-seeding fibrils (Fig. 20c).[34] FapCS acted as a catalyst and propagated its structural characteristics for promoting Aβ amyloidogenesis *in vitro*, *in silico*, and in a zebrafish model of AD. The robust seeding capacity for Aβ by FapCS induced multiple pathological indicators, including behavior, cognitive memory function, cerebral Aβ burden, synaptic health, production of reactive oxygen species (ROS), and cell degeneration in both neuronal cells and zebrafish. Both CsgA and CsgB can cross-seed with the prostatic acid phosphatase fragment of $PAP_{248–286}$ (Fig. 20d). Acting as catalytic agents, they have a moderate impact on the nucleation rate and a significant effect on enhancing fiber growth from existing nuclei.[361] This suggests a more intricate scenario in which cross-seeding partially bypasses the nucleation step but has limited influence on fiber elongation.

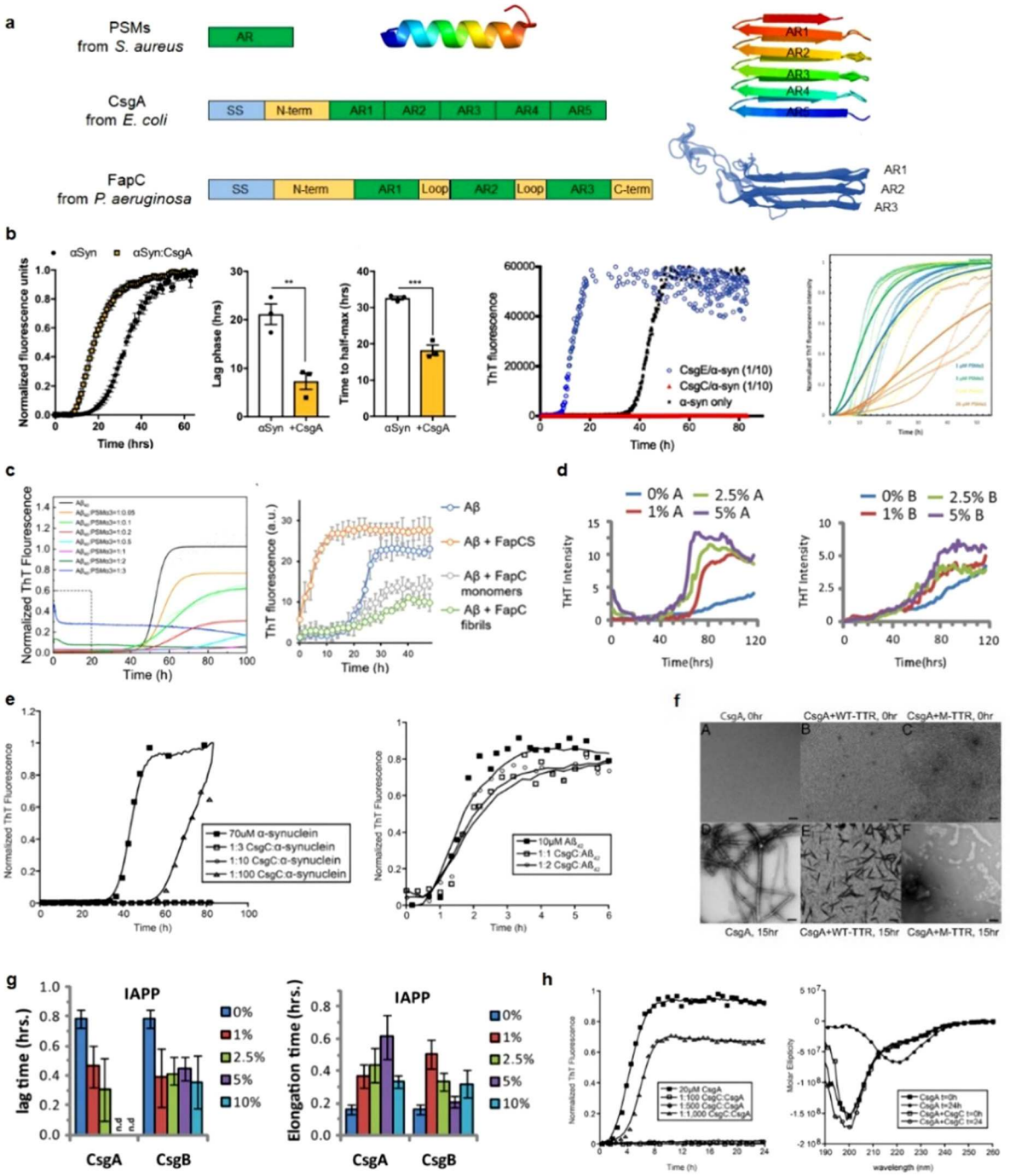

Fig. 20 Cross-seeding interactions between bacterial-secreted peptides and amyloid peptides. (a) Schematic representation of distinct bacterial biofilm-forming functional amyloids. Signal sequences (SS) are depicted in blue, amyloid regions (AR) in green, and loop/linker and terminus regions in yellow. PSMs are short proteins adopting a cross-α fibrillar structure (PDB: 5I55). CsgA forms a β-helix with five imperfect AR repeats stacking on top of each other (PDB: 8ENQ), while FapC also forms a β-helix with three ARs stacking on top of each other (FapC model modified from ref. 372 Copyright © 2018 The Authors). (b) CsgA (Reproduced with permission from ref. 27 Copyright © 2020 eLife Science Publications Ltd.) CsgE (Reproduced with permission from ref. 28 Copyright © 2015 Chorell *et al.*) and PSMα1 (Reproduced with permission from ref. 369 Copyright © 2021 MDPI (Basel, Switzerland)) have demonstrated the ability to accelerate αSyn amyloidogenesis. (c) PSMα3 exhibits a promotional effect on the aggregation of $A\beta_{40}$. (Reproduced with permission from ref. 370 Copyright © 2023 MDPI (Basel, Switzerland)). Similarly, FapCS plays a catalytic role in promoting Aβ amyloidogenesis. (Reproduced with permission from ref. 34 Copyright © 2023 John Wiley & Sons, Inc.) (d) Both CsgA and CsgB can cross-seed with the prostatic acid phosphatase fragment of PAP248-286, facilitating its conversion into the amyloid SEVI. (Reproduced with permission from ref. 361 Copyright © 2013 PeerJ. Inc.) (e) CsgC inhibits the amyloid assembly of αSyn, while demonstrating no inhibitory effect on $A\beta_{42}$ aggregation. (Reproduced with permission from ref. 29 Copyright © 2015 Elsevier Inc.) (f) TTR and its mutants selectively inhibit the conversion of CsgA into amyloid-like fibrils. (Reproduced with permission from ref. 373 Copyright © 2017 National Academy of Sciences) (g) Cross-seeding between CsgA/CsgB and hIAPP results in a reduction in the lag-time but a significant inhibition of hIAPP elongation.[361] (h) CsgC can inhibit CsgA amyloid formation at sub-stoichiometric concentrations and maintain CsgA in a non-β-sheet-rich conformation.[29]

In contrast to findings indicating that bacterial amyloid acts as a trigger, promoting amyloid aggregation through cross-seeding, some studies observed an opposite aspect: bacterial curli possesses a potent and selective inhibitor of amyloid formation. CsgC inhibited amyloid assembly of αSyn, while having no inhibition effect on $A\beta_{42}$ aggregation *in vitro* (Fig. 20e).[29] Human wild-type tetrameric transthyretin (TTR, associated with AD) and its mutants were found to exert a selective inhibitory effect on the conversion of CsgA into amyloid-like fibrils *in vitro* (Fig. 20f).[373] Notably, this effect was observed specifically with CsgA and not CsgB, indicating that the inhibitory mechanism is likely linked to its cross-seeding interaction with CsgA. Furthermore, transthyretin exhibited a comparable inhibitory effect on amyloid formation and subsequent toxicity induced by Aβ,[374,375] hIAPP,[376] and HypF-N[377] in both *in vitro* experiments and mouse models.

Adding to the complexity, the cross-seeding of Csg with various amyloid proteins led to intricate outcomes, which were dependent on the specific amyloid sequences and concentrations at play. When CsgA and CsgB were cross-seeded with hIAPP, they caused a reduction in the lag-time of hIAPP amyloid formation but significantly inhibited hIAPP elongation (Fig. 20g).[361] On the other hand, the impact of CsgA and CsgB on the fibrillization rate of $A\beta_{40}$ was more nuanced. The fibrillization rate demonstrated a modest decrease at lower concentrations of both CsgA and CsgB, while it slightly increased at higher concentrations.[361] These findings suggest that microbial amyloid proteins may possess broad cross-seeding activity, but they could serve as both an inhibitor and enhancer of amyloid fibrillization, influenced by the specific amyloid protein involved and the concentrations of the interacting components. Importantly, under exceptional instances, microbial amyloid proteins possess the capability to cross-seed with each other. CsgC was found to inhibit CsgA amyloid formation at sub-stoichiometric concentrations, effectively maintaining CsgA in a non-β-sheet-rich conformation (Fig. 20h).[29] These findings not only provide additional evidence of the intricate interactions between microbial amyloid proteins and their potential modulatory effects (either acceleration, inhibition, or both at different aggregation stages) on amyloid formation pathways, relevant to a conformational relationship underlying their cross-seeding interactions.

These findings along the gut-brain axis highlight the potential interplay and multifaceted nature between microbial amyloids and human amyloid proteins within the gut environment, with complex pathological consequences between amyloid aggregation and bacterial-induced inflammation.[27] Such interplay leads to an interesting hypothesis that exposure to microbial amyloids in the gastrointestinal tract might play a crucial role in accelerating amyloid aggregation and disease progression in both the gut and the brain. The presence of human and microbial amyloids in the circulation and cerebrospinal fluid opens possibilities for multiple cross-seedings between different pairs of amyloidogenic proteins. This includes cross-seeding between α-syn and hIAPP,[378] Aβ and hIAPP,[379] Aβ and α-syn,[380] Aβ and tau,[381] Aβ and transthyretin,[375] hIAPP and insulin.[382] Additionally, cross-seeding can also occur between human and microbial amyloid proteins, such as Natural silk from the silkworm Bombyx mori, the prion protein Sup35 from the yeast Saccharomyces cerevisiae, and the curli protein CsgA from the bacterium *Escherichia coli*, all of which have been shown to enhance the amyloidosis of amyloid protein A (AA) in mice.[36] The cross-seedings between various amyloidogenic proteins, originating from both human and microbial sources, adds another layer of complexity to the gut-brain axis and its association with amyloid-related diseases, microbial-related pathologies, and other neurological disorders such as autism spectrum disorder, depression, and anxiety. This growing understanding of the intricate connections between the gut microbiome, amyloid proteins, and various neurological conditions offers insights into potential therapeutic approaches and preventive measures in the realm of neurodegenerative and neuropsychiatric disorders.

6. Computational understanding of antimicrobial peptides and amyloid peptides

While numerous studies have explored the native antimicrobial activity of AMPs and the misfolding and self-aggregation properties of AMYs, less efforts have been devoted to computational modeling and simulations of the alternative functions of self-aggregation into amyloid-like fibrils of AMPs, the antimicrobial activity of AMPs, and the cross-seeding between them. This exploration is attributed to the absence of atomic structures for these peptides and fewer identified systems involving alternative functions and cross-seeding interactions between AMPs and AMYs.

6.1. Alternative function of antimicrobial peptides and amyloid peptides

Current computational strategies for studying alternative function of AMPs and AMYs predominantly focus on the membrane disruption mode of AMYs and the stable β-structure organization of AMPs.[100] For AMPs, the self-association and multimerization into β-structures play a pivotal role in their activities, with β-structures being widely recognized for their ability to disrupt cell membrane potential. In Fig. 21, PG-1 assembles into fibrils rich in β-structures, featuring both antiparallel and parallel β-sheets. These twisted fibrils exhibit significant structural similarities to classical amyloids. The β-forming PG-1 peptides have the capability to permeate and self-organize into oligomeric pores within various lipid bilayers, leading to non-specific ion leakage and membrane disruption akin to the membrane pores induced by AMPs.[8,114,383] When comparing β-rich AMPs and amyloids like Aβ, besides their shared cytotoxicity and amyloidogenicity, they also possess a common structural motif, contributing to their ability to form channels. Microsecond time-scale MD simulations of uperin-3.5 unveiled two crucial factors of peptide concentrations and helical intermediates that contribute to the formation of β-sheet-rich

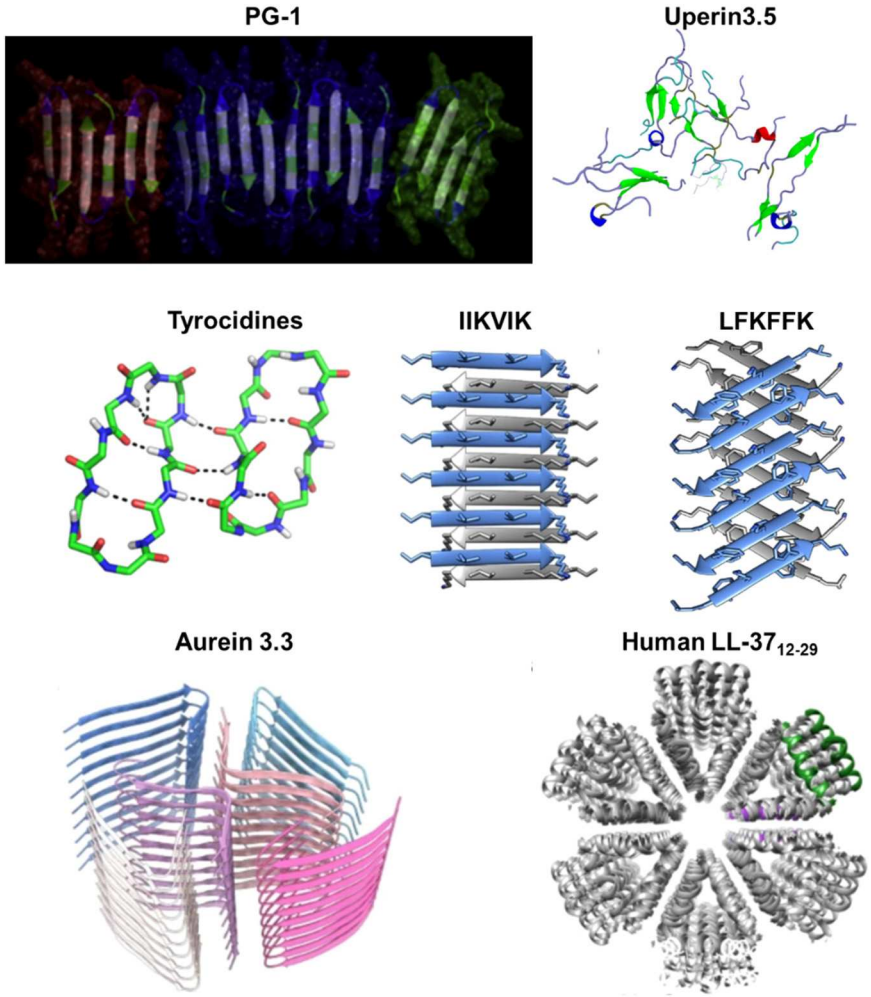

Fig. 21 Computational investigation of self-aggregation propensity of antimicrobial peptides to form amyloid-like fibrils with distinct secondary structures and peptide organizations (cross-β sheets, cross-α sheets, α-helices). Examined peptides include PG-1 (Reproduced with permission from ref. 8 Copyright © 2011 Elsevier Inc.), uperin 3.5 (Reproduced with permission from ref. 384 Copyright © 2023 The Owner Societies), tyrocidines (Reproduced with permission from ref. 196 Copyright © 2013 American Chemistry Society), IIKVIK from PSMα1 and LFKFFK from PSMα3 (Reproduced with permission from ref. 385 Copyright © 2018 Springer Nature Limited), aurein 3.3 (Reproduced with permission from ref. 152 Copyright © 2022 Springer Nature Limited), human LL-37_{17-29} (Reproduced with permission from ref. 155 Copyright © 2020 Springer Nature Limited).

amyloid-like structures.[154,384] Driven by strong hydrophobic interactions, uperin-3.5 rapidly assembled into polymorphic aggregates initially devoid of any β-structures. Subsequently, a gradual structural transition occurred and progressed from random coils to α-helices and ultimately to β-sheets. Although a complete structural transition and formation of β-sheet aggregates were not observed within the typical timescale, a noticeable increase in β-sheet content at the expense of α-helices is evident, suggesting that partial helical conformations may offer a more accessible energetic pathway to the stable formation of amyloid aggregates. Replica Exchange Molecular Dynamics (REMD) simulations of two tyrocidines from Bacillus aneurinolyticus demonstrated their propensity to readily aggregate into distinct dimers with varying orientations (parallel *vs.* antiparallel between two monomers), each adopting a classical β-turn structure.[196] Despite structural similarities among the dimers, the underlying forces of stabilization differ, with some primarily associated by hydrogen bonds and others by hydrophobic interactions. The diverse orientations and organizations of tyrocidine dimers suggest a polymorphic nature in peptide aggregation similar to amyloid peptides.

A combination of computational modeling and x-ray microcrystallography has elucidated atomic structures of short segments from the *Staphylococcus aureus* phenol-soluble modulin (PSM) peptide family.[148,385] PSM peptides demonstrated the capacity to form amyloid-like fibrils, but adopted distinct secondary structures, resulting in diverse cell toxicities. IIKVIK from PSMα1 and IIKIIK from PSMα4 formed classical canonical cross-β amyloid fibrils, where pairs of β-sheets tightly interlocked through a dry interface, creating a steric zipper. In contrast, LFKFFK from PSMα3 self-assembled into novel cross-α fibrils, with α-helices stacking perpendicularly to the fibril axis. The structural disparities among PSMs correlate with distinct functionalities: PSMα3-formed α-helical fibrils

exhibited the highest toxicity to human cells, while PSMα1- and PSMα4-formed β-structure fibrils conveyed minimal toxicity but enhanced biofilm formation. The new discovery of cross-α fibrillation introduces an innovative grasp of the polymorphic structure of amyloid-like fibrils and its influence on cell toxicity. Similarly, a collaboration between cryo-electron microscopy (cryo-EM) and computational modeling has yielded the atomic structure of cross-β fibrils of aurein 3.3. This structure reveals six kinked β-sheet chains arranged in an unconventional in-plane layer.[152] The six-chain organization comprises two inner chains forming an overall S-shape, with two β-strand conformations within a single chain located in an inner area exhibiting $C2_1$ symmetry and four outer chains adopting a V-shape conformation wrapped around this inner cross in $C4_1$ symmetry. Such organization requires strong interlocking β-sheet interactions and precise geometric matching to create tightly staggered β-sheets in both lateral and fibrillar directions. Lastly, diverging from the exclusively β-sheet-rich amyloid-like fibrils formed by AMPs and the cross-α amyloid fibrils of PSMα3, human LL-37_{17-29} adopted a distinct suprahelical fibril structure with unique secondary structure features.[155] LL-37_{17-29} fibrils are formed through the assembly of densely packed helices. In the lateral direction, the cross-section reveals six helices forming a hexameric structure with a central, hydrophobic pore. These helical fibrillar structures prevent LL-37_{17-29} from stacking on top of each other perpendicular to the fibril axis, and as a result, they do not bind to the amyloid indicator dye Thioflavin T. Nevertheless, LL-37_{17-29} fibrils exhibit remarkable thermal stability, retaining their structural integrity without disassembling even after exposure to an 80 °C heat shock.

Computational investigations into the antimicrobial activities of AMYs predominantly focus on their membrane disruption mechanisms. These mechanisms have been discussed in preceding sections and will not be reiterated here. These computational studies highlight the structure–function relationship between amyloid aggregation and antimicrobial activity for AMPs at the structural level. Various AMPs demonstrate the capability to self-assemble into amyloid fibrillar structures, each exhibiting distinct secondary structures and peptide organizations (cross-β sheets, cross-α sheets, α-helices), with specific functional roles in the eradication of bacterial cells.

6.2. Cross-seeding between antimicrobial peptides and amyloid peptides

Fundamentally, the tightly packed β-sheet configuration acts as a structural base and a template for interaction during amyloid cross-seeding. This high degree of structural resemblance helps diminish barriers across species, enhancing the binding and recognition between various species and thus encouraging the formation of heterogeneous amyloid assemblies. The only recent computational study married molecular docking and MD simulations to investigate the binding structures between the HNP-1 dimer and amyloid pentamers formed by Aβ and hIAPP.[24] HNP-1 showed strong affinity for both the β-sheet and U-turn regions of Aβ and hIAPP pentamers. This dual binding mode indicates possible pathways through which HNP-1 inhibits amyloid formation. By binding to these regions, HNP-1 not

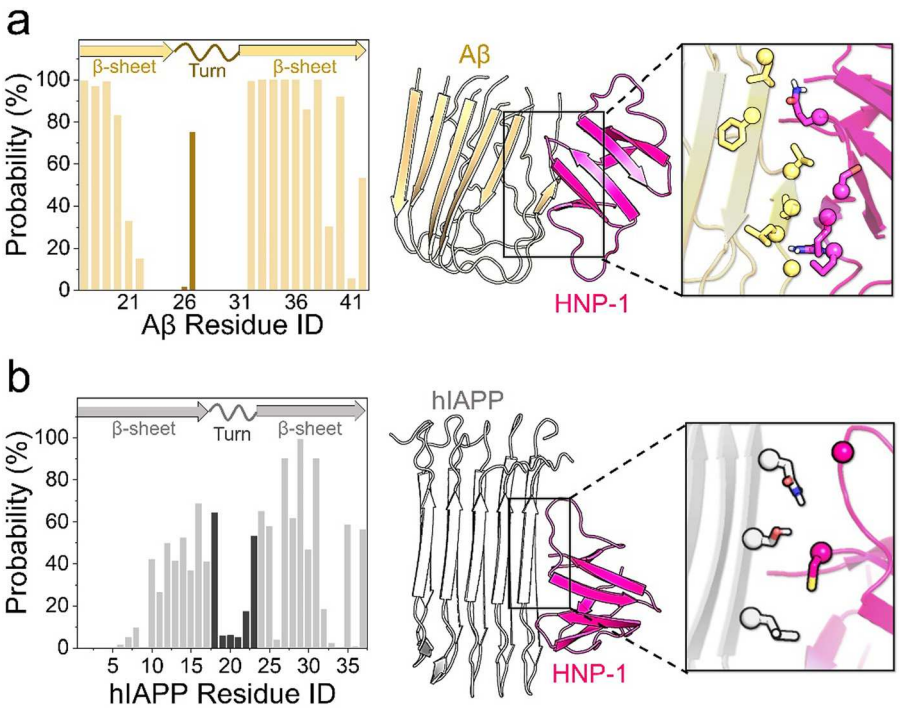

Fig. 22 Computational exploration of cross-seeding between (a) HNP-1 and Aβ and (b) HNP-1 and hIAPP by MD simulations. HNP-1 demonstrates favorable bindings to both the β-sheet and U-turn regions of Aβ and hIAPP oligomers but exhibiting distinct residue binding preferences in each case.

only interferes with the lateral associations and extension processes of amyloid aggregation but also alters the primary and secondary structures of Aβ or hIAPP, enhancing its ability to inhibit amyloid formation. The interaction of HNP-1 with amyloid aggregates also highlighted specific interfacial residues and their preferences for binding. In the Aβ pentamer, HNP-1 strongly interacts with Leu17, Val18, Phe19, and Phe20 from the N-terminal β-sheet, and Ile32, Gly33, Leu34, Met35, Val36, Gly37, Gly38, and Val40 from the C-terminal β-sheet (Fig. 22a). In contrast, HNP-1 showed a preference for binding to Leu27, Ser29, and Asn31 from the C-terminal β-sheet of hIAPP (Fig. 22b).

In contrast to the growing body of experimental findings revealing new alternative functions (*e.g.*, plantaricin A, longipin, melittin, dermaseptin S9, magainin 2, temporin B, Indolicidin) and identifying AMP-AMY cross-seeding systems, there has been a limited number of computational simulations that follow or parallel these experimental investigations at nanoscale or atomic scale. The scarcity of computational studies may trace back to the fundamental challenges associated with protein (mis)folding and structural transitions during the aggregation process, whether involving the same or different peptides. Overcoming high energy barriers within long timescales, on the order of microseconds and beyond, is a crucial aspect that needs to be addressed in exploring these intricate phenomena by current computational approaches. Nonetheless, there is substantial potential for further computational studies in this area.

7. Conclusions and perspectives

AMYs and AMPs belong to distinct families in terms of sequence identity, structural characteristics, gene information, biological function, and pathological implications. However, recent studies revealed intriguing overlaps and interconnections between these two peptide families, hinting at a deeper pathological relationship. Despite their apparent differences, increasing evidence suggests that both AMYs and AMPs share certain structural and functional features, likely acquired through natural evolution. Both AMYs and AMPs exhibit a propensity to adopt β-sheet-rich structures upon aggregation and possess common membrane-disruption mechanisms. These shared characteristics, including peptide self-assembly, oligomerization, the presence of β-rich structures, and common modes of membrane interaction—such as the creation of membrane pores and membrane thinning—observed in both AMPs and AMYs, not only open the door for AMYs to acquire antimicrobial activity and AMPs to exhibit amyloidogenic properties, but also hold potential implications for other membrane-activating peptides and proteins. These common structure-function traits provide possible targets for designing universal defense strategies against viral and amyloid-related diseases. Although challenging to design, approaches such as stabilizing membranes, inhibiting pore formation through small drugs or peptides, and preventing peptide oligomerization or structural transitions toward β-structures could represent therapeutic strategies applicable across a spectrum of diseases, including emerging threats like COVID-19.

More importantly, the cross-seeding phenomenon between AMYs and AMPs is found to play a significant role in the pathogenesis of neurodegenerative diseases and host defense against microbial infections. Cross-seeding involves mutual induction and propagation of peptide aggregation, leading to the formation of mixed amyloid complexes. This interplay is associated with the progression and exacerbation of neurodegenerative disorders, such as Alzheimer's, Parkinson's, and amyotrophic lateral sclerosis. Cross-seeding highlights the remarkable adaptive nature of AMYs and AMPs, allowing them to contribute to the innate immune response and combat microbial pathogens. Understanding the intricate connection between AMYs and AMPs through cross-seeding mechanisms will help uncover their roles in disease pathology and potential therapeutic interventions.

With only a few studies to date, exploration of the AMY-AMP connection may start with comparative studies that assess the antimicrobial activity of AMYs and the amyloidogenic properties of AMPs. From a bioinformatic perspective, several amyloid datasets, such as TANGO,[47] ZipperDB,[58] Waltz-DB2.0,[386] Zyggregator,[387] and PASTA2,[388] have been developed for the identification of amyloid-like aggregation-prone regions in protein or peptide sequences. These datasets, primarily derived from amyloid sequences, offer valuable predictive information for the propensity of specific segments in amyloid proteins and the identification of hotspots within these sequences. However, the predictive accuracy and reliability of these datasets may be compromised when applied to non-amyloid proteins or sequences that do not originate from amyloidogenic regions. Given the increasingly complex pathological interplay between amyloid peptide aggregation and antimicrobial peptide activity, conducting comparative sequence analysis between membrane-activating peptides (*e.g.*, cell penetrating peptides, glycopeptides, lipopeptides) and AMYs and AMPs would facilitate *de novo* peptide design approaches. This involves employing techniques such as high-throughput combinatorial library screening, structure–activity relationship modeling, and predictive algorithms, AI/ML models, with the integration of non-coded modifications, to advance both peptide chemistry and understanding of intricate mechanisms in protein-membrane interactions.

Despite the recent rapid advancements in data-driven artificial intelligence (AI) and machine learning (ML), there is a lack of comprehensive computational studies aimed at screening large antimicrobial datasets to identify AMPs with amyloidogenic properties, as well as amyloid datasets to identify AMYs with antimicrobial activity. Developing innovative data/model-driven deep learning algorithms will serve to facilitate the rational design of peptides or the repurposing of existing AMPs and AMYs with dual antimicrobial and amyloidogenic properties. Utilizing large datasets of AMPs and smaller datasets of AMYs, AI/ML-driven models would permit extracting valuable structure–property features, enabling the discovery and design

of peptides with specific characteristics such as β-structure self-assembly sequences, membrane-disruption actions, and antimicrobial activity. The design outcomes, successful or failed, can be used as feedback to refine and optimize the AI/ML models through iterative training processes. This iterative approach ultimately enhances the efficiency of peptide design, leading to the development of highly effective and novel peptide candidates.

In addition to AI/ML modeling, the investigation of AMP-AMY cross-seeding remains crucial for understanding both host defense mechanisms and amyloid aggregation processes. Molecular simulations, including molecular docking and molecular dynamics, are powerful tools for identifying and exploring the binding modes between AMPs and AMYs at both atomic and coarse-grained levels. Simulations can provide useful information such as binding residues, binding sites, structural characteristics, affinity, and specificity of the peptide interactions. Computational mutagenesis techniques can further validate the key binding sequences, quaternary structures, and hotspot residues involved in these peptide interactions. Advancements in hardware technologies (*e.g.*, GPU-based simulations) and innovative algorithms (*e.g.*, graph theory) hold promise for mapping out the complex interaction patterns within specific AMP-AMY systems. By leveraging these computational approaches, researchers can gain a deeper understanding of the intricate interplay between AMPs and AMYs and shed light on their potential roles in host defense and amyloid-related diseases.

In addition to computational efforts, it is vital to conduct *in vitro* and *in vivo* experimental research to further explore the complementary functions of AMPs and AMYs. A key aspect to investigate is the self-assembly properties of both peptide families for determining the effective states of peptide monomers, oligomers, or fibrils for antimicrobial activity in the case of AMYs and for neurotoxicity towards neuron cells in the case of AMPs. These experimental studies will contribute to expanding the pool of datasets for AMPs and AMYs with dual anti-amyloid and antibacterial activities. This iterative process, which combine experimental validation with computationally informed design, would accelerate the discovery, development, and optimization of new self-assembled peptides, which could be further translated into sustainable and cost-effective therapeutic interventions.

Cross-seeding between these peptide families has significant biological importance and scientific interest. Aggregation through both acceleration and inhibition demonstrated the ability to reduce amyloid-induced cytotoxicity. The pathological implications of this relationship extend beyond the mere formation of amyloid fibrils. Mechanistically, cross-seeding between AMYs and AMPs contributes to the ''microbial infection hypothesis'' and the ''neuroinflammation hypothesis''. The bidirectional communication between amyloid proteins and gut microbiota highlights the critical role of the brain-gut-microbiota axis in the pathogenesis of neurodegenerative diseases. In a broader perspective, it is important to investigate the potential cross-seeding interactions between specific pathogen-related proteins (*e.g.*, viral capsid proteins, bacterial surface proteins, or fungal amyloid proteins) and amyloid peptides (*e.g.*, Aβ, tau, hIAPP, α-synuclein, and prions), including their direct assembly, aggregation, and fibrillation. Unraveling the interplay between pathogen-related proteins and amyloid peptides holds the key to understanding the mechanisms underlying amyloid formation in infectious diseases and neurodegenerative disorders. Furthermore, by exploring the potential impact of these cross-seeding interactions on disease pathology, novel therapeutic targets and strategies for intervention may be uncovered, paving the way for future advancements in combating these debilitating conditions.

As briefly summarized from the above, AMPs and AMYs appear to be two sides of the same coin. Despite some progress, the connection between AMPs and AMYs is still unclear. Firstly, there is a lack of studies that explore the underlying mechanisms and interactions between these two peptide families. The precise molecular crosstalk and interplay between AMPs and AMYs are not yet fully understood. Secondly, the existing literature primarily focuses on individual aspects of either AMPs or AMYs, with limited emphasis on their overlapping properties and functional connections. This hinders a comprehensive understanding of the complex relationship between these peptides. Additionally, the available datasets for AMPs and AMYs are often limited in size and diversity, which restricts the accuracy and generalizability of predictive models. Further research could unravel this intricate connection. Endeavors will not only deepen our fundamental understanding of the intricate workings of the innate immune system and the pathogenesis of neurodegenerative diseases, but also hold great potentials for advancing therapeutic interventions and innovative approaches in both antimicrobial strategies and neurodegenerative disease treatments.

Declarations

Ethics approval and consent to participate: not applicable; consent for publication: yes; availability of data and materials: all data are available in the main text or the supplementary materials.

Author contributions

The manuscript was written with contributions from all authors, who have all approved the final version.

Data availability

No primary research results, software or code have been included and no new data were generated or analysed as part of this review.

Conflicts of interest

There is no competing interests.

Acknowledgements

We thank financial support from NSF-CBET-2107619. This project has been funded in whole or in part with federal funds from the National Cancer Institute, National Institutes of Health, under contract HHSN261200800001E. The content of this publication does not necessarily reflect the views or policies of the Department of Health and Human Services, nor does mention of trade names, commercial products or organizations imply endorsement by the US Government. This Research was supported [in part] by the Intramural Research Program of the NIH, National Cancer Institute, Center for Cancer Research and the Intramural Research Program of the NIH Clinical Center.

References

1 C. Soto and S. Pritzkow, *Nat. Neurosci.*, 2018, **21**, 1332–1340.
2 J. Gandhi, A. C. Antonelli, A. Afridi, S. Vatsia, G. Joshi, V. Romanov, I. V. J. Murray and S. A. Khan, *Rev. Neurosci.*, 2019, **30**, 339–358.
3 A. Gamez, P. Yuste-Checa, S. Brasil, A. Briso-Montiano, L. R. Desviat, M. Ugarte, C. Perez-Cerda and B. Perez, *Clin. Genet.*, 2018, **93**, 450–458.
4 P. H. Nguyen, A. Ramamoorthy, B. R. Sahoo, J. Zheng, P. Faller, J. E. Straub, L. Dominguez, J. E. Shea, N. V. Dokholyan, A. De Simone, B. Ma, R. Nussinov, S. Najafi, S. T. Ngo, A. Loquet, M. Chiricotto, P. Ganguly, J. McCarty, M. S. Li, C. Hall, Y. Wang, Y. Miller, S. Melchionna, B. Habenstein, S. Timr, J. Chen, B. Hnath, B. Strodel, R. Kayed, S. Lesne, G. Wei, F. Sterpone, A. J. Doig and P. Derreumaux, *Chem. Rev.*, 2021, **121**, 2545–2647.
5 J. A. Hardy and G. A. Higgins, *Science*, 1992, **256**, 184–185.
6 V. Baltutis, P. D. O'Leary and L. L. Martin, *Chempluschem*, 2022, **87**, e202200240.
7 B. L. Kagan, H. Jang, R. Capone, F. Teran Arce, S. Ramachandran, R. Lal and R. Nussinov, *Mol. Pharm.*, 2012, **9**, 708–717.
8 H. Jang, F. T. Arce, M. Mustata, S. Ramachandran, R. Capone, R. Nussinov and R. Lal, *Biophys. J.*, 2011, **100**, 1775–1783.
9 H. Zhao, R. Sood, A. Jutila, S. Bose, G. Fimland, J. Nissen-Meyer and P. K. Kinnunen, *Biochim. Biophys. Acta*, 2006, **1758**, 1461–1474.
10 A. N. Calabrese, Y. Liu, T. Wang, I. F. Musgrave, T. L. Pukala, R. F. Tabor, L. L. Martin, J. A. Carver and J. H. Bowie, *Chembiochem*, 2016, **17**, 239–246.
11 R. Urrutia, R. A. Cruciani, J. L. Barker and B. Kachar, *FEBS Lett.*, 1989, **247**, 17–21.
12 D. W. Juhl, E. Glattard, M. Lointier, P. Bampilis and B. Bechinger, *Front. Cell Infect. Microbiol.*, 2020, **10**, 526459.
13 L. Caillon, J. A. Killian, O. Lequin and L. Khemtemourian, *PLoS One*, 2013, **8**, e75528.
14 L. Wang, Q. Liu, J.-C. Chen, Y.-X. Cui, B. Zhou, Y.-X. Chen, Y.-F. Zhao and Y.-M. J. B. C. Li, *Biol. Chem.*, 2012, **393**, 641–646.
15 S. C. Park, J. C. Moon, S. Y. Shin, H. Son, Y. J. Jung, N. H. Kim, Y. M. Kim, M. K. Jang and J. R. Lee, *Biochem. Biophys. Res. Commun.*, 2016, **478**, 924–928.
16 H. Zheng, H. Li, J. Zhang, H. Fan, L. Jia, W. Ma, S. Ma, S. Wang, H. You, Z. Yin and X. Li, *J. Biol. Chem.*, 2020, **295**, 2570–2581.
17 S. J. Soscia, J. E. Kirby, K. J. Washicosky, S. M. Tucker, M. Ingelsson, B. Hyman, M. A. Burton, L. E. Goldstein, S. Duong and R. E. J. P. O. Tanzi, *PloS one*, 2010, **5**, e9505.
18 N. B. Last and A. D. Miranker, *Proc. Natl. Acad. Sci. U. S. A.*, 2013, **110**, 6382–6387.
19 M. L. Gosztyla, H. M. Brothers and S. R. Robinson, *J. Alzheimers Dis.*, 2018, **62**, 1495–1506.
20 U. H. Iqbal, E. Zeng and G. M. Pasinetti, *Int. J. Mol. Sci.*, 2020, **21**, 4920.
21 K. Bourgade, H. Garneau, G. Giroux, A. Y. Le Page, C. Bocti, G. Dupuis, E. H. Frost and T. Fulop, Jr., *Biogerontology*, 2015, **16**, 85–98.
22 M. Zhang, J. Zhao and J. Zheng, *Soft Matter*, 2014, **10**, 7425–7451.
23 Y. Tang, D. Zhang, X. Gong and J. Zheng, *Chem. Sci.*, 2022, **13**, 7143–7156.
24 Y. Zhang, Y. Liu, Y. Tang, D. Zhang, H. He, J. Wu and J. Zheng, *Chem. Sci.*, 2021, **12**, 9124–9139.
25 E. De Lorenzi, M. Chiari, R. Colombo, M. Cretich, L. Sola, R. Vanna, P. Gagni, F. Bisceglia, C. Morasso and J. S. Lin, *J. Alzheimer's Dis.*, 2017, **59**, 1213–1226.
26 V. Armiento, K. Hille, D. Naltsas, J. S. Lin, A. E. Barron and A. Kapurniotu, *Angew. Chem., Int. Ed.*, 2020, **59**, 12837–12841.
27 T. R. Sampson, C. Challis, N. Jain, A. Moiseyenko, M. S. Ladinsky, G. G. Shastri, T. Thron, B. D. Needham, I. Horvath, J. W. Debelius, S. Janssen, R. Knight, P. Wittung-Stafshede, V. Gradinaru, M. Chapman and S. K. Mazmanian, *Elife*, 2020, **9**, e53111.
28 E. Chorell, E. Andersson, M. L. Evans, N. Jain, A. Gotheson, J. Aden, M. R. Chapman, F. Almqvist and P. Wittung-Stafshede, *PLoS One*, 2015, **10**, e0140194.
29 M. L. Evans, E. Chorell, J. D. Taylor, J. Aden, A. Gotheson, F. Li, M. Koch, L. Sefer, S. J. Matthews, P. Wittung-Stafshede, F. Almqvist and M. R. Chapman, *Mol. Cell*, 2015, **57**, 445–455.
30 B. Ma and R. Nussinov, *J. Mol. Biol.*, 2012, **421**, 172–184.
31 B. Ren, Y. Zhang, M. Zhang, Y. Liu, D. Zhang, X. Gong, Z. Feng, J. Tang, Y. Chang and J. Zheng, *J. Mater. Chem. B*, 2019, **7**, 7267–7282.
32 E. A. Newcombe, J. Camats-Perna, M. L. Silva, N. Valmas, T. J. Huat and R. Medeiros, *J. Neuroinflammation*, 2018, **15**, 1–26.
33 K. Kowalski and A. Mulak, *J. Neurogastroenterol. Motil.*, 2019, **25**, 48–60.
34 I. Javed, Z. Zhang, J. Adamcik, N. Andrikopoulos, Y. Li, D. E. Otzen, S. Lin, R. Mezzenga, T. P. Davis, F. Ding and P. C. Ke, *Adv. Sci.*, 2020, **7**, 2001299.
35 Y. Tang, D. Zhang, X. Gong and J. Zheng, *Biophys. Chem.*, 2022, **281**, 106735.

36 K. Lundmark, G. T. Westermark, A. Olsén and P. Westermark, *Proc. Natl. Acad. Sci. U. S. A.*, 2005, **102**, 6098–6102.
37 Z. Wang and G. Wang, *Nucleic Acids Res.*, 2004, **32**, D590–592.
38 G. Wang, X. Li and Z. Wang, *Nucleic Acids Res.*, 2009, **37**, D933–937.
39 S. Thomas, S. Karnik, R. S. Barai, V. K. Jayaraman and S. Idicula-Thomas, *Nucleic Acids Res.*, 2010, **38**, D774–780.
40 P. G. A. Aronica, L. M. Reid, N. Desai, J. Li, S. J. Fox, S. Yadahalli, J. W. Essex and C. S. Verma, *J. Chem. Inf. Model.*, 2021, **61**, 3172–3196.
41 L. T. Nguyen, E. F. Haney and H. J. Vogel, *Trends Biotechnol.*, 2011, **29**, 464–472.
42 R. Mani, S. D. Cady, M. Tang, A. J. Waring, R. I. Lehrer and M. Hong, *Proc. Natl. Acad. Sci. U. S. A.*, 2006, **103**, 16242–16247.
43 R. I. Lehrer and T. Ganz, *Curr. Opin. Immunol.*, 1999, **11**, 23–27.
44 M. Stefani, *FEBS J*, 2010, **277**, 4602–4613.
45 H. H. Tsai, K. Gunasekaran and R. Nussinov, *Structure*, 2006, **14**, 1059–1072.
46 B. H. Gan, J. Gaynord, S. M. Rowe, T. Deingruber and D. R. Spring, *Chem. Soc. Rev.*, 2021, **50**, 7820–7880.
47 A. M. Fernandez-Escamilla, F. Rousseau, J. Schymkowitz and L. Serrano, *Nat. Biotechnol.*, 2004, **22**, 1302–1306.
48 K. Matsuzaki, S. Yoneyama, O. Murase and K. Miyajima, *Biochemistry*, 1996, **35**, 8450–8456.
49 M. P. Cabrera, D. S. Alvares, N. B. Leite, B. M. de Souza, M. S. Palma, K. A. Riske and J. R. Neto, *Langmuir*, 2011, **27**, 10805–10813.
50 M. I. Ivanova, M. J. Thompson and D. Eisenberg, *Proc. Natl. Acad. Sci. U. S. A.*, 2006, **103**, 4079–4082.
51 M. Castle, A. Nazarian, S. S. Yi and P. Tempst, *J. Biol. Chem.*, 1999, **274**, 32555–32564.
52 J. Portelinha, S. S. Duay, S. I. Yu, K. Heilemann, M. D. J. Libardo, S. A. Juliano, J. L. Klassen and A. M. Angeles-Boza, *Chem. Rev.*, 2021, **121**, 2648–2712.
53 C. B. Park, H. S. Kim and S. C. Kim, *Biochem. Biophys. Res. Commun.*, 1998, **244**, 253–257.
54 T. J. Falla, D. N. Karunaratne and R. E. Hancock, *J. Biol. Chem.*, 1996, **271**, 19298–19303.
55 M. B. Ulmschneider, M. S. Sansom and A. D. Nola, *Biophys. J.*, 2006, **90**, 1650–1660.
56 M. Torrent, J. Valle, M. V. Nogues, E. Boix and D. Andreu, *Angew. Chem., Int. Ed.*, 2011, **50**, 10686–10689.
57 L. Jin, X. Bai, N. Luan, H. Yao, Z. Zhang, W. Liu, Y. Chen, X. Yan, M. Rong, R. Lai and Q. Lu, *J. Med. Chem.*, 2016, **59**, 1791–1799.
58 M. J. Thompson, S. A. Sievers, J. Karanicolas, M. I. Ivanova, D. Baker and D. Eisenberg, *Proc. Natl. Acad. Sci. U. S. A.*, 2006, **103**, 4074–4078.
59 J. Zheng, B. Ma, C. J. Tsai and R. Nussinov, *Biophys. J.*, 2006, **91**, 824–833.
60 A. T. Petkova, Y. Ishii, J. J. Balbach, O. N. Antzutkin, R. D. Leapman, F. Delaglio and R. Tycko, *Proc. Natl. Acad. Sci. U. S. A.*, 2002, **99**, 16742–16747.
61 A. T. Petkova, R. D. Leapman, Z. Guo, W. M. Yau, M. P. Mattson and R. Tycko, *Science*, 2005, **307**, 262–265.
62 N. F. Dupuis, C. Wu, J. E. Shea and M. T. Bowers, *J. Am. Chem. Soc.*, 2009, **131**, 18283–18292.
63 M. Sunde, L. C. Serpell, M. Bartlam, P. E. Fraser, M. B. Pepys and C. C. Blake, *J. Mol. Biol.*, 1997, **273**, 729–739.
64 K. T. Nguyen, J. T. King and Z. Chen, *J. Phys. Chem. B*, 2010, **114**, 8291–8300.
65 S. H. White, W. C. Wimley and M. E. Selsted, *Curr. Opin. Struct. Biol.*, 1995, **5**, 521–527.
66 S. Troeira Henriques, N. Lawrence, S. Chaousis, A. S. Ravipati, O. Cheneval, A. H. Benfield, A. G. Elliott, A. M. Kavanagh, M. A. Cooper, L. Y. Chan, Y. H. Huang and D. J. Craik, *ACS Chem. Biol.*, 2017, **12**, 2324–2334.
67 C. P. Hill, J. Yee, M. E. Selsted and D. Eisenberg, *Science*, 1991, **251**, 1481–1485.
68 G. Guigas and M. Weiss, *Biophys. J.*, 2006, **91**, 2393–2398.
69 A. Zemel, A. Ben-Shaul and S. May, *Biophys. J.*, 2004, **86**, 3607–3619.
70 G. Wang, *J. Biol. Chem.*, 2008, **283**, 32637–32643.
71 A. S. Ladokhin and S. H. White, *J. Mol. Biol.*, 1999, **285**, 1363–1369.
72 K. Matsuzaki, K. Sugishita, M. Harada, N. Fujii and K. Miyajima, *Biochim. Biophys. Acta*, 1997, **1327**, 119–130.
73 S. Ludtke, K. He and H. Huang, *Biochemistry*, 1995, **34**, 16764–16769.
74 S. M. Gregory, A. Cavenaugh, V. Journigan, A. Pokorny and P. F. Almeida, *Biophys. J.*, 2008, **94**, 1667–1680.
75 D. Andreu, R. B. Merrifield, H. Steiner and H. G. Boman, *Proc. Natl. Acad. Sci. U. S. A.*, 1983, **80**, 6475–6479.
76 C. Auvynet, C. El Amri, C. Lacombe, F. Bruston, J. Bourdais, P. Nicolas and Y. Rosenstein, *FEBS J*, 2008, **275**, 4134–4151.
77 S. Malekkhaiat Häffner and M. Malmsten, *Curr. Opin. Colloid Interface Sci.*, 2018, **38**, 56–79.
78 Y. Tang, D. Zhang, Y. Zhang, Y. Liu, X. Gong, Y. Chang, B. Ren and J. Zheng, *ACS Appl. Bio Mater.*, 2020, **3**, 8286–8308.
79 Y. Miller, B. Ma and R. Nussinov, *Chem. Rev.*, 2010, **110**, 4820–4838.
80 A. A. Strömstedt, L. Ringstad, A. Schmidtchen and M. Malmsten, *Curr. Opin. Colloid Interface Sci.*, 2010, **15**, 467–478.
81 S. M. Butterfield and H. A. Lashuel, *Angew. Chem., Int. Ed.*, 2010, **49**, 5628–5654.
82 M. Zhang, B. Ren, H. Chen, Y. Sun, J. Ma, B. Jiang and J. Zheng, *Israel J. Chem.*, 2017, **57**, 586–601.
83 E. Gazit, I. R. Miller, P. C. Biggin, M. S. Sansom and Y. Shai, *J. Mol. Biol.*, 1996, **258**, 860–870.
84 L. Chen, X. Li, L. Gao and W. Fang, *J. Phys. Chem. B*, 2015, **119**, 850–860.
85 H. Bouvrais, P. Meleard, T. Pott, K. J. Jensen, J. Brask and J. H. Ipsen, *Biophys. Chem.*, 2008, **137**, 7–12.
86 Y. Pouny, D. Rapaport, A. Mor, P. Nicolas and Y. Shai, *Biochemistry*, 1992, **31**, 12416–12423.

87 S. Kobayashi, K. Takeshima, C. B. Park, S. C. Kim and K. Matsuzaki, *Biochemistry*, 2000, **39**, 8648–8654.
88 E. E. Ambroggio, F. Separovic, J. H. Bowie, G. D. Fidelio and L. A. Bagatolli, *Biophys. J.*, 2005, **89**, 1874–1881.
89 M. Monette and M. Lafleur, *Biophys. J.*, 1995, **68**, 187–195.
90 A. B. Reiss, H. A. Arain, M. M. Stecker, N. M. Siegart and L. J. Kasselman, *Rev. Neurosci.*, 2018, **29**, 613–627.
91 A. K. Bishoyi, P. H. Roham, K. Rachineni, S. Save, M. A. Hazari, S. Sharma and A. Kumar, *Biol. Chem.*, 2021, **402**, 133–153.
92 Y. C. Wong and D. Krainc, *Nat. Med.*, 2017, **23**, 1–13.
93 A. Aguzzi and J. Falsig, *Nat. Neurosci.*, 2012, **15**, 936–939.
94 I. R. Mellor and M. S. Sansom, *Proc. R. Soc. London, Ser. B*, 1990, **239**, 383–400.
95 L. Beven, S. Castano, J. Dufourcq, A. Wieslander and H. Wroblewski, *Eur. J. Biochem.*, 2003, **270**, 2207–2217.
96 Y. Higashimoto, H. Kodama, M. Jelokhani-Niaraki, F. Kato and M. Kondo, *J. Biochem.*, 1999, **125**, 705–712.
97 R. G. Panchal, M. L. Smart, D. N. Bowser, D. A. Williams and S. Petrou, *Curr. Pharm. Biotechnol.*, 2002, **3**, 99–115.
98 R. Capone, F. G. Quiroz, P. Prangkio, I. Saluja, A. M. Sauer, M. R. Bautista, R. S. Turner, J. Yang and M. Mayer, *Neurotox Res*, 2009, **16**, 1–13.
99 R. Lal, H. Lin and A. P. Quist, *Biochim. Biophys. Acta*, 2007, **1768**, 1966–1975.
100 H. Jang, J. Zheng, R. Lal and R. Nussinov, *Trends Biochem. Sci.*, 2008, **33**, 91–100.
101 N. Arispe, J. C. Diaz and O. Simakova, *Biochim. Biophys. Acta*, 2007, **1768**, 1952–1965.
102 B. Leitgeb, A. Szekeres, L. Manczinger, C. Vagvolgyi and L. Kredics, *Chem. Biodiversity*, 2007, **4**, 1027–1051.
103 Y. Bessin, N. Saint, L. Marri, D. Marchini and G. Molle, *Biochim. Biophys. Acta*, 2004, **1667**, 148–156.
104 D. Raimondo, G. Andreotti, N. Saint, P. Amodeo, G. Renzone, M. Sanseverino, I. Zocchi, G. Molle, A. Motta and A. Scaloni, *Proc. Natl. Acad. Sci. U. S. A.*, 2005, **102**, 6309–6314.
105 H. Jang, F. T. Arce, S. Ramachandran, R. Capone, R. Lal and R. Nussinov, *J. Mol. Biol.*, 2010, **404**, 917–934.
106 J. Zhao, Y. Luo, H. Jang, X. Yu, G. Wei, R. Nussinov and J. Zheng, *Biochim. Biophys. Acta*, 2012, **1818**, 3121–3130.
107 L. Y. Tan, K. H. Tang, L. Y. Y. Lim, J. X. Ong, H. Park and S. Jung, *Biomolecules*, 2022, **12**, 507.
108 R. Kayed, E. Head, J. L. Thompson, T. M. McIntire, S. C. Milton, C. W. Cotman and C. G. Glabe, *Science*, 2003, **300**, 486–489.
109 N. Arispe, H. B. Pollard and E. Rojas, *Proc. Natl. Acad. Sci. U. S. A.*, 1993, **90**, 10573–10577.
110 P. Walsh, G. Vanderlee, J. Yau, J. Campeau, V. L. Sim, C. M. Yip and S. Sharpe, *J. Biol. Chem.*, 2014, **289**, 10419–10430.
111 X. Li, M. Wan, L. Gao and W. Fang, *Sci. Rep.*, 2016, **6**, 21614.
112 H. Jang, J. Zheng and R. Nussinov, *Biophys. J.*, 2007, **93**, 1938–1949.
113 H. Jang, F. T. Arce, R. Capone, S. Ramachandran, R. Lal and R. Nussinov, *Biophys. J.*, 2009, **97**, 3029–3037.
114 H. Jang, F. Teran Arce, S. Ramachandran, R. Capone, R. Lal and R. Nussinov, *J. Phys. Chem. B*, 2010, **114**, 9445–9451.
115 L. Connelly, H. Jang, F. T. Arce, R. Capone, S. A. Kotler, S. Ramachandran, B. L. Kagan, R. Nussinov and R. Lal, *J. Phys. Chem. B*, 2012, **116**, 1728–1735.
116 A. Quist, I. Doudevski, H. Lin, R. Azimova, D. Ng, B. Frangione, B. Kagan, J. Ghiso and R. Lal, *Proc. Natl. Acad. Sci. U. S. A.*, 2005, **102**, 10427–10432.
117 T. A. Mirzabekov, M. C. Lin and B. L. Kagan, *J. Biol. Chem.*, 1996, **271**, 1988–1992.
118 H. A. Lashuel, B. M. Petre, J. Wall, M. Simon, R. J. Nowak, T. Walz and J. P. T. Lansbury, *J. Mol. Biol.*, 2002, **322**, 1089–1102.
119 Y. Hirakura, I. Carreras, J. D. Sipe and B. L. Kagan, *Amyloid*, 2002, **9**, 13–23.
120 L. Wang, H. A. Lashuel, T. Walz and W. Colon, *Proc. Natl. Acad. Sci. U. S. A.*, 2002, **99**, 15947–15952.
121 M. Mustata, R. Capone, H. Jang, F. T. Arce, S. Ramachandran, R. Lal and R. Nussinov, *J. Am. Chem. Soc.*, 2009, **131**, 14938–14945.
122 Y. Hirakura and B. L. Kagan, *Amyloid*, 2001, **8**, 94–100.
123 H. Jang, B. Ma, R. Lal and R. Nussinov, *Biophys. J.*, 2008, **95**, 4631–4642.
124 R. Capone, M. Mustata, H. Jang, F. T. Arce, R. Nussinov and R. Lal, *Biophys. J.*, 2010, **98**, 2644–2652.
125 J. H. Viles, *Angew. Chem., Int. Ed.*, 2023, **62**, e202215785.
126 D. Gimenez, O. L. Sanchez-Munoz and J. Salgado, *Langmuir*, 2015, **31**, 3146–3158.
127 P. D. Rakowska, H. Jiang, S. Ray, A. Pyne, B. Lamarre, M. Carr, P. J. Judge, J. Ravi, U. I. Gerling, B. Koksch, G. J. Martyna, B. W. Hoogenboom, A. Watts, J. Crain, C. R. Grovenor and M. G. Ryadnov, *Proc. Natl. Acad. Sci. U. S. A.*, 2013, **110**, 8918–8923.
128 F. Jiao, F. Dehez, T. Ni, X. Yu, J. S. Dittman, R. Gilbert, C. Chipot and S. Scheuring, *Nat. Commun.*, 2022, **13**, 5039.
129 A. W. Hodel, J. A. Rudd-Schmidt, J. A. Trapani, I. Voskoboinik and B. W. Hoogenboom, *Faraday Discuss.*, 2021, **232**, 236–255.
130 D. Sun, J. Forsman and C. E. Woodward, *Langmuir*, 2015, **31**, 752–761.
131 A. A. Langham, A. S. Ahmad and Y. N. Kaznessis, *J. Am. Chem. Soc.*, 2008, **130**, 4338–4346.
132 R. Talandashti, F. Mehrnejad, K. Rostamipour, F. Doustdar and A. Lavasanifar, *J. Phys. Chem. B*, 2021, **125**, 7163–7176.
133 F. A. Daison, N. Kumar, S. Balakrishnan, K. Venugopal, S. Elango and P. Sokkar, *J. Chem. Inf. Model*, 2022, **62**, 40–48.
134 R. Pokhrel, N. Bhattarai, P. Baral, B. S. Gerstman, J. H. Park, M. Handfield and P. P. Chapagain, *Phys. Chem. Chem. Phys.*, 2019, **21**, 12530–12539.
135 A. Catte, M. R. Wilson, M. Walker and V. S. Oganesyan, *Soft Matter*, 2018, **14**, 2796–2807.
136 M. Bhattacharya, N. Jain, P. Dogra, S. Samai and S. Mukhopadhyay, *J. Phys. Chem. Lett.*, 2013, **4**, 480–485.

137 L. A. Morozova-Roche, V. Zamotin, M. Malisauskas, A. Ohman, R. Chertkova, M. A. Lavrikova, I. A. Kostanyan, D. A. Dolgikh and M. P. Kirpichnikov, *Biochemistry*, 2004, **43**, 9610–9619.
138 H. Jang, F. T. Arce, S. Ramachandran, B. L. Kagan, R. Lal and R. Nussinov, *J. Phys. Chem. B*, 2013, **117**, 11518–11529.
139 S. Younger, H. Jang, H. A. Davies, M. J. Niemiec, J. G. N. Garcia, R. Nussinov, R. Q. Migrino, J. Madine and F. T. Arce, *Biophys. J.*, 2020, **118**, 2769–2782.
140 Y. Yang, H. Distaffen, S. Jalali, A. J. Nieuwkoop, B. L. Nilsson and C. L. Dias, *ACS Chem. Neurosci.*, 2022, **13**, 2766–2777.
141 M. Maurer and T. Lazaridis, *J. Chem. Inf. Model*, 2023, **63**, 7171–7179.
142 S. Luca, W. M. Yau, R. Leapman and R. Tycko, *Biochemistry*, 2007, **46**, 13505–13522.
143 T. Luhrs, C. Ritter, M. Adrian, D. Riek-Loher, B. Bohrmann, H. Dobeli, D. Schubert and R. Riek, *Proc. Natl. Acad. Sci. U. S. A.*, 2005, **102**, 17342–17347.
144 K. Iwata, T. Fujiwara, Y. Matsuki, H. Akutsu, S. Takahashi, H. Naiki and Y. Goto, *Proc. Natl. Acad. Sci. U. S. A.*, 2006, **103**, 18119–18124.
145 N. Arispe, H. B. Pollard and E. Rojas, *Proc. Natl. Acad. Sci. U. S. A.*, 1996, **93**, 1710–1715.
146 Y. Hirakura, W. W. Yiu, A. Yamamoto and B. L. Kagan, *Amyloid*, 2000, **7**, 194–199.
147 H. Jang, F. T. Arce, S. Ramachandran, R. Capone, R. Azimova, B. L. Kagan, R. Nussinov and R. Lal, *Proc. Natl. Acad. Sci. U. S. A.*, 2010, **107**, 6538–6543.
148 E. Tayeb-Fligelman, N. Salinas, O. Tabachnikov and M. Landau, *Structure*, 2020, **28**(301–313), e306.
149 R. S. Sayegh, I. F. Batista, R. L. Melo, K. A. Riske, S. Daffre, G. Montich and P. I. da Silva Jr, *PLoS One*, 2016, **11**, e0167953.
150 P. K. Singh, D. Ghosh, D. Tewari, G. M. Mohite, E. Carvalho, N. N. Jha, R. S. Jacob, S. Sahay, R. Banerjee, A. K. Bera and S. K. Maji, *PLoS One*, 2015, **10**, e0120346.
151 R. Sood, Y. Domanov and P. K. Kinnunen, *J. Fluoresc.*, 2007, **17**, 223–234.
152 R. Bucker, C. Seuring, C. Cazey, K. Veith, M. Garcia-Alai, K. Grunewald and M. Landau, *Nat. Commun.*, 2022, **13**, 4356.
153 Y. Tang, D. Zhang, X. Gong and J. Zheng, *J. Mater. Chem. B*, 2023, **11**, 7920–7932.
154 S. Ray, S. Holden, A. K. Prasad, L. L. Martin and A. S. Panwar, *J. Phys. Chem. B*, 2020, **124**, 11659–11670.
155 Y. Engelberg and M. Landau, *Nat. Commun.*, 2020, **11**, 3894.
156 Y. Tang, D. Zhang and J. Zheng, *ACS Chem. Neurosci.*, 2023, **14**, 3143–3155.
157 Y. Zhang, Y. Tang, Y. Liu, D. Zhang and J. Zheng, *Adv. Funct. Mater.*, 2021, **31**, 2102978.
158 S. K. Maji, M. H. Perrin, M. R. Sawaya, S. Jessberger, K. Vadodaria, R. A. Rissman, P. S. Singru, K. P. Nilsson, R. Simon, D. Schubert, D. Eisenberg, J. Rivier, P. Sawchenko, W. Vale and R. Riek, *Science*, 2009, **325**, 328–332.
159 S. L. Gras, A. K. Tickler, A. M. Squires, G. L. Devlin, M. A. Horton, C. M. Dobson and C. E. MacPhee, *Biomaterials*, 2008, **29**, 1553–1562.
160 H. Sakai, K. Watanabe, Y. Asanomi, Y. Kobayashi, Y. Chuman, L. Shi, T. Masuda, T. Wyttenbach, M. T. Bowers, K. Uosaki and K. Sakaguchi, *Adv. Funct. Mater.*, 2013, **23**, 4881–4887.
161 D. Li, E. M. Jones, M. R. Sawaya, H. Furukawa, F. Luo, M. Ivanova, S. A. Sievers, W. Wang, O. M. Yaghi, C. Liu and D. S. Eisenberg, *J. Am. Chem. Soc.*, 2014, **136**, 18044–18051.
162 D. Chen, X. Liu, Y. Chen and H. Lin, *Appl. Microbiol. Biotechnol.*, 2022, **106**, 7711–7720.
163 M. Pasupuleti, M. Roupe, V. Rydengard, K. Surewicz, W. K. Surewicz, A. Chalupka, M. Malmsten, O. E. Sorensen and A. Schmidtchen, *PLoS One*, 2009, **4**, e7358.
164 R. Hari-Dass, C. Shah, D. J. Meyer and J. G. Raynes, *J. Biol. Chem.*, 2005, **280**, 18562–18567.
165 X. Zhan, B. Stamova, L. W. Jin, C. DeCarli, B. Phinney and F. R. Sharp, *Neurology*, 2016, **87**, 2324–2332.
166 D. C. Emery, D. K. Shoemark, T. E. Batstone, C. M. Waterfall, J. A. Coghill, T. L. Cerajewska, M. Davies, N. X. West and S. J. Allen, *Front. Aging Neurosci.*, 2017, **9**, 195.
167 E. Y. Lee, Y. Srinivasan, J. de Anda, L. K. Nicastro, C. Tukel and G. C. L. Wong, *Front. Immunol.*, 2020, **11**, 1629.
168 M. I. Ivanova, Y. Lin, Y. H. Lee, J. Zheng and A. Ramamoorthy, *Biophys. Chem.*, 2021, **269**, 106507.
169 O. Tavassoly, F. Safavi and I. Tavassoly, *ACS Chem. Neurosci.*, 2020, **11**, 3704–3706.
170 S. A. Semerdzhiev, M. A. A. Fakhree, I. Segers-Nolten, C. Blum and M. Claessens, *ACS Chem. Neurosci.*, 2022, **13**, 143–150.
171 A. K. Jana, A. B. Greenwood and U. H. E. Hansmann, *J. Phys. Chem. B*, 2021, **125**, 9155–9167.
172 D. D. Li Puma, R. Piacentini, L. Leone, K. Gironi, M. E. Marcocci, G. De Chiara, A. T. Palamara and C. Grassi, *Stem Cells*, 2019, **37**, 1467–1480.
173 M. Ortega and B. M. Ances, *J. Neuroimmune Pharmacol.*, 2014, **9**, 483–491.
174 D. Bortolotti, V. Gentili, A. Rotola, E. Caselli and R. Rizzo, *Alzheimers Res Ther*, 2019, **11**, 104.
175 F. Pistollato, S. Sumalla Cano, I. Elio, M. Masias Vergara, F. Giampieri and M. Battino, *Nutr. Rev.*, 2016, **74**, 624–634.
176 C. Roubaud-Baudron, P. Krolak-Salmon, I. Quadrio, F. Megraud and N. Salles, *Neurobiol. Aging*, 2012, **33**(1009), e1011–1009.
177 C. J. Hammond, L. R. Hallock, R. J. Howanski, D. M. Appelt, C. S. Little and B. J. Balin, *BMC Neurosci.*, 2010, **11**, 121.
178 D. Vigasova, M. Nemergut, B. Liskova and J. Damborsky, *Microb. Cell Fact.*, 2021, **20**, 25.
179 Y. Tang, D. Zhang, Y. Zhang, Y. Liu, Y. Miller, K. Gong and J. Zheng, *Commun. Biol.*, 2022, **5**, 417.
180 I. Blasko, R. Veerhuis, M. Stampfer-Kountchev, M. Saurwein-Teissl, P. Eikelenboom and B. Grubeck-Loebenstein, *Neurobiol. Dis.*, 2000, **7**, 682–689.
181 J. W. Kinney, S. M. Bemiller, A. S. Murtishaw, A. M. Leisgang, A. M. Salazar and B. T. Lamb, *Alzheimer's Dementia: Transl. Res. Clin. Interventions*, 2018, **4**, 575–590.

182 Z. Wang, P. Vilekar, J. Huang and D. F. Weaver, *ACS Chem. Neurosci.*, 2020, **11**, 4152–4168.
183 P. M. Hwang, N. Zhou, X. Shan, C. H. Arrowsmith and H. J. Vogel, *Biochemistry*, 1998, **37**, 4288–4298.
184 H. Zhao, A. Jutila, T. Nurminen, S. A. Wickstrom, J. Keski-Oja and P. K. Kinnunen, *Biochemistry*, 2005, **44**, 2857–2863.
185 H. Chu, M. Pazgier, G. Jung, S.-P. Nuccio, P. A. Castillo, M. F. de Jong, M. G. Winter, S. E. Winter, J. Wehkamp, B. Shen, N. H. Salzman, M. A. Underwood, R. M. Tsolis, G. M. Young, W. Lu, R. I. Lehrer, A. J. Bäumler and C. L. Bevins, *Science*, 2012, **337**, 477–481.
186 M. Torrent, F. Odorizzi, M. V. Nogues and E. Boix, *Biomacromolecules*, 2010, **11**, 1983–1990.
187 R. Gossler-Schofberger, G. Hesser, M. M. Reif, J. Friedmann, B. Duscher, J. L. Toca-Herrera, C. Oostenbrink and A. Jilek, *Arch. Biochem. Biophys.*, 2012, **522**, 100–106.
188 R. Gossler-Schofberger, G. Hesser, M. Muik, C. Wechselberger and A. Jilek, *FEBS J*, 2009, **276**, 5849–5859.
189 N. Salinas, E. Tayeb-Fligelman, M. D. Sammito, D. Bloch, R. Jelinek, D. Noy, I. Usón and M. Landau, *Proc. Natl. Acad. Sci. U. S. A.*, 2021, **118**, e2014442118.
190 P. Ragonis-Bachar, B. Rayan, E. Barnea, Y. Engelberg, A. Upcher and M. Landau, *Biomacromolecules*, 2022, **23**, 3713–3727.
191 J. Davagnino, M. Herrero, D. Furlong, F. Moreno and R. Kolter, *Proteins: Struct., Funct., Bioinf.*, 1986, **1**, 230–238.
192 S. Bieler, L. Estrada, R. Lagos, M. Baeza, J. Castilla and C. Soto, *J. Biol. Chem.*, 2005, **280**, 26880–26885.
193 S. Gour, V. Kumar, M. Rana and J. K. Yadav, *J. Pept. Sci.*, 2019, **25**, e3178.
194 G. Fimland, J. Pirneskoski, J. Kaewsrichan, A. Jutila, P. E. Kristiansen, P. K. Kinnunen and J. Nissen-Meyer, *Biochim. Biophys. Acta*, 2006, **1764**, 1132–1140.
195 A. Stern, W. A. Gibbons and L. C. Craig, *Proc. Natl. Acad. Sci. U. S. A.*, 1968, **61**, 734–741.
196 G. Munyuki, G. E. Jackson, G. A. Venter, K. E. Kover, L. Szilagyi, M. Rautenbach, B. M. Spathelf, B. Bhattacharya and D. van der Spoel, *Biochemistry*, 2013, **52**, 7798–7806.
197 M. Garvey, S. Meehan, S. L. Gras, H. J. Schirra, D. J. Craik, N. L. Van der Weerden, M. A. Anderson, J. A. Gerrard and J. A. Carver, *Biochim. Biophys. Acta*, 2013, **1834**, 1615–1623.
198 S. Gour, V. Kaushik, V. Kumar, P. Bhat, S. C. Yadav and J. K. Yadav, *J. Pept. Sci.*, 2016, **22**, 201–207.
199 K. Liu, L. Yang, X. Peng, J. Wang, J. R. Lu and H. Xu, *Langmuir*, 2020, **36**, 1737–1744.
200 Z. Shen, Z. Guo, L. Zhou, Y. Wang, J. Zhang, J. Hu and Y. Zhang, *Biomater. Sci.*, 2020, **8**, 2031–2039.
201 X. T. Mai, J. Huang, J. Tan, Y. Huang and Y. Chen, *J. Pept. Sci.*, 2015, **21**, 561–568.
202 J. Blazyk, R. Wiegand, J. Klein, J. Hammer, R. M. Epand, R. F. Epand, W. L. Maloy and U. P. Kari, *J. Biol. Chem.*, 2001, **276**, 27899–27906.
203 N. Harmouche, C. Aisenbrey, F. Porcelli, Y. Xia, S. E. D. Nelson, X. Chen, J. Raya, L. Vermeer, C. Aparicio, G. Veglia, S. U. Gorr and B. Bechinger, *Biochemistry*, 2017, **56**, 4269–4278.
204 V. Balhara, R. Schmidt, S. U. Gorr and C. Dewolf, *Biochim. Biophys. Acta*, 2013, **1828**, 2193–2203.
205 Z. Oren, J. Hong and Y. Shai, *Eur. J. Biochem.*, 1999, **259**, 360–369.
206 D. L. Lee and R. S. Hodges, *Biopolymers*, 2003, **71**, 28–48.
207 R. Bellavita, E. Buommino, B. Casciaro, F. Merlino, F. Cappiello, N. Marigliano, A. Saviano, F. Maione, R. Santangelo, M. L. Mangoni, S. Galdiero, P. Grieco and A. Falanga, *Antibiotics*, 2022, **11**, 1285.
208 Z. Y. Ong, S. J. Gao and Y. Y. Yang, *Adv. Funct. Mater.*, 2013, **23**, 3682–3692.
209 J. M. Rausch, J. R. Marks and W. C. Wimley, *Proc. Natl. Acad. Sci. U. S. A.*, 2005, **102**, 10511–10515.
210 D. Rapaport and Y. Shai, *J. Biol. Chem.*, 1991, **266**, 23769–23775.
211 K. Matsuzaki, O. Murase, N. Fujii and K. Miyajima, *Biochemistry*, 1995, **34**, 6521–6526.
212 V. N. Kokryakov, S. S. L. Harwig, E. A. Panyutich, A. A. Shevchenko, G. M. Aleshina, O. V. Shamova, H. A. Korneva and R. I. Lehrer, *FEBS lett.*, 1993, **327**, 231–236.
213 M. Frohm, B. Agerberth, G. Ahangari, M. Ståhle-Bäckdahl, S. Lidén, H. Wigzell and G. H. Gudmundsson, *J. Biol. Chem.*, 1997, **272**, 15258–15263.
214 R. Sood, Y. Domanov, M. Pietiäinen, V. P. Kontinen and P. K. J. Kinnunen, *Biochim. Biophys. Acta, Biomembr.*, 2008, **1778**, 983–996.
215 E. Y. Lee, C. Zhang, J. Di Domizio, F. Jin, W. Connell, M. Hung, N. Malkoff, V. Veksler, M. Gilliet and P. Ren, *Nat. Commun.*, 2019, **10**, 1012.
216 P. Chairatana and E. M. Nolan, *J. Am. Chem. Soc.*, 2014, **136**, 13267–13276.
217 E. Soravia, G. Martini and M. Zasloff, *FEBS Lett.*, 1988, **228**, 337–340.
218 G. Diamond, M. Zasloff, H. Eck, M. Brasseur, W. L. Maloy and C. L. Bevins, *Proc. Natl. Acad. Sci. U. S. A.*, 1991, **88**, 3952–3956.
219 O. Lequin, A. Ladram, L. Chabbert, F. Bruston, O. Convert, D. Vanhoye, G. Chassaing, P. Nicolas and M. Amiche, *Biochemistry*, 2006, **45**, 468–480.
220 J. H. Bowie, F. Separovic and M. J. Tyler, *Peptides*, 2012, **37**, 174–188.
221 A. Pastore, F. Raimondi, L. Rajendran and P. A. Temussi, *Commun. Biol.*, 2020, **3**, 135.
222 L. Silvestro, K. Gupta, J. N. Weiser and P. H. Axelsen, *Biochemistry*, 1997, **36**, 11452–11460.
223 H. S. McHaourab, J. S. Hyde and J. B. Feix, *Biochemistry*, 1994, **33**, 6691–6699.
224 S. L. Puan, P. Erriah, M. M. A.-A. Baharudin, N. M. Yahaya, W. N. I. W. A. Kamil, M. S. M. Ali, S. A. Ahmad, S. N. Oslan, S. Lim and S. Sabri, *Appl. Microbiol. Biotechnol.*, 2023, **107**, 5569–5593.
225 J. Nissen-Meyer and I. F. Nes, *Arch. Microbiol.*, 1997, **167**, 67–77.
226 M. A. Riley and J. E. Wertz, *Annu. Rev. Microbiol.*, 2002, **56**, 117–137.
227 M. A. Riley, *Annu. Rev. Genet.*, 1998, **32**, 255–278.

228 M. Herrero and F. Moreno, *J. Gen. Microbiol.*, 1986, **132**, 393–402.
229 V. D. Lorenzo, *Arch. Microbiol.*, 1984, **139**, 72–75.
230 D. Destoumieux-Garzon, X. Thomas, M. Santamaria, C. Goulard, M. Barthelemy, B. Boscher, Y. Bessin, G. Molle, A. M. Pons, L. Letellier, J. Peduzzi and S. Rebuffat, *Mol. Microbiol.*, 2003, **49**, 1031–1041.
231 V. De Lorenzo and A. Pugsley, *Antimicrob. Agents Chemother.*, 1985, **27**, 666–669.
232 C. Hetz, M. R. Bono, L. F. Barros and R. Lagos, *Proc. Natl. Acad. Sci. U. S. A.*, 2002, **99**, 2696–2701.
233 P. Aguilera, A. Marcoleta, P. Lobos-Ruiz, R. Arranz, J. M. Valpuesta, O. Monasterio and R. Lagos, *Front. Microbiol.*, 2016, **7**, 35.
234 R. H. Perez, T. Zendo and K. Sonomoto, *Microb. Cell Fact.*, 2014, **13**, 1–13.
235 P. D. Cotter, C. Hill and R. P. Ross, *Nat. Rev. Microbiol.*, 2005, **3**, 777–788.
236 A. Thakur, Master thesis, University of Horticulture & Forestry Nauni (Solan), India, 2017.
237 J. Nakayama, Y. Abe, Y. Ono, A. Isogai and A. Suzuki, *Biosci. Biotechnol. Biochem.*, 1995, **59**, 703–705.
238 J. P. Tam, S. Wang, K. H. Wong and W. L. Tan, *Pharmaceuticals*, 2015, **8**, 711–757.
239 W. F. Broekaert, B. P. Cammue, M. F. De Bolle, K. Thevissen, G. W. De Samblanx, R. W. Osborn and K. Nielson, *CRC Crit. Rev. Plant Sci.*, 1997, **16**, 297–323.
240 Y. Jin, J. Hammer, M. Pate, Y. Zhang, F. Zhu, E. Zmuda and J. Blazyk, *Antimicrob. Agents Chemother.*, 2005, **49**, 4957–4964.
241 H. Kamimori, J. Blazyk and M. I. Aguilar, *Biol. Pharm. Bull.*, 2005, **28**, 148–150.
242 H. Youssef and C. E. DeWolf, *Langmuir*, 2019, **36**, 660–665.
243 G. Bell and P. H. Gouyon, *Microbiology*, 2003, **149**, 1367–1375.
244 Z. Y. Ong, J. Cheng, Y. Huang, K. Xu, Z. Ji, W. Fan and Y. Y. Yang, *Biomaterials*, 2014, **35**, 1315–1325.
245 G. Zhong, J. Cheng, Z. C. Liang, L. Xu, W. Lou, C. Bao, Z. Y. Ong, H. Dong, Y. Y. Yang and W. Fan, *Adv. Healthcare Mater.*, 2017, **6**, 1601134.
246 F. Chiti and C. M. Dobson, *Annu. Rev. Biochem.*, 2006, **75**, 333–366.
247 M. G. Iadanza, M. P. Jackson, E. W. Hewitt, N. A. Ranson and S. E. Radford, *Nat. Rev. Mol. Cell Biol.*, 2018, **19**, 755–773.
248 D. Otzen and R. Riek, *Cold Spring Harbor Perspect. Biol.*, 2019, **11**, a033860.
249 N. Van Gerven, R. D. Klein, S. J. Hultgren and H. Remaut, *Trends Biotechnol.*, 2015, **23**, 693–706.
250 B. Dai, C. J. Sargent, X. Gui, C. Liu and F. Zhang, *Biomacromolecules*, 2019, **20**, 2015–2023.
251 W. A. Eimer, D. K. V. Kumar, N. K. N. Shanmugam, A. S. Rodriguez, T. Mitchell, K. J. Washicosky, B. György, X. O. Breakefield, R. E. Tanzi and R. D. J. N. Moir, *Neuron*, 2018, **99**(56–63), e53.
252 M. R. White, R. Kandel, S. Tripathi, D. Condon, L. Qi, J. Taubenberger and K. L. Hartshorn, *PloS one*, 2014, **9**, e101364.
253 Y. Liao, H. Chen, C. Qiu, H. Shen, Z. He, Z. Song and W. Zhou, *Research Square*, 2023, DOI: **10.21203/rs.3.rs-3300215/v1**.
254 M. R. White, R. Kandel, I. N. Hsieh, X. De Luna and K. L. Hartshorn, *PLoS One*, 2018, **13**, e0194001.
255 P. Spitzer, M. Condic, M. Herrmann, T. J. Oberstein, M. Scharin-Mehlmann, D. F. Gilbert, O. Friedrich, T. Gromer, J. Kornhuber, R. Lang and J. M. Maler, *Sci. Rep.*, 2016, **6**, 32228.
256 N. M. Hemmaragala, H. Abrahamse and B. P. George, *IET Nanobiotechnol.*, 2017, **11**, 377–382.
257 C. Kokotidou, S. V. R. Jonnalagadda, A. A. Orr, G. Vrentzos, A. Kretsovali, P. Tamamis and A. Mitraki, *Biomolecules*, 2019, **10**, 7.
258 X. Sha, P. Li, Y. Feng, D. Xia, X. Tian, Z. Wang, Y. Yang, X. Mao and L. Liu, *ACS Appl. Bio Mater.*, 2020, **3**, 3648–3655.
259 E. L. Beatman, A. Massey, K. D. Shives, K. S. Burrack, M. Chamanian, T. E. Morrison and J. D. Beckham, *J. Virol.*, 2016, **90**, 2767–2782.
260 T. Yamada, B. Kluve-Beckerman, J. J. Liepnieks and M. D. Benson, *Biochim. Biophys. Acta*, 1994, **1226**, 323–329.
261 A. Erman, K. Lakota, K. Mrak-Poljsak, M. G. Blango, V. Krizan-Hergouth, M. A. Mulvey, S. Sodin-Semrl and P. Veranic, *PLoS One*, 2012, **7**, e32933.
262 J. Gong, J. Wu, M. Ikeh, L. Tao, Y. Zhang, J. Bing, C. J. Nobile and G. Huang, *Antimicrob. Agents Chemother.*, 2019, **64**, e01975-19.
263 M. Lavie, C. Voisset, N. Vu-Dac, V. Zurawski, G. Duverlie, C. Wychowski and J. Dubuisson, *Hepatology*, 2006, **44**, 1626–1634.
264 Z. Cai, L. Cai, J. Jiang, K.-S. Chang, D. R. van der Westhuyzen and G. Luo, *J. Virol.*, 2007, **81**, 6128–6133.
265 T. Sato, P. Kienlen-Campard, M. Ahmed, W. Liu, H. Li, J. I. Elliott, S. Aimoto, S. N. Constantinescu, J. N. Octave and S. O. Smith, *Biochemistry*, 2006, **45**, 5503–5516.
266 N. Nalivaeva, N. Belyaev, I. Zhuravin and A. Turner, *Int. J. Alzheimers Dis*, 2012, **2012**, 383796.
267 J. Hardy and D. J. Selkoe, *Science*, 2002, **297**, 353–356.
268 R. Penninkilampi, H. M. Brothers and G. D. Eslick, *J. Neuroimmune Pharmacol.*, 2017, **12**, 194–203.
269 K. G. Yiannopoulou and S. G. Papageorgiou, *J. Cent. Nerv. Syst. Dis.*, 2020, **12**, 1179573520907397.
270 S. Gilman, M. Koller, R. S. Black, L. Jenkins, S. G. Griffith, N. C. Fox, L. Eisner, L. Kirby, M. B. Rovira, F. Forette, J. M. Orgogozo and A. N. S. Team, *Neurology*, 2005, **64**, 1553–1562.
271 J. M. Orgogozo, S. Gilman, J. F. Dartigues, B. Laurent, M. Puel, L. C. Kirby, P. Jouanny, B. Dubois, L. Eisner, S. Flitman, B. F. Michel, M. Boada, A. Frank and C. Hock, *Neurology*, 2003, **61**, 46–54.
272 A. Schneeberger, S. Hendrix, M. Mandler, N. Ellison, V. Burger, M. Brunner, L. Frolich, N. Mimica, J. Hort, M. Rainer, D. Imarhiagbe, A. Kurz, O. Peters, H. J. Gertz, L. Tierney, F. Mattner, W. Schmidt and B. Dubois, *J. Prev. Alzheimers Dis.*, 2015, **2**, 103–114.

273 R. Vandenberghe, M. E. Riviere, A. Caputo, J. Sovago, R. P. Maguire, M. Farlow, G. Marotta, R. Sanchez-Valle, P. Scheltens, J. M. Ryan and A. Graf, *Alzheimers Dement*, 2017, **3**, 10–22.
274 R. D. Moir, R. Lathe and R. E. Tanzi, *Alzheimers Dement*, 2018, **14**, 1602–1614.
275 D. K. Kumar, S. H. Choi, K. J. Washicosky, W. A. Eimer, S. Tucker, J. Ghofrani, A. Lefkowitz, G. McColl, L. E. Goldstein, R. E. Tanzi and R. D. Moir, *Sci. Transl. Med.*, 2016, **8**, 340ra372.
276 L. De Vlieger, R. E. Vandenbroucke and L. Van Hoecke, *Drug Discovery Today*, 2022, **27**, 103340.
277 M. Sochocka, K. Zwolinska and J. Leszek, *Curr. Neuropharmacol.*, 2017, **15**, 996–1009.
278 W. R. Lin, M. A. Wozniak, R. J. Cooper, G. K. Wilcock and R. F. Itzhaki, *J. Pathol.*, 2002, **197**, 395–402.
279 R. Piacentini, G. De Chiara, D. D. Li Puma, C. Ripoli, M. E. Marcocci, E. Garaci, A. T. Palamara and C. Grassi, *Front. Pharmacol.*, 2014, **5**, 97.
280 K. Bourgade, A. Le Page, C. Bocti, J. M. Witkowski, G. Dupuis, E. H. Frost and T. Fulop, Jr., *J Alzheimers Dis.*, 2016, **50**, 1227–1241.
281 D. K. Kumar, W. A. Eimer, R. E. Tanzi and R. D. Moir, *Neurodegener Dis Manag*, 2016, **6**, 345–348.
282 M. Torrent, D. Pulido, M. V. Nogues and E. Boix, *PLoS Pathog*, 2012, **8**, e1003005.
283 H. Jang, L. Connelly, F. T. Arce, S. Ramachandran, B. L. Kagan, R. Lal and R. Nussinov, *J. Chem. Theory Comput.*, 2013, **9**, 822–833.
284 Y. R. Huang and R. T. Liu, *Int. J. Mol. Sci.*, 2020, **21**, 4477.
285 E. Portelius, G. Brinkmalm, A. J. Tran, H. Zetterberg, A. Westman-Brinkmalm and K. Blennow, *Neurodegener. Dis.*, 2009, **6**, 87–94.
286 A. Guntert, H. Dobeli and B. Bohrmann, *Neuroscience*, 2006, **143**, 461–475.
287 J. C. J. A. C. N. Phillips, *ACS Chem. Neurosci.*, 2019, **10**, 2843–2847.
288 L. Gu and Z. Guo, *Biochem. Biophys. Res. Commun.*, 2021, **534**, 292–296.
289 M. Ahmed, J. Davis, D. Aucoin, T. Sato, S. Ahuja, S. Aimoto, J. I. Elliott, W. E. Van Nostrand and S. O. Smith, *Nat. Struct. Mol. Biol.*, 2010, **17**, 561–567.
290 C. J. Pike, M. J. Overman and C. W. Cotman, *J. Biol. Chem.*, 1995, **270**, 23895–23898.
291 D. Meral and B. Urbanc, *Biophys. J.*, 2013, **104**, 389a.
292 J. P. Colletier, A. Laganowsky, M. Landau, M. Zhao, A. B. Soriaga, L. Goldschmidt, D. Flot, D. Cascio, M. R. Sawaya and D. Eisenberg, *Proc. Natl. Acad. Sci. U. S. A.*, 2011, **108**, 16938–16943.
293 C. Kokotidou, S. V. R. Jonnalagadda, A. A. Orr, M. Seoane-Blanco, C. P. Apostolidou, M. J. van Raaij, M. Kotzabasaki, A. Chatzoudis, J. M. Jakubowski, E. Mossou, V. T. Forsyth, E. P. Mitchell, M. W. Bowler, A. L. Llamas-Saiz, P. Tamamis and A. Mitraki, *FEBS Lett.*, 2018, **592**, 1777–1788.
294 R. A. DeFronzo, E. Ferrannini, L. Groop, R. R. Henry, W. H. Herman, J. J. Holst, F. B. Hu, C. R. Kahn, I. Raz, G. I. Shulman, D. C. Simonson, M. A. Testa and R. Weiss, *Nat. Rev. Dis. Primers*, 2015, **1**, 15019.
295 S. Chatterjee, K. Khunti and M. J. Davies, *Lancet*, 2017, **389**, 2239–2251.
296 P. Westermark and E. J. D. Wilander, *Diabetologia*, 1983, **24**, 342–346.
297 S. Chakraborty, B. Chatterjee and S. J. B. C. Basu, *Biophys. Chem.*, 2012, **168**, 1–9.
298 R. A. Noel, D. K. Braun, R. E. Patterson and G. L. Bloomgren, *Diabetes Care*, 2009, **32**, 834–838.
299 S. Sharma and P. Tripathi, *J. Nutr. Biochem.*, 2019, **63**, 101–108.
300 A. K. Sikalidis and A. Maykish, *Biomedicines*, 2020, **8**, 8.
301 C. Naing, J. W. Mak, S. I. Ahmed and M. Maung, *World J. Gastroenterol.*, 2012, **18**, 1642.
302 S. G. Yoo, K. D. Han, K. H. Lee, Y. La, D. E. Kwon and S. H. Han, *Diabetes Metab. J.*, 2019, **43**, 815–829.
303 J. Sato, A. Kanazawa, F. Ikeda, T. Yoshihara, H. Goto, H. Abe, K. Komiya, M. Kawaguchi, T. Shimizu and T. Ogihara, *Diabetes Care*, 2014, **37**, 2343–2350.
304 A. Bener, R. Micallef, M. Afifi, M. Derbala, H. M. Al-Mulla and M. A. J. T. J. G. Usmani, *Turk J. Gastroentero.*, 2007, **18**, 225–229.
305 C. Wang, D. Gao and B. Kaltenboeck, *J. Infect. Dis.*, 2009, **200**, 279–287.
306 S. Al Mubarak, A. A. Robert, J. K. Baskaradoss, K. Al-Zoman, A. Al Sohail, A. Alsuwyed and S. Ciancio, *J. Infect. Public Health*, 2013, **6**, 296–301.
307 M. Y. Donath, M. Boni-Schnetzler, H. Ellingsgaard and J. A. Ehses, *Physiology*, 2009, **24**, 325–331.
308 M. Boni-Schnetzler, J. Thorne, G. Parnaud, L. Marselli, J. A. Ehses, J. Kerr-Conte, F. Pattou, P. A. Halban, G. C. Weir and M. Y. Donath, *J. Clin. Endocrinol. Metab.*, 2008, **93**, 4065–4074.
309 S. Kim, J. H. Seo and Y. H. Suh, *Parkinsonism Relat. Disord.*, 2004, **10**(Suppl 1), S9–S13.
310 L. Breydo, J. W. Wu and V. N. Uversky, *Biochim. Biophys. Acta*, 2012, **1822**, 261–285.
311 M. C. Bennett, *Pharmacol. Ther.*, 2005, **105**, 311–331.
312 O. EI-Agnaf and G. J. B. S. T. Irvine, *Biochem. Soc. Trans.*, 2002, **30**, 559–565.
313 C. R. Fields, N. Bengoa-Vergniory and R. Wade-Martins, *Front. Mol. Neurosci.*, 2019, **12**, 299.
314 D. L. Fortin, M. D. Troyer, K. Nakamura, S. Kubo, M. D. Anthony and R. H. Edwards, *J. Neurosci.*, 2004, **24**, 6715–6723.
315 D. Sulzer and R. H. Edwards, *J. Neurochem.*, 2019, **150**, 475–486.
316 C. R. Pacheco, C. N. Morales, A. E. Ramirez, F. J. Munoz, S. S. Gallegos, P. A. Caviedes, L. G. Aguayo and C. M. Opazo, *J. Neurochem.*, 2015, **132**, 731–741.
317 K. J. Vargas, S. Makani, T. Davis, C. H. Westphal, P. E. Castillo and S. S. Chandra, *J. Neurosci.*, 2014, **34**, 9364–9376.
318 F. Savini, M. R. Loffredo, C. Troiano, S. Bobone, N. Malanovic, T. O. Eichmann, L. Caprio, V. C. Canale,

Y. Park, M. L. Mangoni and L. Stella, *Biochim. Biophys. Acta Biomembr.*, 2020, **1862**, 183291.
319 Y. Luo and Y. Song, *Int. J. Mol. Sci.*, 2021, **22**, 11401.
320 W. Y. Lin, M. S. Lin, Y. H. Weng, T. H. Yeh, Y. S. Lin, P. Y. Fong, Y. R. Wu, C. S. Lu, R. S. Chen and Y. Z. Huang, *JAMA Neurol.*, 2019, **76**, 1019–1027.
321 H. Wang, X. Liu, C. Tan, W. Zhou, J. Jiang, W. Peng, X. Zhou, L. Mo and L. Chen, *Brain Behav.*, 2020, **10**, e01549.
322 S. G. Chen, V. Stribinskis, M. J. Rane, D. R. Demuth, E. Gozal, A. M. Roberts, R. Jagadapillai, R. Liu, K. Choe, B. Shivakumar, F. Son, S. Jin, R. Kerber, A. Adame, E. Masliah and R. P. Friedland, *Sci. Rep.*, 2016, **6**, 34477.
323 I. Poggiolini, D. Saverioni and P. Parchi, *Int. J. Cell Biol.*, 2013, **2013**, 910314.
324 R. A. Moore, L. M. Taubner and S. A. Priola, *Curr. Opin. Struct. Biol.*, 2009, **19**, 14–22.
325 H. Bueler, A. Aguzzi, A. Sailer, R. A. Greiner, P. Autenried, M. Aguet and C. Weissmann, *Cell*, 1993, **73**, 1339–1347.
326 J. R. Silveira, G. J. Raymond, A. G. Hughson, R. E. Race, V. L. Sim, S. F. Hayes and B. J. N. Caughey, *Nature*, 2005, **437**, 257–261.
327 P. Tixador, L. Herzog, F. Reine, E. Jaumain, J. M. Chapuis, A. L. Dur, H. Laude and V. Beringue, *PLoS Pathog*, 2010, **6**, e1000859.
328 A. R. Castle and A. C. Gill, *Front. Mol. Biosci.*, 2017, **4**, 19.
329 R. Linden, V. R. Martins, M. A. Prado, M. Cammarota, I. Izquierdo and R. R. Brentani, *Phys. Rev.*, 2008, **88**, 673–728.
330 F. Prestori, P. Rossi, B. Bearzatto, J. Laine, D. Necchi, S. Diwakar, S. N. Schiffmann, H. Axelrad and E. D'Angelo, *J. Neurosci.*, 2008, **28**, 7091–7103.
331 J. Bremer, F. Baumann, C. Tiberi, C. Wessig, H. Fischer, P. Schwarz, A. D. Steele, K. V. Toyka, K.-A. Nave and J. Weis, *Nat. Neurosci.*, 2010, **13**, 310–318.
332 P. C. Konturek, K. Bazela, V. Kukharskyy, M. Bauer, E. G. Hahn and D. Schuppan, *World J. Gastroenterol.*, 2005, **11**, 7651–7656.
333 J. Pammer, W. Weninger and E. Tschachler, *Am. J. Pathol.*, 1998, **153**, 1353–1358.
334 M. D. Beer, T. Yuan, M. Kindy, B. Asztalos, P. Roheim and F. D. Beer, *J. Lipid Res.*, 1995, **36**, 526–534.
335 A. Butler and A. S. Whitehead, *Immunogenetics*, 1996, **44**, 468–474.
336 R. L. Meek and E. P. Benditt, *J. Exp. Med.*, 1986, **164**, 2006–2017.
337 E. P. Benditt and N. Eriksen, *Am. J. Pathol.*, 1971, **65**, 231–252.
338 C. L. Banka, T. Yuan, M. C. de Beer, M. Kindy, L. K. Curtiss and F. C. de Beer, *J. Lipid Res.*, 1995, **36**, 1058–1065.
339 R. Badolato, J. M. Wang, W. J. Murphy, A. R. Lloyd, D. F. Michiel, L. L. Bausserman, D. J. Kelvin and J. J. Oppenheim, *J. Exp. Med.*, 1994, **180**, 203–209.
340 C. Song, K. Hsu, E. Yamen, W. Yan, J. Fock, P. K. Witting, C. L. Geczy and S. B. Freedman, *Atherosclerosis*, 2009, **207**, 374–383.
341 N. Olsson, A. Siegbahn and G. Nilsson, *Biochem. Biophys. Res. Commun.*, 1999, **254**, 143–146.
342 C. Shah, R. Hari-Dass and J. G. Raynes, *Blood*, 2006, **108**, 1751–1757.
343 M. C. Lin, T. Mirzabekov and B. L. Kagan, *J. Biol. Chem.*, 1997, **272**, 44–47.
344 N. Arispe, E. Rojas and H. B. Pollard, *Proc. Natl. Acad. Sci. U. S. A.*, 1993, **90**, 567–571.
345 L. Obici and G. Merlini, *Swiss Med. Wkly.*, 2012, **142**, w13580.
346 E. R. Eckhardt, J. Witta, J. Zhong, R. Arsenescu, V. Arsenescu, Y. Wang, S. Ghoshal, M. C. de Beer, F. C. de Beer and W. J. de Villiers, *BMC Gastroenterol.*, 2010, **10**, 133.
347 R. Badolato, J. M. Wang, S. L. Stornello, A. N. Ponzi, M. Duse and T. Musso, *J. Leukoc. Biol.*, 2000, **67**, 381–386.
348 J. Gong, J. Bing, G. Guan, C. J. Nobile and G. Huang, *Antimicrob. Agents Chemother.*, 2020, **64**, e00024-20.
349 X. N. Mo, Z. Q. Su, C. L. Lei, D. F. Chen, H. Peng, R. C. Chen, L. Sang, H. K. Wu and S. Y. Li, *Respirology*, 2020, 764.
350 H. Li, X. Xiang, H. Ren, L. Xu, L. Zhao, X. Chen, H. Long, Q. Wang and Q. Wu, *J. Infect.*, 2020, **80**, 646–655.
351 M. R. White, I. N. Hsieh, X. De Luna and K. L. Hartshorn, *J. Leukocyte Biol.*, 2021, **110**, 155–166.
352 H. B. Kramer, K. J. Lavender, L. Qin, A. R. Stacey, M. K. Liu, K. D. Gleria, A. Simmons, N. Gasper-Smith, B. F. Haynes, A. J. McMichael, P. Borrow and B. M. Kessler, *PLoS Pathog*, 2010, **6**, e1000893.
353 S. Makin, *Nature*, 2018, **559**, S4–S7.
354 R. Oliva, S. K. Mukherjee, L. Ostermeier, L. A. Pazurek, S. Kriegler, V. Bader, D. Prumbaum, S. Raunser, K. F. Winklhofer, J. Tatzelt and R. Winter, *Chemistry*, 2021, **27**, 11845–11851.
355 A. Kasus-Jacobi, J. L. Washburn, C. A. Land and H. A. Pereira, *Curr. Alzheimer Res*, 2021, **18**, 414–427.
356 A. F. Gombart, N. Borregaard and H. P. Koeffler, *FASEB J*, 2005, **19**, 1067–1077.
357 L. D. Pound, C. Patrick, C. E. Eberhard, W. Mottawea, G. S. Wang, T. Abujamel, R. Vandenbeek, A. Stintzi and F. W. Scott, *Diabetes*, 2015, **64**, 4135–4147.
358 J. Sun, L. Furio, R. Mecheri, A. M. van der Does, E. Lundeberg, L. Saveanu, Y. Chen, P. van Endert, B. Agerberth and J. Diana, *Immunity*, 2015, **43**, 304–317.
359 S. Grabrucker, M. Marizzoni, E. Silajdzic, N. Lopizzo, E. Mombelli, S. Nicolas, S. Dohm-Hansen, C. Scassellati, D. V. Moretti, M. Rosa, K. Hoffmann, J. F. Cryan, O. F. O'Leary, J. A. English, A. Lavelle, C. O'Neill, S. Thuret, A. Cattaneo and Y. M. Nolan, *Brain*, 2023, **146**, 4916–4934.
360 T. Harach, N. Marungruang, N. Duthilleul, V. Cheatham, K. D. Mc Coy, G. Frisoni, J. J. Neher, F. Fåk, M. Jucker and T. Lasser, *Sci. Rep.*, 2017, **7**, 41802.
361 K. Hartman, J. R. Brender, K. Monde, A. Ono, M. L. Evans, N. Popovych, M. R. Chapman and A. Ramamoorthy, *PeerJ*, 2013, **1**, e5.

362 A. Cattaneo, N. Cattane, S. Galluzzi, S. Provasi, N. Lopizzo, C. Festari, C. Ferrari, U. P. Guerra, B. Paghera, C. Muscio, A. Bianchetti, G. D. Volta, M. Turla, M. S. Cotelli, M. Gennuso, A. Prelle, O. Zanetti, G. Lussignoli, D. Mirabile, D. Bellandi, S. Gentile, G. Belotti, D. Villani, T. Harach, T. Bolmont, A. Padovani, M. Boccardi, G. B. Frisoni and I.-F. Group, *Neurobiol. Aging*, 2017, **49**, 60–68.

363 M. Sanchez-Tapia, A. Mimenza-Alvarado, L. Granados-Dominguez, A. Flores-Lopez, A. Lopez-Barradas, V. Ortiz, C. Perez-Cruz, H. Sanchez-Vidal, J. Hernandez-Acosta, J. A. Avila-Funes, M. Guevara-Cruz, A. R. Tovar and N. Torres, *Nutrients*, 2023, **15**, 932.

364 O. Meza-Barajas, I. Aranda, A. Binmahfooz, A. Newell and S. Jayasinghe, *bioRxiv*, 2019, preprint, DOI: 10.1101/772392.

365 N. Khan, M. Arlantico, E. Feliciano, H. Nguyen and S. Jayasinghe, *FASEB J*, 2018, **32**, lb59.

366 I. Cherny, L. Rockah, O. Levy-Nissenbaum, U. Gophna, E. Z. Ron and E. Gazit, *J. Mol. Biol.*, 2005, **352**, 245–252.

367 C. Wang, C. Y. Lau, F. Ma and C. Zheng, *Proc. Natl. Acad. Sci. U. S. A.*, 2021, **118**, e2106504118.

368 E. Tayeb-Fligelman, O. Tabachnikov, A. Moshe, O. Goldshmidt-Tran, M. R. Sawaya, N. Coquelle, J. P. Colletier and M. Landau, *Science*, 2017, **355**, 831–833.

369 C. Haikal, L. Ortigosa-Pascual, Z. Najarzadeh, K. Bernfur, A. Svanbergsson, D. E. Otzen, S. Linse and J.-Y. Li, *Int. J. Mol. Sci.*, 2021, **22**, 11594.

370 B. Peng, S. Xu, Y. Liang, X. Dong and Y. Sun, *Biomimetics*, 2023, **8**, 459.

371 S. Perov, O. Lidor, N. Salinas, N. Golan, E. Tayeb-Fligelman, M. Deshmukh, D. Willbold and M. Landau, *PLoS Pathog*, 2019, **15**, e1007978.

372 S. L. Rouse, S. J. Matthews and M. S. Dueholm, *J. Mol. Biol.*, 2018, **430**, 3685–3695.

373 N. Jain, J. Aden, K. Nagamatsu, M. L. Evans, X. Li, B. McMichael, M. I. Ivanova, F. Almqvist, J. N. Buxbaum and M. R. Chapman, *Proc. Natl. Acad. Sci. U. S. A.*, 2017, **114**, 12184–12189.

374 J. N. Buxbaum, Z. Ye, N. Reixach, L. Friske, C. Levy, P. Das, T. Golde, E. Masliah, A. R. Roberts and T. Bartfai, *Proc. Natl. Acad. Sci. U. S. A.*, 2008, **105**, 2681–2686.

375 X. Li, X. Zhang, A. R. Ladiwala, D. Du, J. K. Yadav, P. M. Tessier, P. E. Wright, J. W. Kelly and J. N. Buxbaum, *J. Neurosci.*, 2013, **33**, 19423–19433.

376 S. Wasana Jayaweera, S. Surano, N. Pettersson, E. Oskarsson, L. Lettius, A. L. Gharibyan, I. Anan and A. Olofsson, *Biomolecules*, 2021, **11**, 411.

377 R. Cascella, S. Conti, B. Mannini, X. Li, J. N. Buxbaum, B. Tiribilli, F. Chiti and C. Cecchi, *Biochim. Biophys. Acta*, 2013, **1832**, 2302–2314.

378 I. Horvath and P. Wittung-Stafshede, *Proc. Natl. Acad. Sci. U. S. A.*, 2016, **113**, 12473–12477.

379 R. Hu, M. Zhang, H. Chen, B. Jiang and J. Zheng, *ACS Chem. Neurosci.*, 2015, **6**, 1759–1768.

380 P. K. Mandal, J. W. Pettegrew, E. Masliah, R. L. Hamilton and R. Mandal, *Neurochem. Res.*, 2006, **31**, 1153–1162.

381 I. C. Stancu, B. Vasconcelos, D. Terwel and I. Dewachter, *Mol Neurodegener.*, 2014, **9**, 51.

382 P. Liu, S. Zhang, M. S. Chen, Q. Liu, C. Wang, C. Wang, Y. M. Li, F. Besenbacher and M. Dong, *Chem. Commun.*, 2012, **48**, 191–193.

383 H. Jang, B. Ma, T. B. Woolf and R. Nussinov, *Biophys. J.*, 2006, **91**, 2848–2859.

384 A. K. Prasad, L. L. Martin and A. S. Panwar, *Phys. Chem. Chem. Phys.*, 2023, **25**, 12134–12147.

385 N. Salinas, J. P. Colletier, A. Moshe and M. Landau, *Nat. Commun.*, 2018, **9**, 3512.

386 N. Louros, K. Konstantoulea, M. De Vleeschouwer, M. Ramakers, J. Schymkowitz and F. Rousseau, *Nucleic Acids Res.*, 2020, **48**, D389–D393.

387 G. G. Tartaglia and M. Vendruscolo, *Chem. Soc. Rev.*, 2008, **37**, 1395–1401.

388 I. Walsh, F. Seno, S. C. Tosatto and A. Trovato, *Nucleic Acids Res.*, 2014, **42**, W301–307.